HEAT TRANSFER AND FRICTION LOSS ANALYSIS OF A NOVEL ECO-FRIENDLY COLLOIDAL SUSPENSION IN FLOW PASSAGES

KAVIRAJ A/L JAYARAMAN

FACULTY OF ENGINEERING
UNIVERSITY OF MALAYA
KUALA LUMPUR

2019

HEAT TRANSFER AND FRICTION LOSS ANALYSIS OF A NOVEL ECO-FRIENDLY COLLOIDAL SUSPENSION IN FLOW PASSAGES

KAVIRAJ JAYARAMAN

THESIS SUBMITTED IN FULFILMENT OF THE REQUIREMENTS FOR THE DEGREE OF MASTERS OF MECHANICAL ENGINEERING

FACULTY OF ENGINEERING
UNIVERSITY OF MALAYA
KUALA LUMPUR

2019

UNIVERSITY OF MALAYA

ORIGINAL LITERARY WORK DECLARATION

Name of Candidate: Kaviraj Jayaraman

Matric No: KQK180021

Name of Degree: Masters of Mechanical Engineering

Title of Thesis : Heat Transfer and Friction Loss Analysis of a Novel Eco-Friendly

Colloidal Suspension in Flow Passages

Field of Study: Heat Transfer

I do solemnly and sincerely declare that:

(1) I am the sole author/writer of this Work;
(2) This Work is original;
(3) Any use of any work in which copyright exists was done by way of fair dealing and for permitted purposes and any excerpt or extract from, or reference to or reproduction of any copyright work has been disclosed expressly and sufficiently and the title of the Work and its authorship have been acknowledged in this Work;
(4) I do not have any actual knowledge nor do I ought reasonably to know that the making of this work constitutes an infringement of any copyright work;
(5) I hereby assign all and every rights in the copyright to this Work to the University of Malaya ("UM"), who henceforth shall be owner of the copyright in this Work and that any reproduction or use in any form or by any means whatsoever is prohibited without the written consent of UM having been first had and obtained;
(6) I am fully aware that if in the course of making this Work I have infringed any copyright whether intentionally or otherwise, I may be subject to legal action or any other action as may be determined by UM.

Candidate's Signature Date:

Subscribed and solemnly declared before,

Witness's Signature Date:

Name:

Designation:

HEAT TRANSFER AND FRICTION LOSS ANALYSIS OF A NOVEL ECO-FRIENDLY COLLOIDAL SUSPENSION IN FLOW PASSAGES

ABSTRACT

Invention of heat exchanger can be considered as once of the most important inventions of time. Heat exchangers are important equipments with various industrial applications such as power plants, HVAC industry and chemical industries. The are various fluids that are used as working fluid in the heat exchangers. These fluids are water, oil, and ethylene glycol are some of the commonly used working fluids.

A minor improvement in the working principle of heat exchanger may yield a much bigger outcome at a lesser cost. This idea has always interested researchers. Hence, researchers have conducted various studies and investigations to improve the heat exchanger be it from material or heat transfer point of view. In terms of heat transfer, they noticed that the conventional working fluids have a relatively low thermal conductivity and properties. There has been attempts to create solid particles suspended mixture. This invention faced some setback whereby the pressure drop was compromised, sedimentation occurred or even erosion, resulting in higher cost of maintenance.

A group researcher discovered a new class of colloidal suspension fluid that met all the demands and characteristics of a heat exchanger. This novel colloidal suspension mixture was then and now addressed as “nanofluid”.

In this study, phenolic acid functionalized graphene nanoplatelets nanofluids will be synthesized. The thermo-physical properties, thermal conductivity, density, viscosity, specific heat capacity and heat transfer coefficient will be studied upon. The flow of the nanofluid will be of turbulent fully developed type in a circular and square tube. All the nanofluids were prepared without adding surfactant but was put through sonication process. No sedimentation was observed.

The experimental data for all the prepared nanofluids have shown significant enhancement in thermal conductivity and heat transfer coefficient in comparison to the corresponding IV base fluid the water data. In this investigation, some improved empirical correlations were proposed based on the experimental data for evaluation of the Nusselt number and friction factor.

Keywords: Heat exchanger, Nanofluids, Heat transfer Coefficient, Nusselt number, Pressure Drop, Thermo-physical

ABSTRAK

Penciptaan penukar haba boleh dianggap sebagai penemuan masa yang paling penting. Penukar haba adalah peralatan penting dengan pelbagai aplikasi perindustrian seperti loji kuasa, industri HVAC dan industri kimia. Pelbagai cecair yang digunakan sebagai cecair kerja di penukar haba. Cecair ini adalah air, minyak, dan etilena glikol adalah sebahagian daripada cecair kerja yang biasa digunakan.

Penambahbaikan kecil dalam prinsip kerja penukar haba boleh menghasilkan hasil yang lebih besar pada kos yang lebih rendah. Idea ini sentiasa menjadi penyelidik yang berminat. Oleh itu, para penyelidik telah menjalankan pelbagai kajian dan penyiasatan untuk meningkatkan penukar haba dari sudut pandangan material atau haba. Dari segi pemindahan haba, mereka mendapati bahawa cecair kerja konvensional mempunyai kekonduksian terma dan sifat yang agak rendah. Terdapat percubaan untuk mencipta campuran zarah pepejal yang digantung. Ciptaan ini menghadapi beberapa kemunduran di mana penurunan tekanan telah dikompromikan, pemendapan terjadi atau bahkan hakisan, mengakibatkan kos penyelenggaraan yang lebih tinggi.

Seorang penyelidik kumpulan menemui satu kelas cairan penggantungan koloid baru yang memenuhi semua permintaan dan ciri-ciri penukar haba. Campuran penggantungan koloid novel ini kemudiannya ditangani sebagai "nanofluid".

Dalam kajian ini, nanofluid graphene nanopluelet asid fenolik akan disintesis. Ciri-ciri haba fizikal, kekonduksian terma, ketumpatan, kelikatan, kapasiti haba tertentu dan pekali pemindahan haba akan dikaji. Aliran nanofluid akan menjadi jenis yang sepenuhnya dibangunkan bergelombang dalam tabung pekeliling dan persegi. Semua nanofluid disediakan tanpa menambah surfaktan tetapi diletakkan melalui proses sonication. Tiada pemendapan yang diamati.

Data eksperimen untuk semua nanofluid yang telah disediakan telah menunjukkan peningkatan ketara dalam kekonduksian terma dan pekali pemindahan haba berbanding dengan pangkalan data IV yang sama mencairkan data air. Dalam penyiasatan ini, beberapa korelasi empirikal yang lebih baik dicadangkan berdasarkan data eksperimen untuk penilaian nombor Nusselt dan faktor geseran.

Keywords: Heat exchanger, Nanofluids, Heat transfer Coefficient, Nusselt number, Pressure Drop, Thermo-physical

ACKNOWLEDGEMENTS

First and foremost, I would like to express my gratitude to my supervisor Prof. DR.Kazi Md. Salim Newaz for allotting me the title for my research project. His guidance and inputs throughout the project enabled me to complete the research successfully and also in time. In addition, I would like to also thank Dr. Oon Cheen Sean, Postdoctoral Research Fellow for guiding me throughout the research project cycle. His valuable feedbacks, encouragement and teaching had enabled me to complete the thesis in a commendable manner.

Futhermore, I would like to also extend my gratitude to my family members especially my parents for believing and inspiring me throughout my life. They have been my pillar of support throughout these years. Without their unconditional support, this journey would not have been a successful one. I would like further thank my friend, Mr. Sivanesh Kumar, for his assistance and feedbacks throughout the projects. I truly acknowledge his assistance as it was an opportunity to share knowledge and ideas for betterment.

Last but not least, I would like to thank University of Malaya for providing me the place and opportunity to conduct my research project without any inference. Without the proper tools and set up, I would not have been possible to for this experimental test to be carried out.

TABLE OF CONTENTS

LIST OF FIGURES

LIST OF TABLES

LIST OF SYMBOLS AND ABBREVIATIONS

For examples:

DPT	:	Differential Pressure Transmitter
GNP	:	Graphene Nanopletelet
h	:	Heat transfer coefficient, W/m2 K
k	:	Thermal conductivity, W/m K
Nu	:	Nusselt number
q	:	Heat flux, W/m^2

CHAPTER 1: INTRODUCTION

1.1 Background

Flow of fluid in an enclosed channel or tubular structure is governed by various concepts of physics such as fluid mechanics and fluid dynamics. It is essential to analyse the pipe flow as it is an important aspect of engineering application. Over the years various study is being conducted on heat transfer devices, working fluid and surfaces. Cost and space constraints have led to huge effort to develop an efficient heat exchanger.

The efficiency is highly dependent on the type of fluid and the nature of flow in the pipe. Working fluid flowing in the heat exchanger pipes are known to be in turbulent flow condition in nature. Besides that, the overall performance of the heat exchanger can be improved by enhancing the rate of heat transfer in the heat exchanger. Heat transfer coefficient which reflects on the rate of convective heat loss or gain of a fluid moving in a solid is studied.

1.2 Objective of Study

1. To investigate the conduit geometry effect on the heat transfer.
2. Experiment and study the effect of phenolic acid treated GNP concentration to the heat transfer profile.
3. To study the thermos-physical properties of phenolic acid treated GNP
4. Conduct simulation and investigate the effect of phenolic acid treated GNP's concentration to the heat transfer.

1.3 Problem statement

Since the invention of heat exchanger, working fluids such as water, ethyl glycol, oil and many others are used. Unfortunately, these working fluids have a very low thermal properties. Hence, in order to compensate for the low thermal properties, heat exchangers are built in larger scale. By fabricating in a large scale, the coils or pipes will be able to contain more working fluids.

But there is a problem in the form of cost. Fabrication of a large scale heat exchanger is not very much practical to the amount of cost involved as more material is needed. Besides that, assembling and dismantling it would require large amount of manpower. Hence, it was essential to devise an alternative for this problem

Nanofluid is has a much improved thermal charateristics in comparison to the conventional working fluids. This higher much better thermal properties enables the possibility of fabricating a much smaller heat exchanger with better efficiency. Off lately, various research is being conducted to fully utilize nanofluid in heat exchangers as it is not being addressed as an alternative to a decade long problem.

This study would further investigate experimentally and in terms of simulation on the feasibility of using Phenolic acid treated Graphene in heat exchangers.

1.4 Heat Exchanger

Heat exchangers work by transferring heat from a primary fluid to secondary fluid. This fluids do not mix with each other or even come in contact with each other. Conventional example of heat exchangers is that in internal combustion engine. The heat generated by the engine is eliminated by the constantly running coolant fluid around the engine block. Similar principle applies to heat exchangers in power plants. Power plants generated huge amount heat energy which is wastefully emitted into the atmosphere.

Instead, this fluids containing heat is channeled through heat recovery coils. The harvested heat energy is used to pre-heat water which in turn reduces to consumption of fossil fuel. In industries, most commonly used heat exchangers are shell and tube type. Figure 1.1 shows shell and tube type heat exchanger.

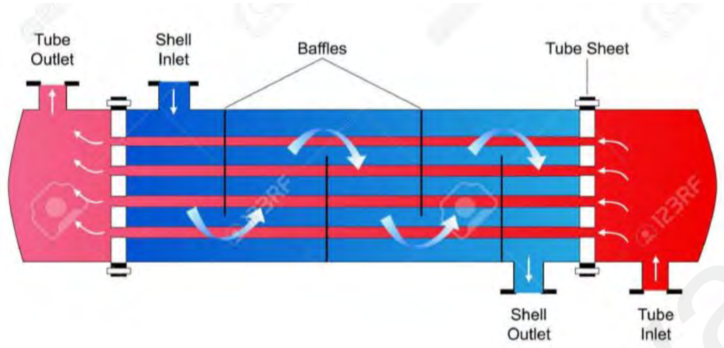

Figure 1.1: Shell and tube type heat exchanger

Heat exchanger considers one of the most common types of exchangers widely used in the industrial processes (Mirzaei, Hajabdollahi, & Fadakar, 2017). Heat transfer rate is highly dependent on various factors such as geometry, working fluid, working pressure, feed water temperature and more (Liu et al., 2016).

1.5 Working Fluid

In real application, numerous working fluids are used in heat exchangers. These working fluids are dependent on the nature of use of the heat exchangers. Most commonly used fluids are oil, water, ethylene glycol and oil. These working fluids inhibit very low thermal conductivity in comparison to solids.

Advancement in nanotechnology have enabled introduction of new age fluid known as nanofluid. Owing to increasing demand, numerous researchers have conducted numerical and experimental research to study the feasibility of nanofluid usage for heat transfer applications. Studies on improving the thermal conductivity of liquids by adding solid started off decades ago. Initially all the studies were conducted with relatively large sized particles (micrometer or milimeter sized). This limited the applicability of the nanofluids due to clogging and abrasion being major drawbacks.

Growth of technology facilitated the possiblity to produce nanoparticles of size lesser than 100nm whereby the nanoparticle dispersed and suspended stably in a colloidal suspension of base fluid. The fluid in general have a high magnitude of thermal conductivity in comparison to base liquid (Kumar, Singh, Redhewal, & Bhandari, 2015). Figure 1.1 below shows difference between stable and unstable colloidal suspension.

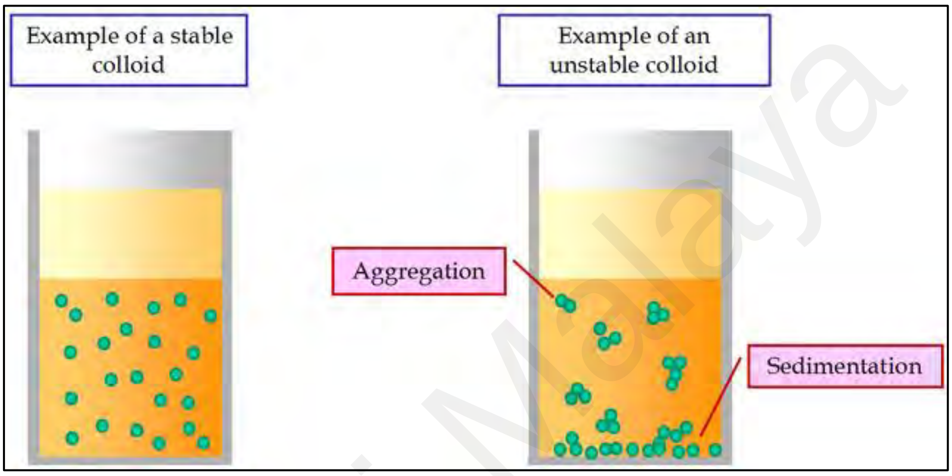

Figure 1.2: Difference between stable and unstable colloidal suspension

With regards to studies conducted by various other researchers, nanofluids have been found to possess enhanced thermophysical properties such as thermal conductivity, thermal diffusivity, viscosity and convective heat transfer coefficients compared to those of base fluids like oil or water (Wong & De Leon, 2010). In addition, since the ratio of surface to volume is high, the nanoparticles tend to remain suspended in the mixture, reducing erosion and clogging.

1.6 Simulation

Computational Fluid Dynamics (CFD) serves as a benchmark for comparison with experimental and numerical study. ANSYS Fluent is used to perform the numerical analysis by developing a mathematical model. This mathematical model was a direct representation of the rig on which the experimental study was done. The data output from the simulation is compared graphically against experimental. The thermal-physical properties of the working fluids are were calculated based on analytical formulas.

1.7 Experimental

Experimental study of pipe flow was conducted on a rig set up in University Malaya CFD lab. The working fluid used in the experimental testing was functionalized Graphene nanoparticles in Gallic acid base liquid. Two different geometries being circular and square was study on to investigate the rate of heat transfer from the solid structure wall to the nanofluid. The surface of the tubular and square pipes were subjected to heat flux from thermal conductors.

For the purpose of this thesis, graphene nanoplatelet (GNP) based nanofluids are used as working fluid to study the suitability of the nanofluids to replace conventionally used working fluids in day to day application (Hosseini et al., 2018). The nanofluids for this study are functionalized with gallic acid and multiple concentrations are prepared. Figure below shows different types of graphene nanoparticles after 10minutes of sonification process (Dul et al., 2017).

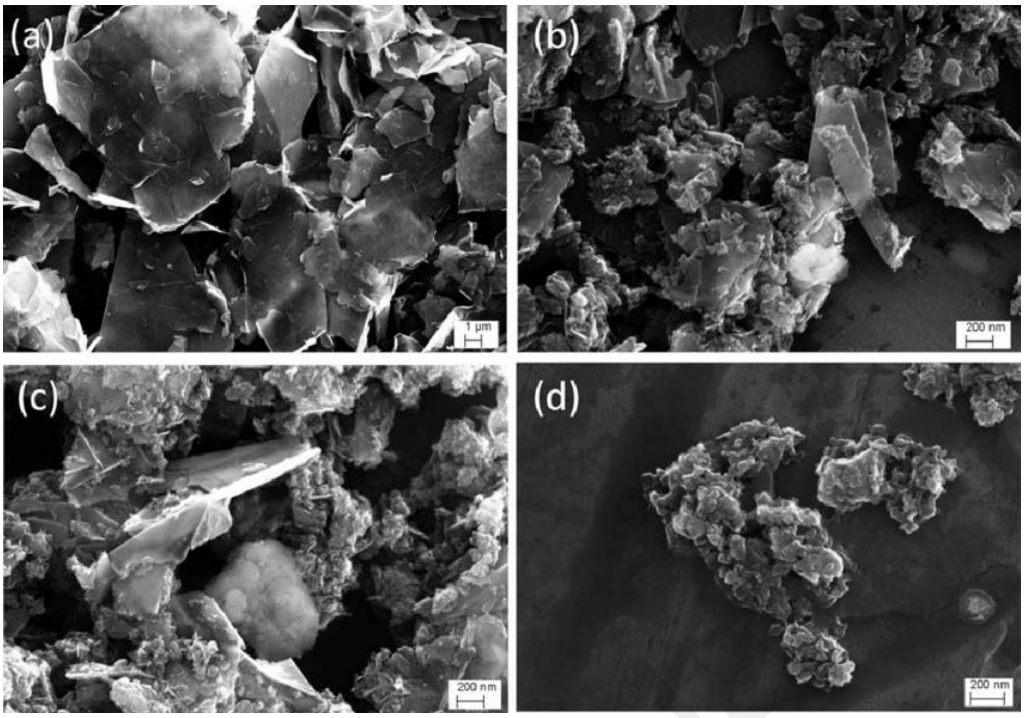

Figure 1.3: SEM images of graphene nanoplatelets after 10 minutes of sonification

CHAPTER 2: LITERATURE REVIEW

Previous works and finding of researchers in relation to study of this thesis will further be acknowledged and cited in this chapter. The findings from previous works are taken into consideration in conducting the experimental and simulation runs.

2.1 Nanofluids

Various studies on nanoparticles have been conducted by researchers in making nanofluids. Copper Oxide (CuO), Aluminium Oxide (Al_2O_3) and Zinc Oxide (ZiO) are some of the prominently used nanoparticles in producing nanofluids in comparison to other types of metal oxides (Khoshvaght-Aliabadi, 2014; Yarmand, Gharehkhani, Kazi, Sadeghinezhad, & Safaei, 2014). In addition to that, carbon based nanofluids such as graphene (GNP) and carbon nanotube (CNT) were largely experimented by researchers (Sabiha, Saidur, Hassani, Said, & Mekhilef, 2015).

Ever since 2004, time frame on which Novoselov et al discovered graphene as a carbon of single layer 2-dimensional lattice, numerous extraordinary thermo-physical and mechanical properties have been identified (Novoselov et al., 2004; Yu, Xie, & Bao, 2009). Graphene nanoplatelets (GNP) are 2-dimensional honey comb lattice structures. The structure is highly dense with multiple layers of graphene crystalline lattice. Figure 2.1 is representation of the lattice structure.

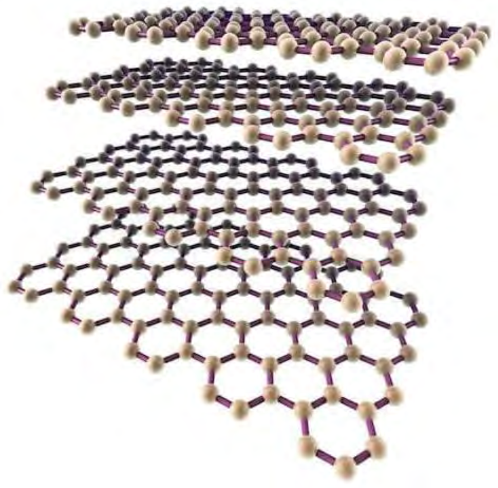

Figure 2.1: Individual graphene sheets stacked together (Side view)

It is highly important to produce nanoplatelets that are evenly dispersed in the lattice. Dispersion is essential because uneven rate of dispersion of the graphene nanoparticles would indeed compromise the overall stability and properties of the structure. Hence, with regards to developing commendable nanoplatelets, functionalization technique is practiced.

Functionalization is process of acid treatment and amino function whereby the graphite is functionalized with oxygen containing functional group. In addition proper sonification or addition of surfactants would be able to produce crystalline lattice with well dispersed graphene nanoparticles (Georgakilas et al., 2012; Le, Du, & Pang, 2014; Sridhar, Jeon, & Oh, 2010).

2.2 Nanofluid preparation

Preparation of nanofluid is the first step in conducting a study or in any applications. Preparation of nanofluid is an intricate process whereby it has to be carefully prepared in order to not tamper with the thermos-physical properties which may eventually affect the final outcome of the testing. Researchers around the world conducting study on nanofluid has indicated two different approaches to prepare nanofluid, namely, one step and two step method.

2.2.1 One step method

Eastman et al. introduced the physical vapor condensation one step method to produce nanofluids in an effort to reduce accumulation of nanoparticles (Eastman, U. S. Choi, Li, Yu, & J. Thompson, 2001). This method eliminates the act of drying, dispersing and storage of nanoparticles. It only involves the process of synthesizing and simultaneously the particles is dispersed in the fluid. The upside of this method is that, the overall stability of the nanofluid will be increased (Y. Li, Zhou, Tung, Schneider, & Xi, 2009). Via this process, it is possible to develop a stable fully suspended nanoparticle and that is fully dispersed in the base fluid. Figure 2.2 shows schematic of one step method.

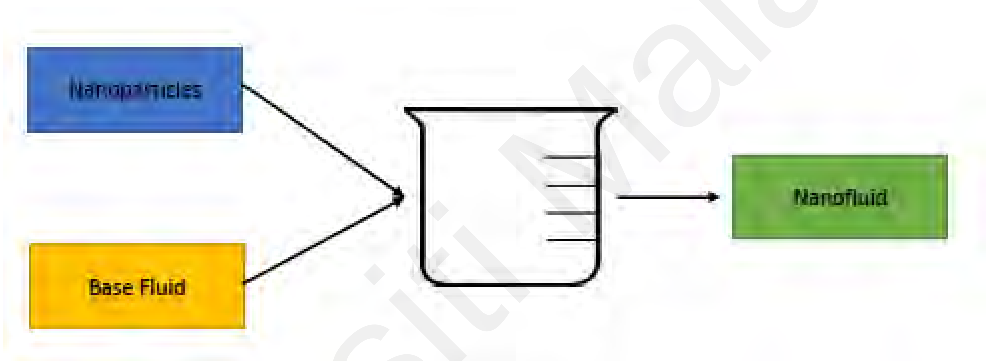

Figure 2.2: One Step Method

One step physical method is has its disadvantages of not being able to me utilized to synthesis nanofluid in a big scale. In addition, the cost of synthesizing is relatively expensive too. Hence, one step chemical method is rapidly developing for various implementations. Besides that, another disadvantage of one step method is that due to incomplete reaction or stabilization, the residual of the reactants remains in the nanoparticles. Due to the presence of impurities, effect analysis of nanoparticle would indeed be hindered.

2.2.2 Two step method

Most commonly practiced method in nanofluid preparation is the two-step method. In this method, the nanoparticles are first produced in the form of dry powder. This is either done chemically or physically. Secondly, the dry powder is mixed in a base fluid and it would be dispersed in the fluid through physical actions such as ultrasonication, intense magnetic agitation, and more.

In comparison to the one step method, the two step method is very much economic to produce nanoparticles in large scale as the processes of synthesizing the nanoparticles have equally advanced. The nanoparticles synthesized from this technique has large surface area which would indeed cause them to aggregate. Hence, to avoid aggregation of the nanoparticles, surfacants is added.

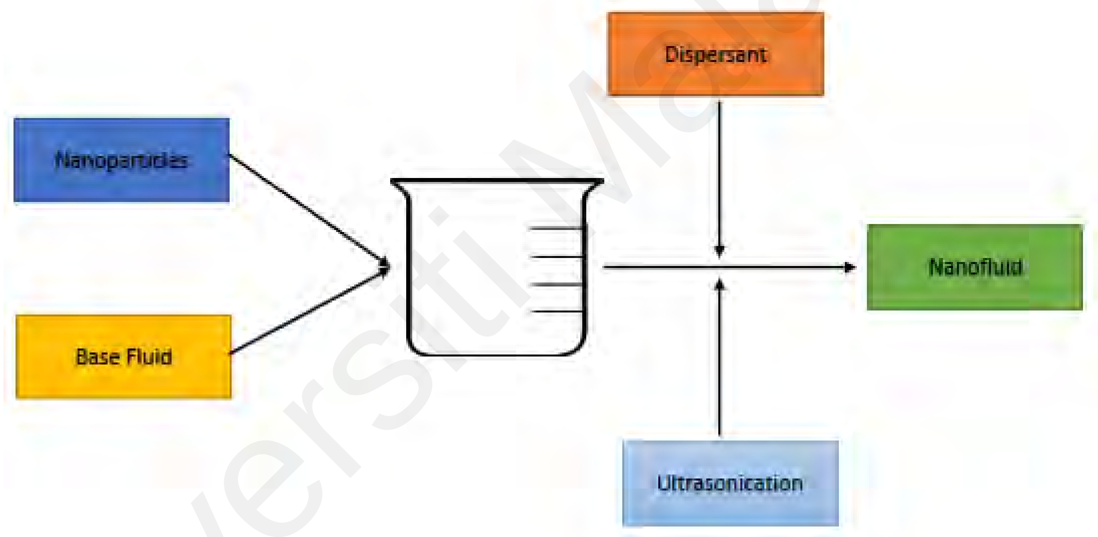

Figure 2.3: Two Step Method

2.3 Nanofluid stability

Due to being in a colloidal suspension, nanofluids are prone to agglomerate. As the nanoparticles have a high surface area to volume ratio, the particles tens to have a remarkable high surface energy. Hence to minimize it's the energy, particles tend to agglomerate. Strong Van der Waals forces between the particles is the driving factor uncontrolled agglomeration.

With that said, it is essential to ensure the nanofluid is in stable state to minimize decreasing suspension properties such as thermal conductivity, increase in specific heat and viscosity (Ghadimi, Saidur, & Metselaar, 2011). The stability of nanofluid is commonly evaluation based on several methods of analysis namely zeta potential analysis, sedimentation method, centrifugation method and spectral analysis method (Mukherjee & Paria, 2013). On the other hand, the stability of the nanofluid may also be enhanced to further minimize agglomeration.

Various studies have been conducted in an effort to increase the stability of nanofluid either via physical or chemical treatment. Some of the recommended methods are addition of surfactant, nanoparticle surface modification, pH control and ultrasonic vibration (Ghadimi et al., 2011). Either all of the listed methods or selected methods may be incorporated into the study to determine the stability properties of corresponding nanofluids (Pantzali, Kanaris, Antoniadis, Mouza, & Paras, 2009).

2.3.1 Ultrasonic vibration

The mixture of phenolic acid treated GNP in distilled water is put through sonification process. Probe sonication process was implemented whereby a sonicator probe is inserted in the mixture of nanoparticle in base fluid. G.Narendar et al. implemented similar technique to prepared the nanofluid colloidal suspension (Narendar, Gupta, Krishnaiah, & Satyanarayana, 2017). R.Gangadevi et al. sonicated the synthesized CuO and Al_2O_3 in distilled water. The mixure was sonicated for 4 hours and it was then stirrer on a magnetic stirrer (Gangadevi, Vinayagam, & Senthilraja, 2018).

Energy emitted from the probe sonicator is transmitted throughout the nanofluid mixture. This ensures that the nanoparticle agglomeration is fully dispersed and homogenized.

2.3.2 Chemical treatment to nanoparticle

Despite various studies conducted to study the practical and basic nanofluid importance, research investigation on the influence of pH control on the thermal conductivity. Off lately, the surface chemical effects is considered to be one of the contributing factors to the thermal conductivity of nanofluids (X. Li, Zhu, & Wang, 2007).

Stability of the nanoparticles in the base fluid is relatable to the electrokinetic properties. Electrokinetic phenomena refers to the flow created in the channel accommodating fluid flow. A well dispersed nanofluid of strong repulsive force can be obtained with high surface charge density (X. Li et al., 2007). As functional hydroxyl group is added to the nanoparticles, a stable colloidal suspension fluid is able to be synthesized. This is due to the alteration in the hrdophobic and hydrophilic nature of the surface (Xie, Lee, Youn, & Choi, 2003).

2.3.3 Surfactant addition

Due to the nature of nanoparticle settling down in an aqueous solution, surfactant can be added to prevent this occurrence. Surfactants act to slow down the deposition or accumulation of nanoparticles in the emulsion. It improves the stability of the nanofluid by further dispersing the nanoparticle in the aqueous solution. Surfactants can also be addressed as dispersants. Easy and economic method to enhance stability of nanofluids is adding dispersants in two phase system.

Experimental outcome of the study conducted by Hao Peng et al. is that the presence of surfactant enhance the heat transfer in the nanofluid in most of the cases but the heat transfer suffers a significant impact whereby the performance deteriorates with at high surfactant concentration (Peng, Ding, & Hu, 2011). Besides that, I was also proved that an adequate amount of surfactant need to added to nanofluid to provide necessary coating that aids to overcome repulsive forces (Jiang, Gao, & Sun, 2003).

Unfortunately, there are disadvantages in adding surfactant to the nanofluid solution. Since surfactants are to be classified as catalyst, these catalyst have limitations in terms of temperature. The functionality of the surfactants are commonly limited at 60 ºC. Working fluid beyond this temperature would denature or result in the bonding between the nanoparticles to weaken, promoting agglomeration (Assael, Metaxa, Arvanitidis, Christofilos, & Lioutas, 2005; Wang & Mujumdar, 2008).

Currently there is no proper or verified process to select the appropriate surfactant at a sufficient amount. As selecting the most efficient and suitable surfactant is important, hence, widely used surfactants may be taken into consideration as a standard practice. Some of the popular surfactants are cetyltrimethylammoniumbromide (CTAB) (Assael et al., 2005; Pantzali et al., 2009), salt and oleic acid (Hwang et al., 2008), Polyvinylpyrrolidone (PVP) (Zhu et al., 2007) and many more.

2.4 Thermo-physical properties

Heat transfer is closely related to the thermos-physical properties of nanofluids as these are the deciding factors of the efficient and suitability of a particular nanofluid to be used on real world operations such as heat exchanger. Thermal conductivity, viscosity, specific heat capacity and density. These parameters are to be discussed with regards to available studies that has been conducted by researchers previously.

2.4.1 Viscosity of nanofluids

In comparison to common working fluids, nanofluids have a relatively higher viscosity. Hence, it is important to measure the viscosity of the nanofluids to study the heat transfer capacity and suitability.

2.4.1.1 Effects of temperature

In real world application, nanofluids would constantly be subjected to numerous temperature conditions. As a result, to meet this non-constant environment, it is essential to develop and ensure that the novel solution is capable of satisfying the needs and demands. In a study conducted, on a viscostity of silver nanoparticles in distilled water at a temperature range of 50 ºC to 90 ºC, it was concluded that there is 45% improvement in terms of heat transfer. The volumetric concentration of the solution was 0.9% (Godson, Raja, Lal, & Wongwises, 2010). In addition to that, Wongwises and Duang concluded that for viscosity of TiO_2 nanoparticle in water, there is up to 15% heat transfer enhancement for volumetric concentration of 0.2% to 2%. The study was conducted at a temperature range of 15 ºC - 35 ºC (Duangthongsuk & Wongwises, 2009).

2.4.1.2 Effects of base fluid

Water, ethylene glycol or base fluid in a mixture of water and ethylene glycol is commonly used to synthesize nanofluids. The viscosity of the base fluid is an important factor in heat transfer of the particular nanofluid. L.Chen investigated the viscosity relationship with base fluid y using water, glycerol, silicon oil and ethylene glycol as base fluid. It was then concluded that silicon oil and water based nanofluid inhibit much better heat transfer rate. At volume fraction of less than 0.4%, the nanofluids were found to be having lower viscosity compared to its base fluid due to its lubricative effect of nanoparticles. It was also found that at volume fraction higher than 0.4%, the viscosity increases due to increase in nanoparticles in the aqueous solution. Ethylene glycol and glycerol based nanofluids found to have reduced viscosity enhancement at temperature higher than 55ºC (L. Chen, Xie, Li, & Yu, 2008)

In a considerably similar investigation, it was concluded that TiO_2 in water has 23% viscosity improvement at 1.86% volumetric concentration and TiO_2 in EG nanofluid solution had 11% enhancement at 1.2% volumetric concentration (H. Chen, Ding, He, & Tan, 2007). Meanwhile, in separate study with base fluids of 20:80%, 60:40% and 40:60% water and EG solution, a significantly high improvement was concluded in 60:40% nanofluid in comparison to other solutions (Syam Sundar, Venkata Ramana, Singh, & De Sousa, 2012).

2.4.1.3 Effects of nanoparticle geometry and size

Subjected to temperature range of 22 °C to 75 °C and particle size of between 1% and 9.4%, effects due to particle size was studied and it was concluded that the viscosity is highly dependent on the particle volume fraction. The dynamic viscosity increases when the particle size was increased and vice versa (Nguyen et al., 2007).

Timofeeva et al. argued that the viscosity of nanofluid is highly dependent on the it was shown that a higher result was exhibited for elongated particles such as platelets and cylinders in comparison to sphere (Timofeeva et al., 2007). In another study conducted, Chevalier et al. studied the silicon dioxide nanoparticle in ethanol nanofluid at particle geometry of 35, 94 and 190nm. The volume concentration of the solution was at 1.4-7%. They noted that the viscosity increases with reduction in particle size and shape at volume concentration range from 1.4 to 7% and found that viscosity rises with the decrease of particle size (Chevalier, Tillement, & Ayela, 2007).

2.4.2 Nanofluid density

Density properties of a few different types of nanofluids namely antimony-tin oxide, aluminium and zinc oxides were studied. The nanoparticles were in a base fluid of 60:40 EG/W. An Anton-Paar digital meter to measure density was used to monitor the reading (Vajjha, Das, & Mahagaonkar, 2009). The density reading outcome was then compared with a theoretical formulation introduced by Cheremisinoff which was then approved by Pak and Cho through a series of testing. In the tests conducted, the density was evaluated are 25 ºC only for titanium oxide and aluminium oxide nanofluids. The nanofluids were in a concentration of 4.5% (Cheremisinoff, 1986; Pak & Cho, 1998).

Upon comparing the theoretical and analytical results, it was concluded that as the volumetric concentration increases, the nanofluid density increases. This is due to the fact that the particles in the nanofluid possess a higher density in comparison to the base fluid. Besides that, it was also observed that, the density of nanofluid decreases as the temperature decreases (Vajjha et al., 2009). Unfortunately, there are not much study conducted on the density of the nanofluid. Further study shall be conducted to investigate the density properties of nanofluid.

2.4.3 Thermal conductivity

As the terms suggests, thermal conductivity refers to the heat transfer capability of a particular solution or material. This was one of the driving force for researchers to study the effect on thermal conductivity when nanoparticles were added to a base fluid. Thermal conductivity is affected by factors such as volume fraction of particles, temperature, nature of base fluid, type of material of particle and more. In addition, numerous ways have been studied to enhance the thermal conductivity of nanofluids. Following section would enlist the studies conducted by researchers in an effort to enhance the themal conductivity.

2.4.3.1 Enhancement of nanofluid thermal conductivity

All the studies conducted with regards to enhance the thermal conductivity of nanofluid proves that the thermal conductivity does indeed increases with the addition of nanoparticles.

Patel et al. identified up to 21% increase in thermal conductivity of the water based nanofluid with silver nanoparticles at a volumetric concentration of 0.00026%. In addition, gold nanoparticles was used in the study and an enhancement of 7-14% was reported for gold nanoparticle in water based fluid at a volume concentration of 0.011% (Patel et al., 2003).

In another study conducted by Eastman et al, oil and water was used as base fluid with copper oxide and aluminium oxide nanoparticles. For base fluid volume fraction 5% nanoparticles, a 60% enhancement was observed. Besides that, they also concluded that one step method yields a better enhancement data than two step method (Eastman, S. Choi, Li, J. Thompson, & Lee, 1996).

2.5 Numerical Analysis

Studies were conducted to study the heat transfer in backward step flow. The numerical study was conducted on ANSYS FLUENT platform which enables creation and simulation based on a mathematical model (Oon et al., 2018). Previously a studied was conducted to determine the thermal properties of nanofluid in annular passage (Oon, Togun, Kazi, Badarudin, & Sadeghinezhad, 2013). In addition, laminar flow in a passage was also studied previously by Al-Aswadi et. al (Al-aswadi, Mohammed, Shuaib, & Campo, 2010)

CHAPTER 3: METHODOLOGY

Any study would require complete experimental set-up before the particular is started off. There are some procedures that need to be followed to ensure the experimental run yields a desired output. Set-up for this study is done as per standard procedures as advised. Overall methodology of the test would be thoroughly explained in the following sections.

3.1 Preparation of nanofluid

Graphene nanoplatelets used in this study was obtained from BT Science Sdn. Bhd. The nanaplatelets are of width 2µm, specific surface area of $750m^2/g$ and purity 99.5%. Hydrogen peroxide (30%) was obtained from Sigma-Aldrich. Lastly, phenolic acid was procured from BT Science Sdn. Bhd.

Two step method was utilized to prepare the Phenolic acid treated GNP. Gallic acid served as additive and distilled water was the base liquid in the preparation. Hydrogen peroxide (H_2O_2) was a reducing agent and heat was added as a thermal initiator to catalyse the reaction. H_2O_2 was used as it does not produce toxic waste deeming it as environmental friendly.

5 gram of GNP nanoparticles, 15 gram phenolic acid was poured into a beaker filled with 1000 ml of distilled water. The beaker was placed in a hot plate stirrer and left for 20 minutes. Upon the mixture attaining uniform black suspension, 35 ml of concentrated hydrogen peroxide was poured into the solution and stirred. The mixture was then sonicated in the probe-sonicator in order for the nanoparticles to disperse completely in the distilled water.

Following this, the functionalized was then centrifuged to segregate the denser nanoparticles. It was also washed multiple times until the pH value turns neutral. Finally the funtionalized GNP is dried overnight in the oven at 50°C. The phenolic acid GNP's were prepared in a concentration of 0.1%, 0.05% and 0.0025%. Figure below shows the flow of phenolic acid functionalized GNP (Sadri et al., 2017).

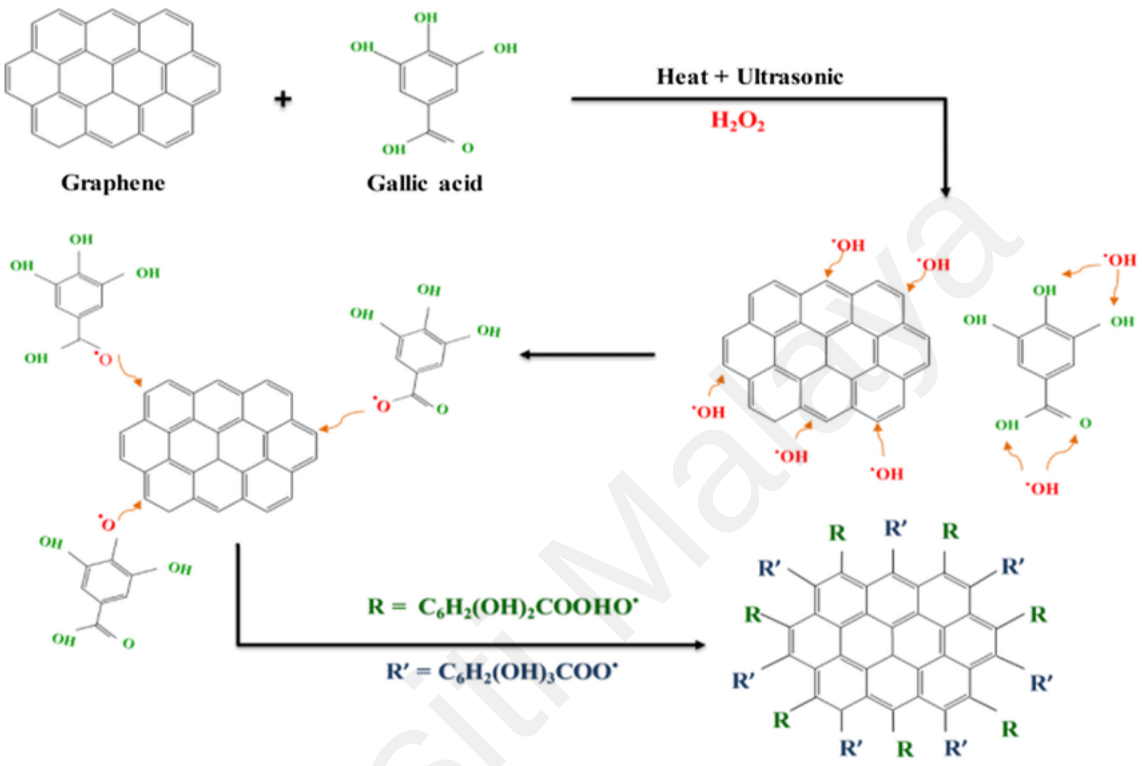

Figure 3.1: Phenolic Acid functionalized GNP molecular breakdown

3.2 Experimental Set Up

Rig for the experiment was set up in University Malaya CFD Lab. The rig consists of multiple mechanical and electronical parts for data observation and collection. Figure 3.1 is the schematic representation of experimental set up for the thesis. The set-up includes heater, flow loop connections, chiller for cooling purpose and data logger for collection of data. Figure 3.2 is the photograph of the rig set up in the lab on which the study was conducted.

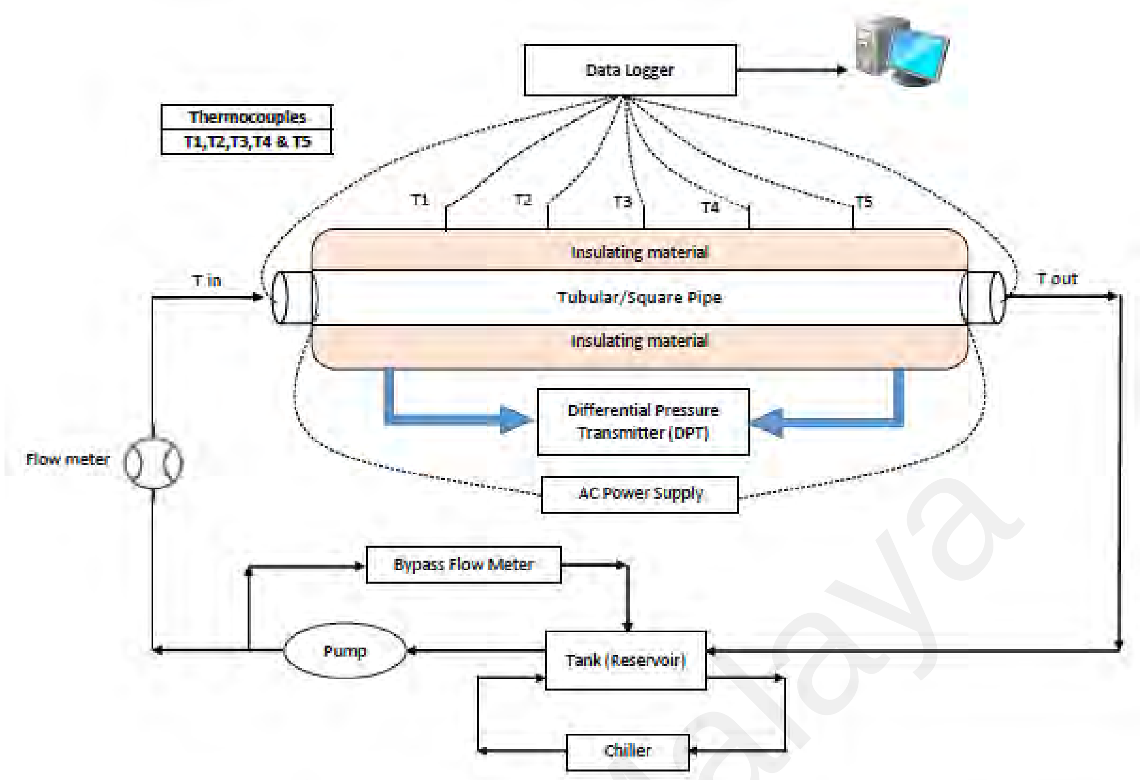

Figure 3.2: Schematic representation of experimental set up rig

Figure 3.3: Photograph of the rig used to conduct the experiment

Flow loop of the rig has a set up consisting of reservoir, chiller, pump and flow rate meter. The reservoir or commonly referred to as tank houses the nanofluids during experimental runs. A mechanical stirrer is fitted into the tank to maintain a constant movement throughout the fluid in order to avoid nanoparticles from settling down. The stirrer was set at fixed revolution of 600 rpm. The reservoir has a total tank capacity of 14 litres. In the study, only 6 litres of either distilled water or nanofluid is used

On the other hand, the chiller is connected to the system to imitate the operating principle of heat exchanger. The chiller temperature was set at 18˚C throughout the test. As the nanofluids absorb heat from the surface of the circular or square pipe, the absorbed heat has to be removed in order to prevent overheating of the system. Besides that, the chiller helps to create a steady state condition to avoid fluctuation of temperature data. Meanwhile, the pump is one of the most crucial elements whereby it helps to pump the working fluid throughout the pipeline to be circulated through the test section and then be discharged back to the reservoir.

Differential Pressure Transducer (DPT) is fitted to the rig on opposite ends to study the pressure drop across the circular and square test sections. A digital meter is connected to the transducer to indicate the pressure drop across the tubes. DPT was essential in determining the friction factor of the nanofluids.

As indicated in the Figure 3.1, this study was conducted on 2 different channels or tubes. One being cylinder and another being square. The inner and outer diameters of the circular tube is 10 mm and 12.8mm respectively. As of the square section, the inner and outer width of each cross sectional sides are 10mm and 12.8mm respectively. Both the circular and square test sections are of 1.2 metre length.

Entire surface of the test sections are wound with heater. The heater generates constant heat flux on the wall boundary from the power supplied from the main via a transformer. As indicated and shown in both the schematic and photograph, thermocouple is placed on the test sections are different intervals. The purpose of the thermocouple is to record temperature on the wall at particular intervals. The thermocouples are placed at intervals of 0.2 m, 0.4 m, 0.6 m, 0.8 m and 1.0 m from the inlet of the circular and square test channels.

Meanwhile, the inlet temperature and outlet temperature is recorded from thermocouple inserted into the flow stream of nanofluid. All the thermocouples used in on the set-up are T-type thermocouples. These type of thermocouple are sensitive at low temperature, hence satisfying the purpose of the application.

3.2.1 Data logger

Graphtec midi Logger GL220 as shown in Figure 3.4 is used to record the surface temperature of the test channels. All the thermocouples were linked to the logger and the temperature rise and drop were monitored at real time. A total of 10 thermocouples can be connected to the logger as there are 10 input channels available. The logger is capable of recording data at an interval of 10 milliseconds to 1 hour.

As of the flow rate meter, Burkert Electromagnetic Flow Meter is used to continuous monitor and control the flow measurement of the working fluid. In addition, a pressure transducer is fitted onto the test channel at outlet and inlet to facilitate the reading of pressure drop across the rig by the DPT.

Figure 3.4: Graphtec midi Logger GL220

3.2.2 Test channel

The test section on which the experimental runs were conducted on it made out of stainless steel with the dimensions as indicated earlier. Grooves is prepared on the surface of the tube to place the thermocouples and it was ensured that the holes were not hollow to prevent the thermocouple from being in direct contact with fluid flowing in the tube since the aim was to record the surface temperature instead of the fluid temperature. A holder like structure with slot was installed onto the test section. Epoxy was used as adhesive to attach the holder at the points with grooves. Thermocouples were then inserted fully into the slot until it gets in contact with the surface of the test section.

3.3 Nanofluid properties

Thermo-physical properties of colloidal suspension fluid can be altered by dispersing nanoparticles in the base fluid. Numerous studies have been conducted by researchers to improve the thermos-physical properties of suspension fluid. Correlations developed for the suspension fluids can be utilized to compare the experimental and evaluated data of nanofluids. With regards to that, any improvements be it to the nanoparticles or suspension fluid can be made for betterment purposes.

Main aim of study in the field of nanofluids is to obtain a much improved thermal conductivity. Various related studies have been conducted to correlate the experimental and analytical results. This study was further researched by Crosser and Hamilton whereby they studied the effect of size of, volume percentage of nanoparticle and type of nanoparticles base fluid as per equation (1).

$$K_{nf} = \frac{K_{bf}\left[K_p+(n-1)K_{bf}-(n-1)\emptyset_p\left(K_{bf}-K_p\right)\right]}{K_p+(n-1)K_{bf}-\emptyset_p\left(K_{bf}-K_p\right)} \quad (1)$$

whereby, K_{nf} is the nanofluid thermal conductivity, K_p is the nanoparticle thermal conductivity, K_{bf} is the base fluid thermal conductivity and the ratio of thickness of nanolayer to original radius of particle is represented as β. Commonly, a value of 0.1 is selected for β in calculating the thermal conductivity of nanofluids. Experimental value of the shape factor in equation (1) is $n = \frac{3}{\varphi}$ is incorporated whereby Ψ represents the nanoparticles sphericity.

Usually the thermos-physical properties of nanofluid is dependent on the pH, host fluid, size and volumetric concentration values of the nanoparticles. The effective density (ρ_{nf}) of the nanofluid is calculated by applying mass balance of the mixture of host fluid and solid nanoparticles. This can be obtained from equation (2).

$$\rho_{nf} = \left(1-\emptyset_p\right)\rho_{bf} + \emptyset_p\rho_p \quad (2)$$

whereby, $\rho_{bf,}$ ϕ_P and ρ_p, are host fluid density, fractional volume of solid nanoparticles and the density of particles respectively. The formula was further improved by Xuan. Y and W. Roetzel (Xuan & Roetzel, 2000) as per equation (3)

$$C_{p,nf} = \frac{[(1-\emptyset_p)\, \rho_{bf} C_{bf} + \emptyset_p\, \rho_p C_p]}{\rho_{nf}} \quad (3)$$

One of the most important properties of nanofluid is viscosity. Pumping power, pressure drop and heat transfer are highly dependent on it. Sharma, K et al (M Hussein, Sharma, Abu Bakar, & Kadirgama, 2013) has conducted study to identify the properties by taking into account volume portion, diameter of particle and temperature as of equation (4)

$$\mu_{nf} = \left[(1+\varphi_p)^{11.3} \left(1+\frac{T_{nf}}{70}\right)^{-0.038} \left(1+\frac{d_p}{170}\right)^{-0.061} \right] \mu_{bf} \quad (4)$$

Table 3.1 below shows thermos-physical properties of the materials tested in this study with respect to their corresponding concentrations. Correlations listed previously were used to calculate the thermos-physical properties of the nanofluids.

Table 3-1: Thermo-physical properties of working fluids

	Distilled water	**GNP0.025%**	**GNP 0.05%**	**GNP 0.1%**
k (W/m.K)	0.615	0.63	0.65	0.67
µ (Pa. s)	0.00092	0.00093	0.000945	0.00096
ρ (m^3/kg)	996.85	997	997.15	997.3
C_p (J/kg. K)	4099	4032	4014	3810

One of the most important characteristics of nanofluids is calculating the pressure drop across the inlet and outlet of the test channel. Pressure drop aids to determine the pump power requirement as different working fluids have different viscosity. The pressure drop in the test channel is calculated with respect to Fanning friction coefficient (C_f)

$$C_f = \frac{2\tau_s}{\rho V^2} \quad (5)$$

where, sheer stress is indicated as τ_s and V denotes the average velocity. Darcy friction coefficient f can be correlated with Fanning friction coefficient, C_f as shown in equation (6).

$$C_f = \frac{f}{4} \tag{6}$$

In order to calculate the pressure drop in channels, property of friction factor has to be evaluated. This is highly dependent on the Reynolds number and nature of flow, turbulent or laminar. As of laminar flow, the friction factor can be computed as per equation (7).

$$f = \frac{64}{R_e} \tag{7}$$

Experiment for this thesis is carried out in turbulent flow nature. The respective friction factor is calculated from Moody's chart or empirical equations and the roughness of surface is computed from the tables (Yuan, Tao, Li, & Tian, 2016). Theoretical pressure drop is as equation (8).

$$\Delta P = f\left(\frac{L}{D}\right)\frac{\rho V^2}{2} \tag{8}$$

If the Reynold's number of different fluids is kept constant, the velocity of different nanofluids will change with regard to the concentration. This is because, the relationship between Re and V may be altered by density and viscosity as indicated in equation (9)

$$V = \frac{Re\mu}{\rho D} \tag{9}$$

On the other hand, the pressure drop per unit length can be computed by substituting the velocity from equation (9) to equation (8) yielding equation (10)

$$\frac{\Delta P}{L} = \frac{Re^2 f}{2D^3}\ \vartheta.\mu \tag{10}$$

In addition, Pethukov equation (11) can be deployed in the case of turbulent flow to determine the friction factor

$$f = (0.79 lnRe - 1.64)^{-2} \tag{11}$$

The heat transfer coefficient, heat flux and Nusselt number through the ducts computation have been studied by various researchers. Most commonly, the correlations developed relies mainly on the flow type, fluid type and fluid properties. For any fully developed flow in tubular tubes and numerous boundary conditions, Gnielinski equation can be used to calculate the Nusselt number based on equation (12)

$$Nu = \frac{\left(\frac{f}{8}\right)(Re-1000)(Pr)}{1+12.7\sqrt{\frac{f}{8}}\,(Pr^{\frac{2}{3}}-1)}\left[1+\left(\frac{D}{L}\right)^{\frac{2}{3}}\right]k_c \tag{12}$$

where, K_c is taken into consideration as factor. K_c for fluids can be represented as Equation (13)

$$K_c = \left(\frac{Pr}{Pr_s}\right)^{0.11} \tag{13}$$

In the equation (13), Pr can be computed from equation (14). Meanwhile, Pr_s is referred to as Prandtl number at the T_s which is surface temperature.

$$\mathrm{Pr} = \mu\frac{C_p}{K} \tag{14}$$

Furthermore, an experimental correlation to calculate Nusselt number at fully developed flow though the channels was developed by Dittus and Boelter. The respective equation is as the following

$$Nu = 0.023\, Re^{0.8}\, Pr^{n} \tag{15}$$

whereby, n = 0.3 for cool fluid and n = 0.4 for heated fluid.

With regards to equation (12) and (15), in the case of forced convection turbulent flow, Prandtl number and Reynold's number can be taken into consideration as the most important parameters that affect the Nusselt number. In the instance of maintaining Reynold's number at constant value, much bigger impact to the Nusselt number would be implicated by the Prandtl number.

Parameters that could affect the Nusselt number was studied by Xuan.Y and W.Roetzel (Xuan & Roetzel, 2000) and a new generic function that takes into account the factors of influence is included along in the equation (16)

$$Nu_{nf} = f\left[Re, Pr, \frac{K_p}{K_{bf}} \frac{(\rho C_p)_p}{(\rho C_p)_{bf}}\ \emptyset, flow\ geometry, particle\ geometry\right] \tag{16}$$

As show in equation (1), from Newton;s Law of Cooling, the average convective heat transfer coefficient value can be computed from equation (17)

$$h = \frac{NuK}{D} = \frac{q}{T_s - T_b} \tag{17}$$

whereby, heat flux is denoted as q, T_s refers to the inner surface temperature and T_b refers to the flowing fluid's bull temperature. Based on the fluid temperature and temperature of surface at specific locations on the test channel, the local Nusselt number at a specific section of the tube can be evaluated.

In order to calculate the corresponding velocity, the thermos-physical properties of fluid have to be considered upon addition of nanoparticles. Hence, at constant Reynold's number, the velocity of nanofluid can be evaluated as equation (18)

$$V_{nf} = \frac{\rho_{bf}}{\rho_{nf}} \frac{\mu_{nf}}{\mu_{bf}} V_{bf} \tag{18}$$

Whereby, V_{bf} is represented as the base fluid velocity and equation (9) can be used to calculate V_{bf}.

3.4 ANSYS Simulation

Apart from experimental runs, simulation was done on ANSYS Fluent. The simulation is done for both circular and square test sections. Simulation was done for all the GNP concentrations and also for water. The thermos-physical properties for the simulation run was based on data in Table 3.1. Three different nanofluid elements and one distilled water fluid elements was created in ANSYS. Steel was used as the surface material of the test section

As of the circular tube, only top half of the circular tube was drawn and simulated. This is due to the steady state condition of the fluid flow. Figure 3.1 shows the circular tube cross section that was developed on ANSYS platform.

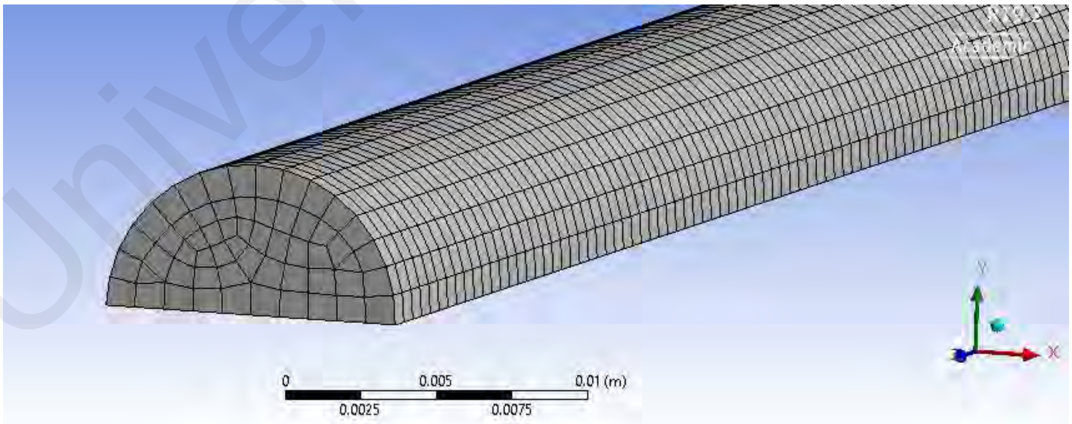

Figure 3.5: Circular tube cross section

Figure 3.6 shows the simulation of square test section developed in the ANSYS Fluent platform. The model was developed as per the rig the study was conducted on.

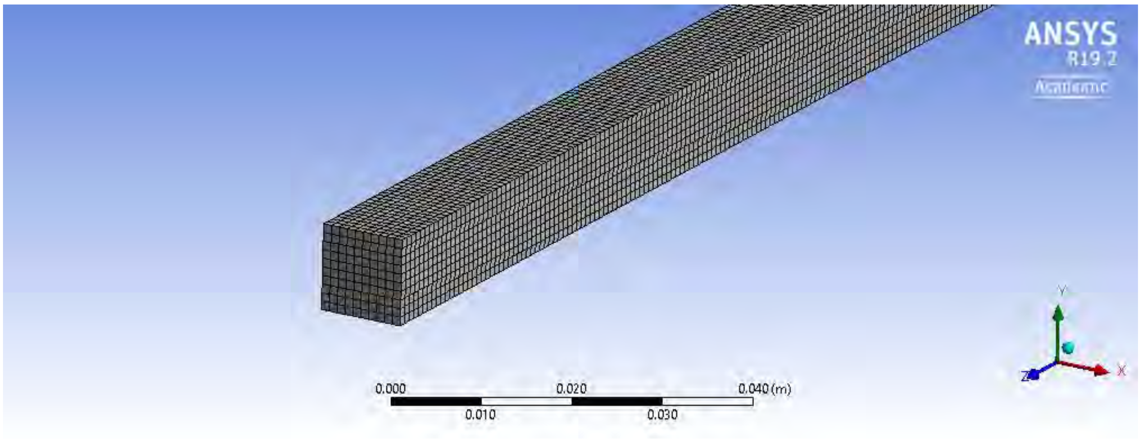

Figure 3.6: Square tube cross section

Both the circular and square cross sections was drawn on the ANSYS Fluent design modeler. The wall, inlet and outlet of the tube was defined to assist data extraction upon computation. The solid models were then meshed with element size of 1 mm. In order to decide on the optimum value of mesh size, mesh independency study was done. The study was conducted by gradually reducing the meshing size until no significant difference was noted in the temperature.

This is then followed by specifying the fluid and solid type. Thermo-physical properties of the fluids were input based on Table 3.1. Boundary conditions were then specified on the wall and inlet. Heat flux on the wall of the test section was calculated based on equation (19) and equation (20) for circular and square test section respectively.

$$\dot{q} = \frac{P}{2\pi r L} \quad (19)$$

$$\dot{q} = \frac{P}{4LD_h} \quad (20)$$

Whereby, $\dot{q}$ is the heat flux supplied by the thermal strip surrounding the test section, P is the power rating of heater, L is the length of test section, r refers to the radius of the circular cross section and D_h indicates the hydraulic diameter of the test section. Inlet velocity was input from the flowrate and the inlet temperature was considered as per the experimental T_{in}.

CHAPTER 4: RESULTS AND DISCUSSION

In this chapter, the outcomes of experimental and simulation run of the study will be discussed thoroughly. Outcome of both the experimental and simulation study will be presented in graphical method to ease comparison study. The concentration of nanofluid studied in the study are 0.0025%, 0.05% and 0.1%. This different concentration of nanofluids are tested on the circular and square test section. Hydraulic diameter of the square tube is similar to that of the circular tube.

4.1 ANSYS Simulation analysis

Test section mathematic model that was design in the ANSYS Fluent platform is used to simulate for analytical data. Mathematical model was developed for both the square and circular. Outcome of the simulation is represented in graphical and tabular form.

4.1.1 Mesh independency study

In order to ensure accuracy of CFD simulation, the meshing of the particular should be taken into serious consideration. The number of nodes and elements are important to suggest on the reliability of a particular element or structure (Kulkarni, Chapman, & Shah, 2016). Hence, as for this study, mesh independency study was done to zero in on the most suitable meshing value. Mesh independency study technically makes the particular reading or data more general as an optimum meshing level it chosen. At this point, the error percentage is relatively negligible. Figure 4.1 shows graph of temperature against distance for mesh independency study.

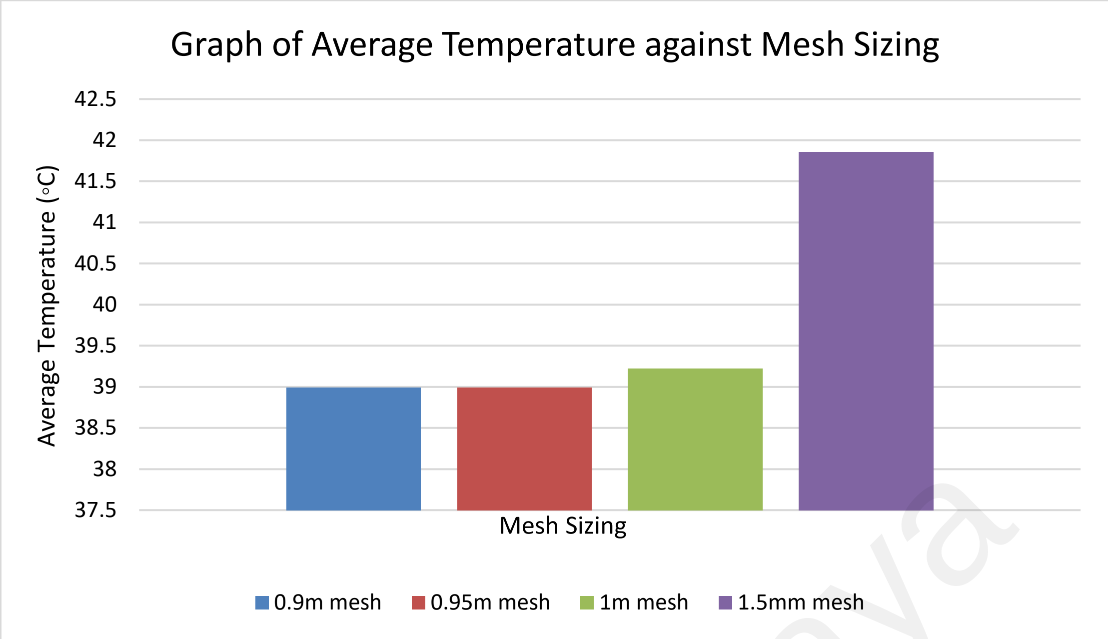

Figure 4.1: Graph of Average temperature against Mesh sizing

From Figure 2.1, it is evident that the accuracy of final output of a simulation decreases as the mesh sizing becomes smaller. For instance, 0.9mm mesh would have the most number of elements in comparison to other mesh sizes. This is because, at lower mesh value, the mathematical model is broken down into more number of nodes. This makes the simulation more accurate as the percentage of error becomes lesser and lesser.

4.1.2 Circular and Square geometry

Both the circular and square geometry have different surface area altogether. This would indeed affect the overall heat transfer process. The temperature, heat transfer coefficient and Nusselt number at local points is discussed further.

4.1.2.1 Circular tube

The following section would discuss the comparison between temperature, heat transfer coefficient and Nusselt number against distance. The data is analysed with respect to the position of the thermocouples. Only graphs of 0.1% GNP and distilled water data will be discussed in this section.

Table 4-1: Table of temperature at local points on test section of distilled water

Temperature (°C)					
Length (m)	**0.2**	**0.4**	**0.6**	**0.8**	**1**
Flow3.5	36.40	36.60	36.85	37.09	37.34
Flow4.5	36.20	36.40	36.65	36.89	37.14
Flow5.5	36.11	36.30	36.51	36.71	36.91
Flow6.5	36.00	36.20	36.42	36.59	36.76
Flow7.5	35.90	36.05	36.25	36.40	36.55
Flow8.5	35.74	35.87	36.00	36.13	36.26

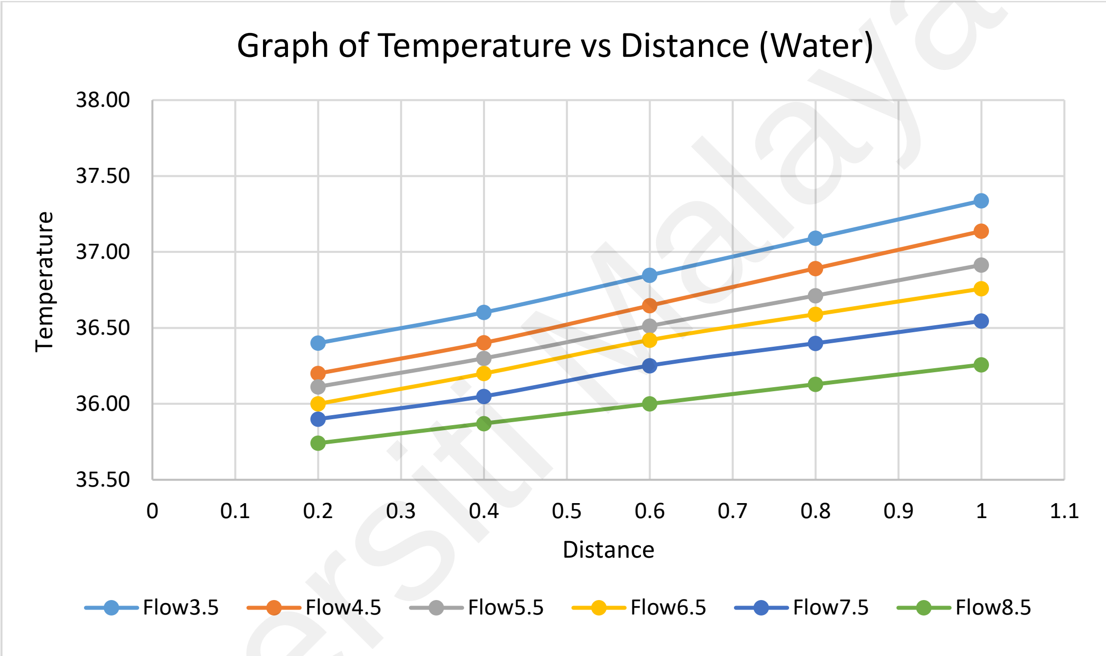

Figure 4.2: Graph of temperature against distance of distilled water

Table 4-2: Table of heat transfer coefficient at local points on test section of distilled water

Heat transfer Coeff (W/m^{2}K)					
Length (m)	**0.2**	**0.4**	**0.6**	**0.8**	**1**
Flow3.5	1269.8533	1243.1390	1212.2089	1182.7805	1154.7471
Flow4.5	1297.4588	1269.5831	1237.3402	1206.6944	1177.5299
Flow5.5	1309.8454	1283.5076	1254.7693	1228.9324	1204.0166
Flow6.5	1326.2912	1297.4588	1267.1572	1244.6945	1223.2651
Flow7.5	1341.1933	1318.9636	1290.1665	1269.9884	1250.5627
Flow8.5	1365.5898	1345.5778	1326.2912	1307.5496	1289.3304

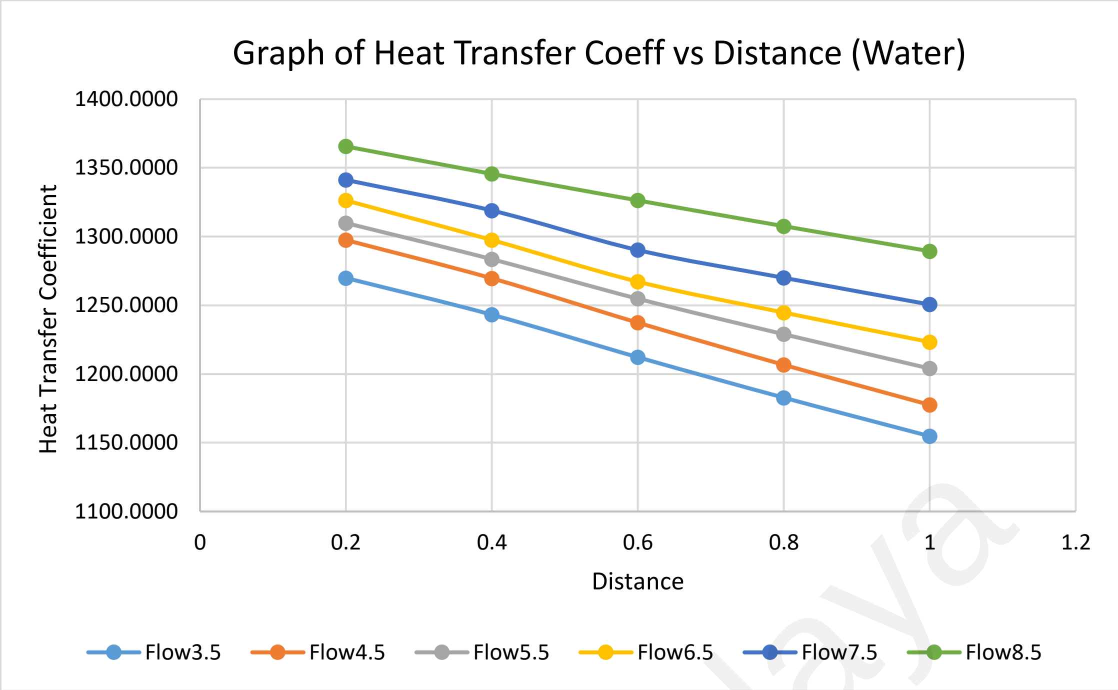

Figure 4.3: Graph of heat transfer coefficient against distance of distilled water

Table 4-3: Table of Nusselt number at local points on test section of distilled water

Nusselt Number					
Length (m)	**0.2**	**0.4**	**0.6**	**0.8**	**1**
Flow3.5	18.9530	18.5543	18.0927	17.6534	17.2350
Flow4.5	19.3651	18.9490	18.4678	18.0104	17.5751
Flow5.5	19.5499	19.1568	18.7279	18.3423	17.9704
Flow6.5	19.7954	19.3651	18.9128	18.5775	18.2577
Flow7.5	20.0178	19.6860	19.2562	18.9551	18.6651
Flow8.5	20.3819	20.0833	19.7954	19.5157	19.2437

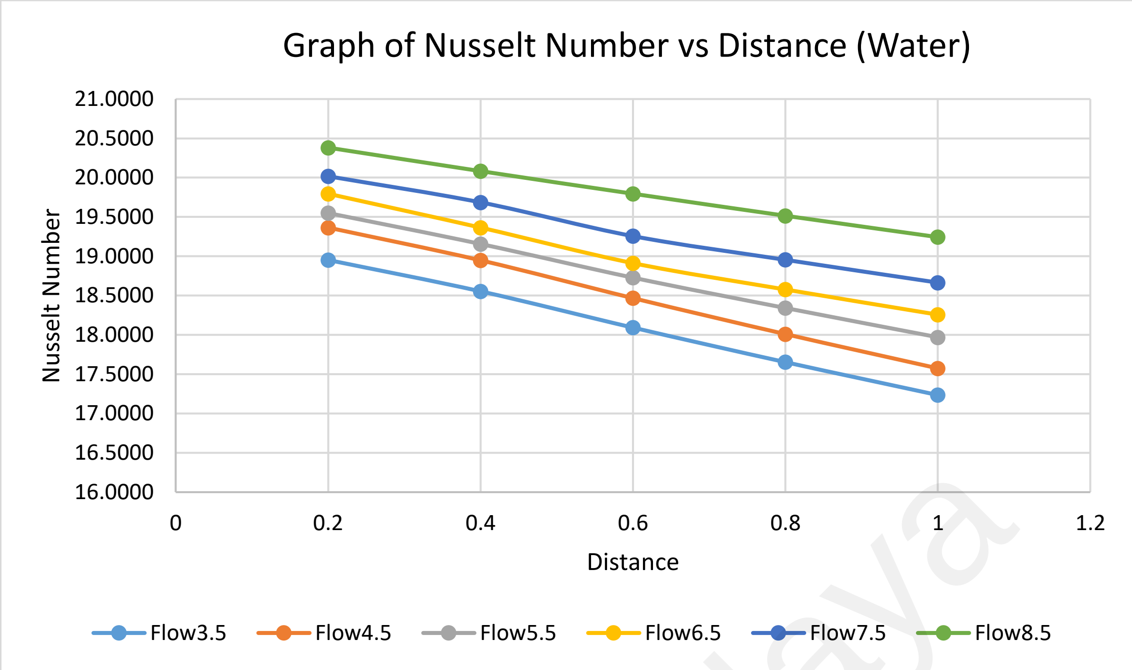

Figure 4.4: Graph of Nusselt number against distance of distilled water

Table 4-4: Table of temperature at local points on test section of 0.1% GNP

Temperature (°C)					
Length (m)	**0.2**	**0.4**	**0.6**	**0.8**	**1**
Flow3.5	37.50	38.20	38.90	39.60	40.30
Flow4.5	37.00	37.60	38.20	38.79	39.39
Flow5.5	36.73	37.15	37.57	37.98	38.40
Flow6.5	36.25	36.70	37.05	37.40	38.00
Flow7.5	36.20	36.47	36.75	37.02	37.30
Flow8.5	36.11	36.20	36.29	36.38	36.48

Table 4-5: Table of heat transfer coefficient at local points on test section of 0.1% GNP

Heat transfer Coeff (W/m2K)					
Length (m)	**0.2**	**0.4**	**0.6**	**0.8**	**1**
Flow3.5	1136.8210	1065.7697	1003.0774	947.3509	897.4903
Flow4.5	1193.3041	1126.0963	1066.0553	1012.0927	963.3299
Flow5.5	1226.4071	1176.0217	1129.6130	1086.7280	1046.9802
Flow6.5	1290.4455	1230.5795	1187.7235	1147.7520	1085.1473
Flow7.5	1297.4588	1259.9346	1224.5200	1191.0418	1159.3454
Flow8.5	1310.5644	1297.4588	1284.6126	1272.0184	1259.6687

Table 4-6: Table of Nusselt number at local points on test section of 0.1% GNP

Nusselt Number					
Length (m)	**0.2**	**0.4**	**0.6**	**0.8**	**1**
Flow3.5	16.9675	15.9070	14.9713	14.1396	13.3954
Flow4.5	17.8105	16.8074	15.9113	15.1059	14.3781
Flow5.5	18.3046	17.5526	16.8599	16.2198	15.6266
Flow6.5	19.2604	18.3669	17.7272	17.1306	16.1962
Flow7.5	19.3651	18.8050	18.2764	17.7767	17.3037
Flow8.5	19.5607	19.3651	19.1733	18.9853	18.8010

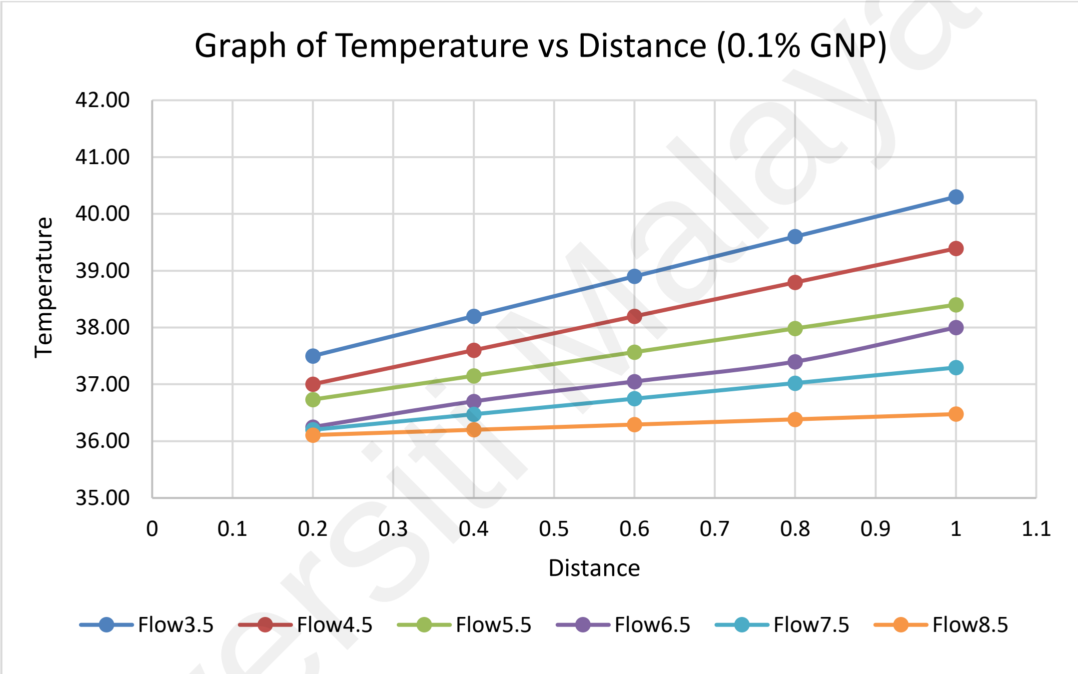

Figure 4.5: Graph of temperature against distance of 0.1% GNP

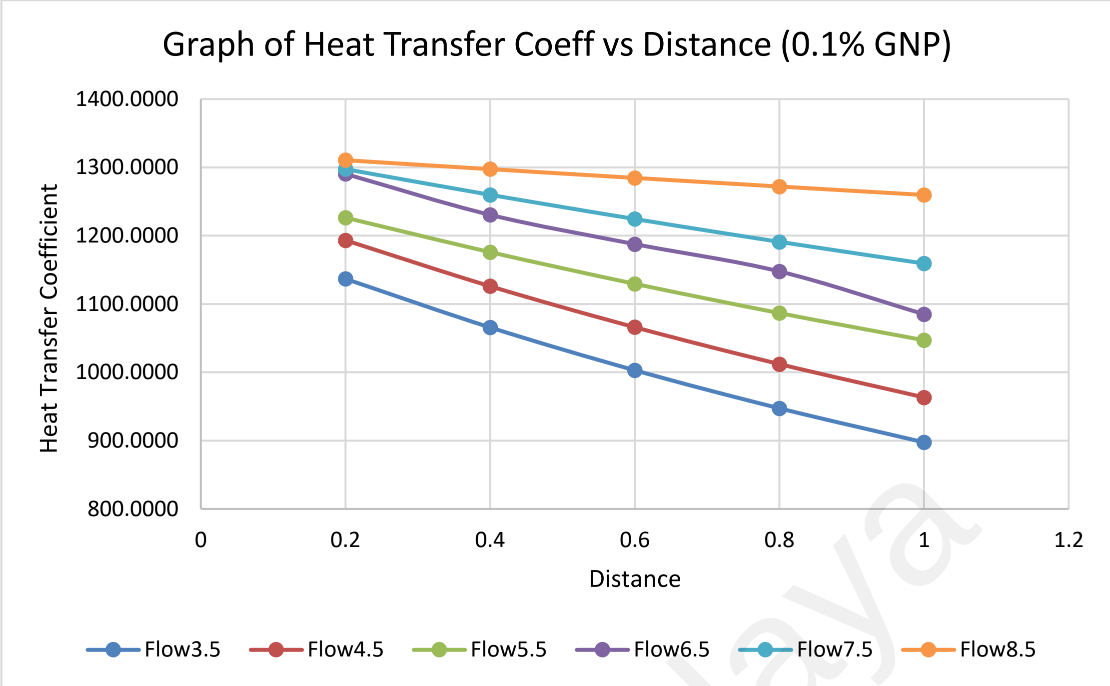

Figure 4.6: Graph of heat transfer coefficient against distance of 0.1% GNP

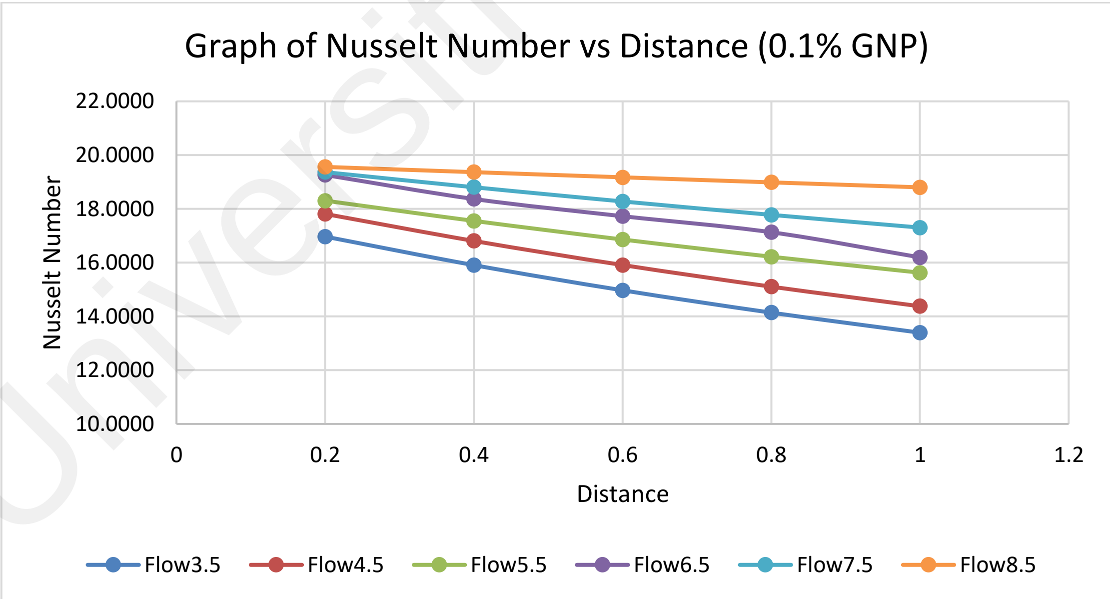

Figure 4.7: Graph of Nusselt number against distance of 0.1% GNP

Figure 4.1, 4.2 and 4.3 represents the simulation data of distilled water. Thermo-physical properties listed in Table 3.1 is used in the simulation of the process. As of Figure 4.1, it can be noted that the temperature is increasing order from T1 to T5. T1 denotes

0.2m and T5 denotes 1.0m. This are the points where the thermocouple was placed on the test section. As the fluid flows in the test section, it absorbs more and more heat from the surface. Hence, the temperature increases along the thermocouple.

Highest temperature of 37.09 ºC was recorded at flowrate of 3.5 L/min while the lowest temperature of 35.74 ºC was recorded at 8.5 L/min for the distilled water run. As of the study with 0.1% GNP, the highest temperature recorded was 40.30 ºC for flowrate of 3.5 L/min meanwhile lowest temperature recorded is 36.11 ºC for flowrate of 8.5 L/min.

From the distilled graphs, it can be observed that 3.5 l/min flowrate has the least heat transfer coefficient of 1154.75 W/m^{2}K at the 1m mark wherelse at 8.5 l/min the heat transfer coefficient is the highest at 1365 W/m^{2}K. As of the Nusselt number,

From the 0.1% GNP graphs, it can be observed that 3.5 l/min flowrate has the least heat transfer coefficient of 897.49 W/m^{2}K at the 1m mark wherelse at 8.5 l/min the heat transfer coefficient is the highest at 1310.67 W/m^{2}K. As of the Nusselt number,

The Nusselt number of the distilled water and 0.1% follows the similar trend of heat transfer coefficient. At 0.2m, flowrate 3.5 l/min has 13.95 for distilled water while it's at 19.67 for 0.1% GNP. The variation in the Nusselt number can be due to the difference on the thermal conductivity of the respective fluids. It is quite evident in Nusselt number as Nusselt number is directly affected by the thermal conductivity of a particular fluid.

4.1.2.2 Square tube

The following section would discuss the comparison between temperature, heat transfer coefficient and Nusselt number against distance. The data is analysed with respect to the position of the thermocouples. Only graphs of 0.1% GNP and distilled water data will be discussed in this section.

Table 4-7: Table of temperature at local points on test section of distilled water

Temperature (°C)					
Length (m)	**0.2**	**0.4**	**0.6**	**0.8**	**1**
Flow3.5	66.40	66.60	66.85	67.09	67.34
Flow4.5	66.20	66.40	66.65	66.89	67.14
Flow5.5	66.11	66.30	66.51	66.71	66.91
Flow6.5	66.00	66.20	66.42	66.59	66.76
Flow7.5	65.90	66.05	66.25	66.40	66.55
Flow8.5	65.74	65.87	66.00	66.13	66.26

Table 4-8: Table of heat transfer coefficient at local points on test section of distilled water

Heat transfer Coeff (Water)					
Length (m)	**0.2**	**0.4**	**0.6**	**0.8**	**1**
Flow3.5	237.9442	236.7305	235.2749	233.8372	232.4169
Flow4.5	239.1582	237.9321	236.4618	235.0095	233.5750
Flow5.5	239.6901	238.5496	237.2637	236.0688	234.8800
Flow6.5	240.3846	239.1582	237.8234	236.8022	235.8016
Flow7.5	241.0026	240.0768	238.8413	237.9502	237.0717
Flow8.5	241.9917	241.1824	240.3846	239.5921	238.8048

Table 4-9: Table of Nusselt number at local points on test section of distilled water

Nusselt Number (Water)					
Length (m)	**0.2**	**0.4**	**0.6**	**0.8**	**1**
Flow3.5	3.5514	3.5333	3.5116	3.4901	3.4689
Flow4.5	3.5695	3.5512	3.5293	3.5076	3.4862
Flow5.5	3.5775	3.5604	3.5412	3.5234	3.5057
Flow6.5	3.5878	3.5695	3.5496	3.5344	3.5194
Flow7.5	3.5971	3.5832	3.5648	3.5515	3.5384
Flow8.5	3.6118	3.5997	3.5878	3.5760	3.5643

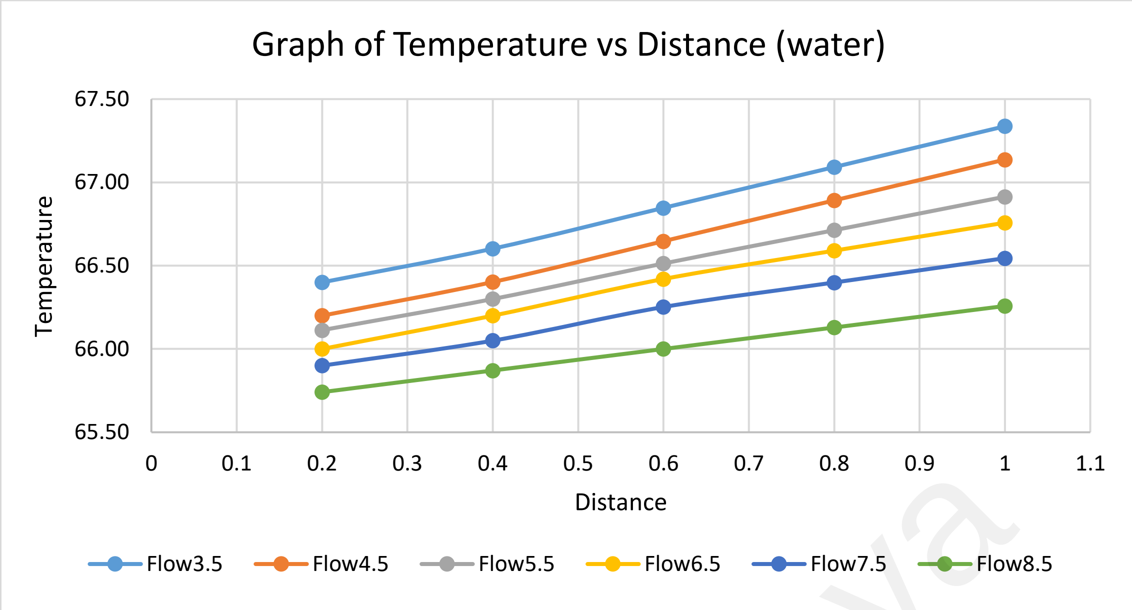

Figure 4.8: Graph of temperature against distance of distilled water

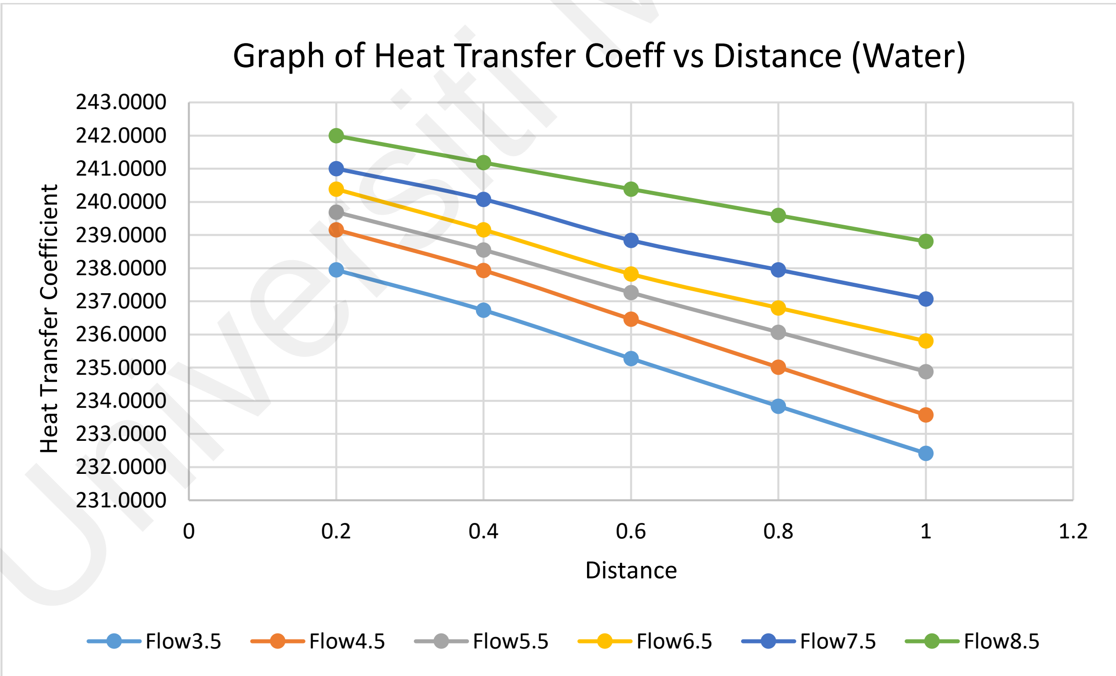

Figure 4.9: Graph of Heat transfer coefficient against distance of distilled water

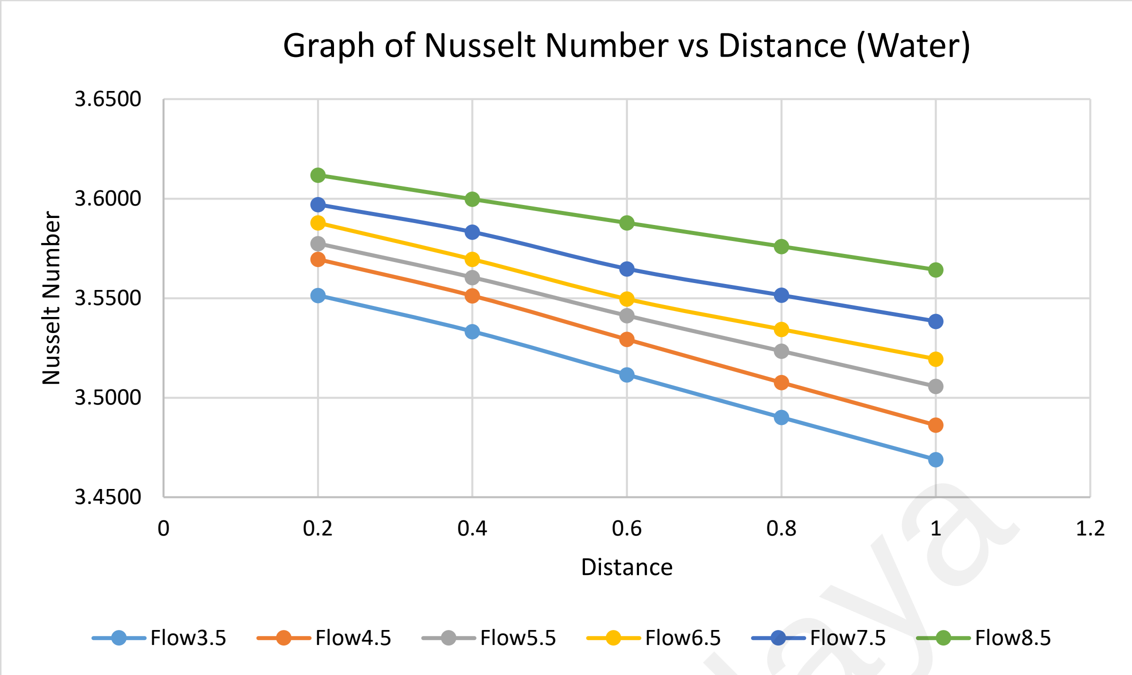

Figure 4.10: Graph of Nusselt number against distance of distilled water

Table 4-10: Table of temperature at local points on test section of 0.1% GNP

Temperature (°C)					
Length (m)	**0.2**	**0.4**	**0.6**	**0.8**	**1**
Flow3.5	63.15	63.50	63.80	64.10	64.40
Flow4.5	62.90	63.21	63.52	63.83	64.14
Flow5.5	62.70	62.95	63.20	63.45	63.70
Flow6.5	62.45	62.70	62.95	63.20	63.45
Flow7.5	62.30	62.50	62.70	62.90	63.10
Flow8.5	61.95	62.10	62.25	62.40	62.55

Table 4-11: Table of heat transfer coefficient at local points on test section of 0.1% GNP

Heat transfer Coeff (W/m^2K)					
Length (m)	**0.2**	**0.4**	**0.6**	**0.8**	**1**
Flow3.5	259.3361	256.8493	254.7554	252.6954	250.6684
Flow4.5	261.1421	258.9064	256.7087	254.5479	252.4233
Flow5.5	262.6050	260.7789	258.9779	257.2016	255.4496
Flow6.5	264.4570	262.6050	260.7789	258.9779	257.2016
Flow7.5	265.5807	264.0845	262.6050	261.1421	259.6953
Flow8.5	268.2403	267.0940	265.9574	264.8305	263.7131

Table 4-12: Table of Nusselt number at local points on test section of 0.1% GNP

Nusselt Number					
Length (m)	**0.2**	**0.4**	**0.6**	**0.8**	**1**
Flow3.5	3.8707	3.8336	3.8023	3.7716	3.7413
Flow4.5	3.8976	3.8643	3.8315	3.7992	3.7675
Flow5.5	3.9195	3.8922	3.8653	3.8388	3.8127
Flow6.5	3.9471	3.9195	3.8922	3.8653	3.8388
Flow7.5	3.9639	3.9416	3.9195	3.8976	3.8760
Flow8.5	4.0036	3.9865	3.9695	3.9527	3.9360

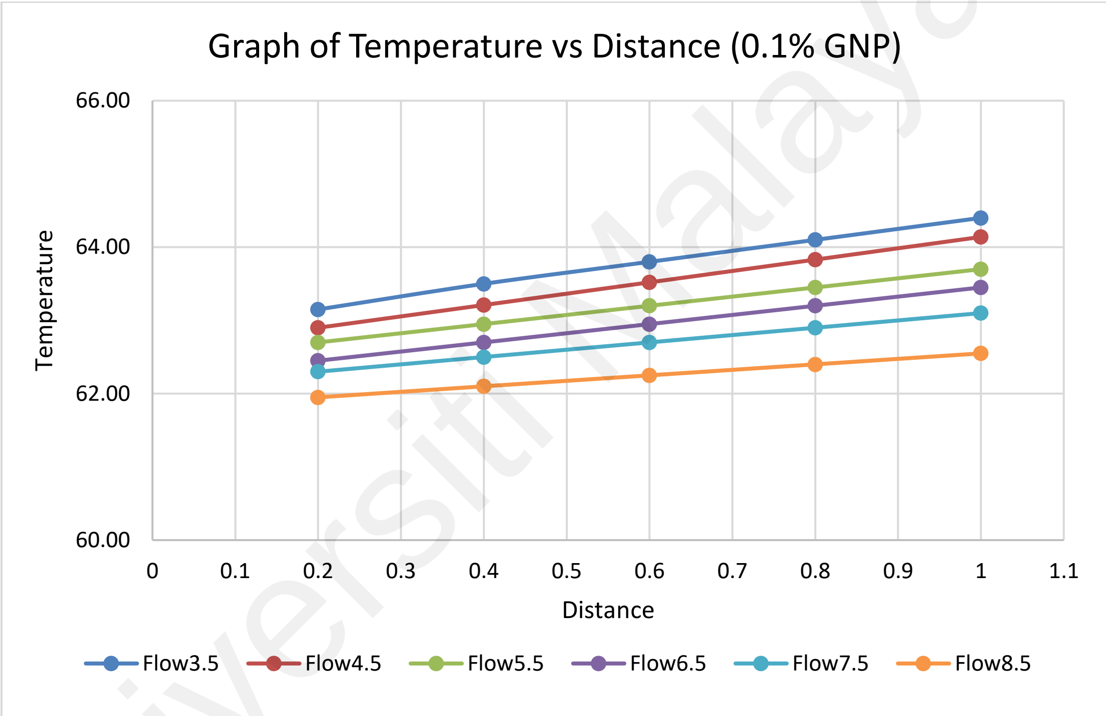

Figure 4.11: Graph of temperature against distance of 0.1% GNP

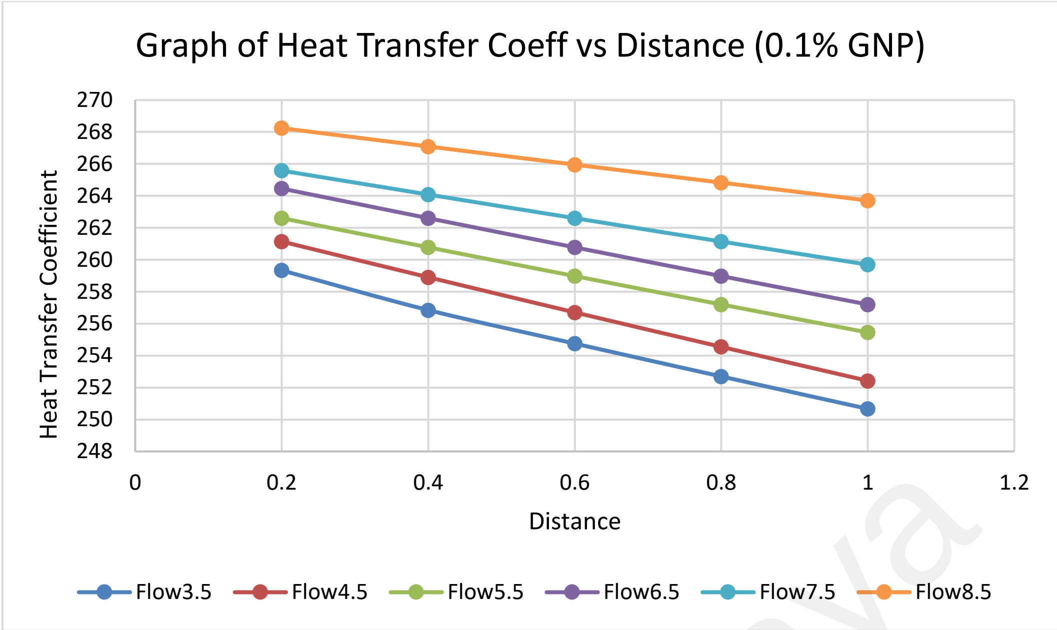

Figure 4.12: Graph of heat transfer coefficient against distance of 0.1% GNP

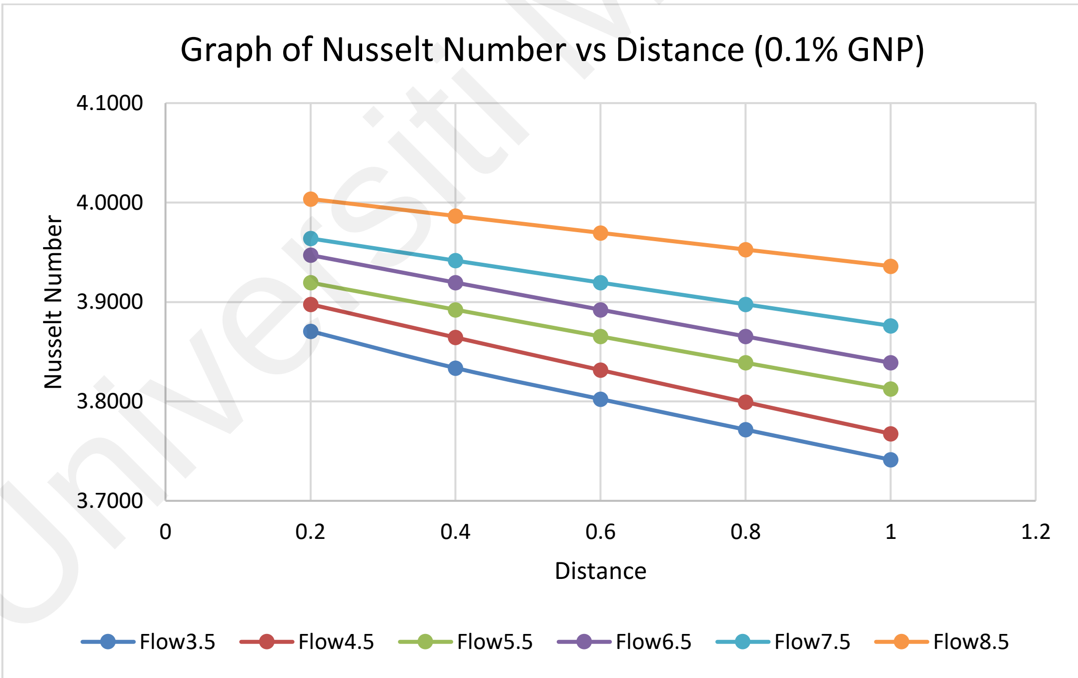

Figure 4.13: Graph of Nusselt number against distance of 0.1% GNP

From the distilled water graphs, Figure 4.7 - 4.9, it can be denoted that the highest temperature of 67.34 °C was recorded at flowrate of 3.5 L/min while the lowest temperature of 65.74 °C was recorded at 8.5 L/min for the distilled water run. Meanwhile, the heat transfer coefficient is highest at 0.2m for flowrate 8.5 l/min at 237.94 W/m^{2}K and lowest at 1m for flowrate 3.5 l/min at 238.80 W/m^{2}K. In addition, the Nusselt number mirrors similar graphical image of heat transfer coefficient as both are interrelated.

From the 0.1% GNP graphs, Figure 4.10 - 4.12, it can be denoted that the highest temperature of 64.40 ºC was recorded at flowrate of 3.5 L/min while the lowest temperature of 61.95 ºC was recorded at 8.5 L/min for the distilled water run. Meanwhile, the heat transfer coefficient is highest at 0.2m for flowrate 8.5 l/min at 268.24 W/m^{2}K and lowest at 1m for flowrate 3.5 l/min at 259.34 W/m^{2}K. In addition, the Nusselt number mirrors similar graphical image of heat transfer coefficient as both are interrelated. More heat is absorbed at in the beginning of the test section at a higher flowrate.

4.1.3 Effect of concentration on heat transfer

Three different concentrations of phenolic acid treated GNP at 0.1%, 0.05% and 0.0025% is study in this work along with distilled water. Both circular and square geometry is run with water and all the said concentrations. Since different concentration have different volume of GNP's in its solution, the effectiveness of removing heat would indeed vary. Hence, the study on the effect of concentration of nanofluid on heat transfer is very much essential.

4.1.3.1 Circular and square tube

Table 4.1 shows the velocity of nanofluid with respect to the flowrates and its corresponding heat transfer coefficients.

Table 4-13: Table of heat transfer coefficient and velocity of circular tube

Flowrate (L/min)	Velocity (m/s)	H avg (water)	H avg (0.1%)	H avg (0.05%)	H avg (0.025%)
3.5	0.583333333	819.35006	1010.101847	959.0187775	900.5459494
4.5	0.75	845.7428898	1072.175637	1008.22192	959.7821658
5.5	0.933333333	884.5761942	1133.150019	1069.229694	1026.344241
6.5	1.083333333	911.6485397	1180.676031	1128.002021	1083.352325
7.5	1.25	941.2199837	1244.478927	1195.817262	1142.01677
8.5	1.416666667	954.1039234	1298.642209	1258.230787	1199.875519

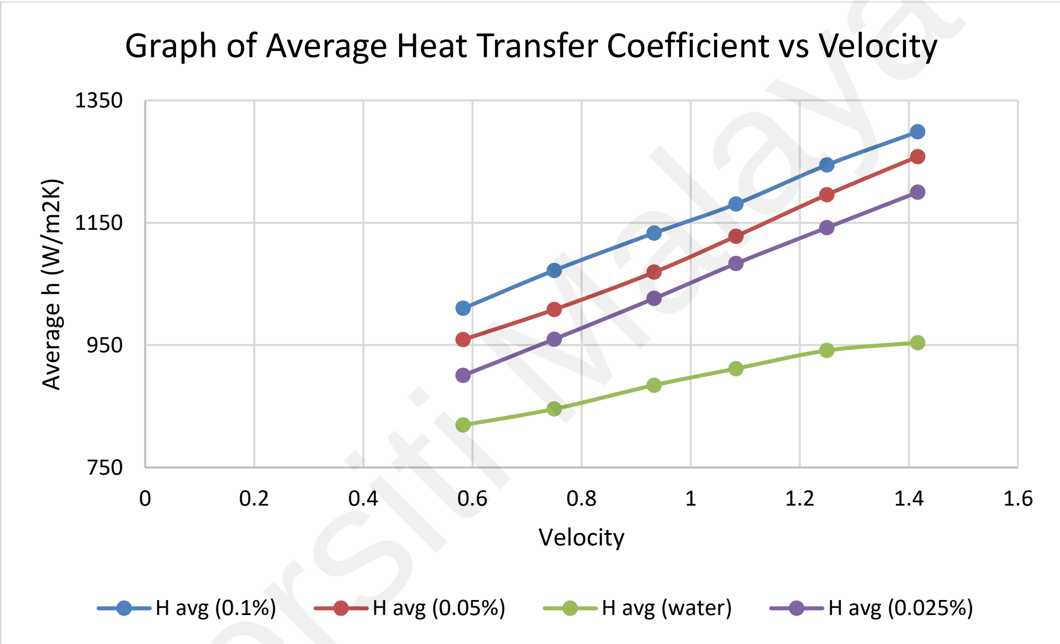

Figure 4.14: Graph of average heat transfer coefficient against velocity

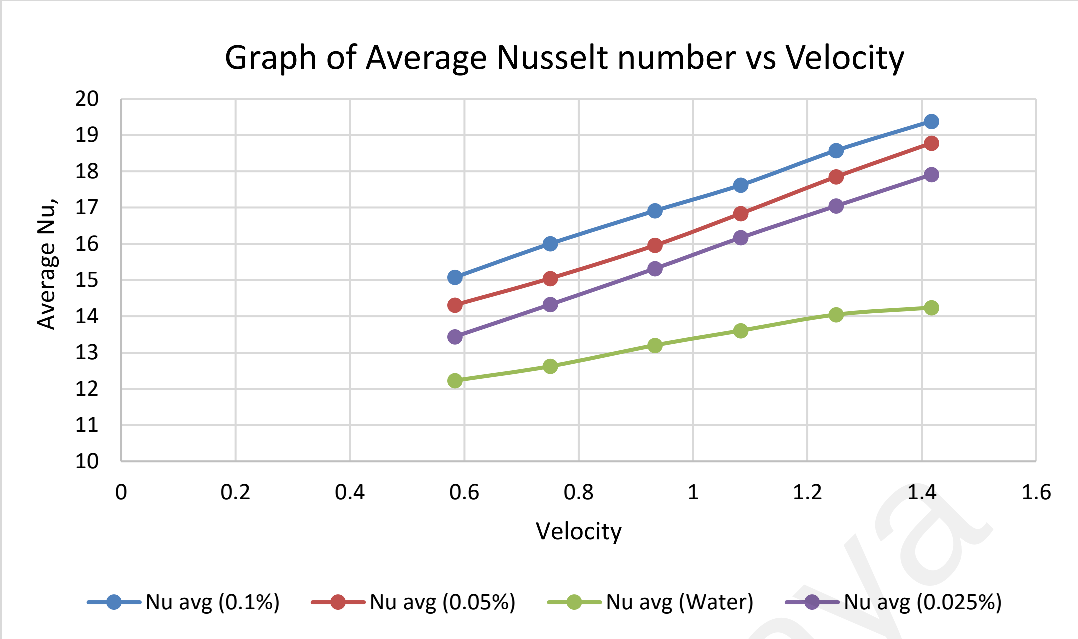

Figure 4.15: Graph of average Nusselt number against velocity

Table 4-14: Table heat transfer coefficient and velocity of square tube

Flowrate (L/min)	Velocity (m/s)	H avg (water)	H avg (0.1%)	H avg (0.05%)	H avg (0.025%)
3.5	0.583333333	235.8305291	254.4556847	248.0584121	241.6365525
4.5	0.75	236.478614	256.7456559	249.840694	243.5270317
5.5	0.933333333	237.2746669	259.0026079	251.7401735	245.432304
6.5	1.083333333	237.8309864	260.804086	253.6220457	246.7241958
7.5	1.25	238.8467704	262.6215275	256.0813958	248.6877385
8.5	1.416666667	239.33629	265.9670792	258.6216737	250.0142236

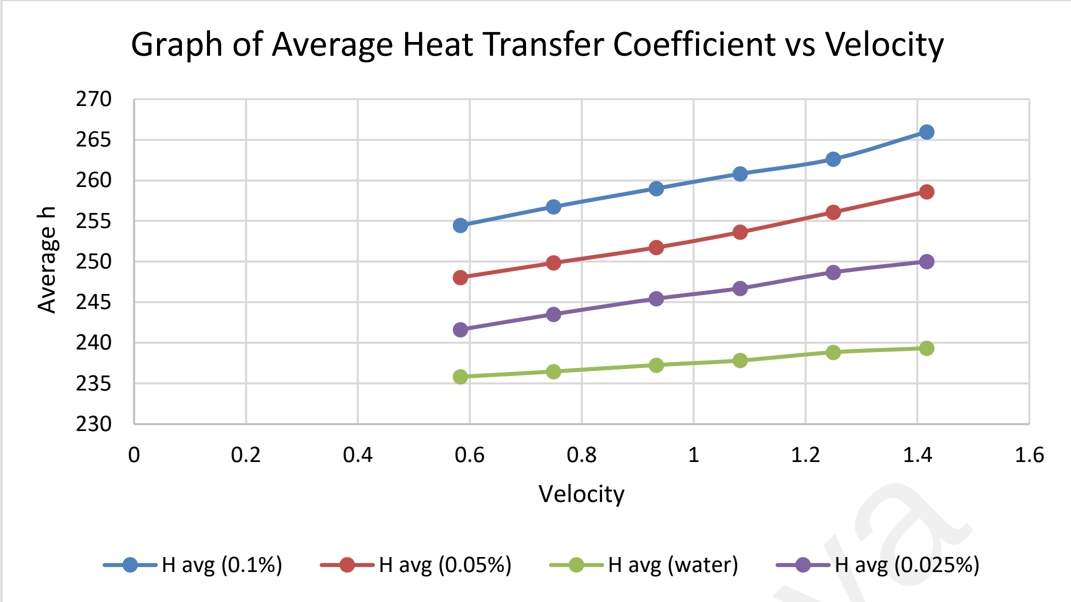

Figure 4.16: Graph of average heat transfer against velocity of square tube

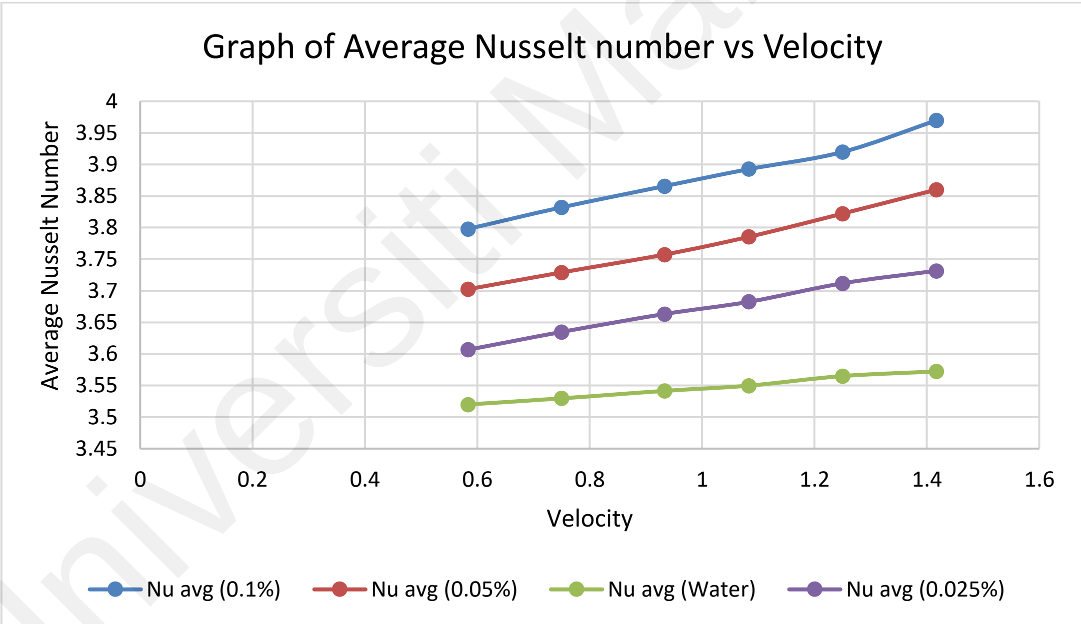

Figure 4.17: Graph of average Nusselt number against velocity of square tube

Figure 4.1 and Figure 4.2 refers to the average heat transfer coefficient against velocity and average Nusselt number against velocity of circular tubes. Figure 4.3 and Figure 4.4 refers to the average heat transfer coefficient against velocity and average Nusselt number against velocity of square tubes. Regardless of the geometry of the test section, it can be noted that as the velocity of the working fluid flowing in the test section increases, the average heat transfer capacity and Nusselt number increases too. In short, it can also be said that the average heat transfer coefficient and Nusselt number is directly proportional to the velocity of the working fluid. As the velocity in the test section increases, more heat is able to be carried away by the working fluid. This is because, if a small element of the test section is taken into consideration, at a higher flowrate, more fluid would have flowed pass the element in comparison to fluid at lower flowrate.

The heat removed from the surface of the test section is conducted into adjacent piping in the jacketed tank. The cooled fluid flows back into the test section to remove more heat. At a higher flowrate, the rate of fluid flowing through the passage is higher. This is represented as average Nusselt number in graphical form.

4.2 Experiment

Experimental runs with nanofluid is made on the test section in the lab. The data collected is presented in graphical method for much better analysis and tabulation.

4.2.1 Effect of conduit geometry

Circular and square conduits have a different overall total surface area. This is directly related to the overall heat transfer of the set up.

4.2.1.1 Water

Table 4-15: Heat transfer coefficient and Nusselt number of water at flowrate 3.5 L/min

	Flowrate 3.5 - Circular		Flowrate 3.5 - Square	
Distance	Heat Transfer Coefficient	Nusselt number	Heat Transfer Coefficient	Nusselt number
0.2	1085.147339	17.78930064	768.442623	12.59742005
0.4	994.7183943	16.30685892	694.4444444	11.38433515
0.6	918.2015948	15.05248516	633.4459459	10.38435977
0.8	852.6157666	13.97730765	582.2981366	9.545871093
1.0	795.7747155	13.04548714	538.7931034	8.832673827

Table 4-16: Heat transfer coefficient and Nusselt number of water at flowrate 6.5 L/min

Flowrate 6.5 - Circular			Flowrate 6.5 - Square	
Distance	Heat Transfer Coefficient	Nusselt number	Heat Transfer Coefficient	Nusselt number
0.2	1193.662073	19.56823071	768.442623	12.59742005
0.4	1085.147339	17.78930064	721.1538462	11.8221942
0.6	994.7183943	16.30685892	679.3478261	11.13684961
0.8	918.2015948	15.05248516	642.1232877	10.52661127
1.0	852.6157666	13.97730765	608.7662338	9.979774324

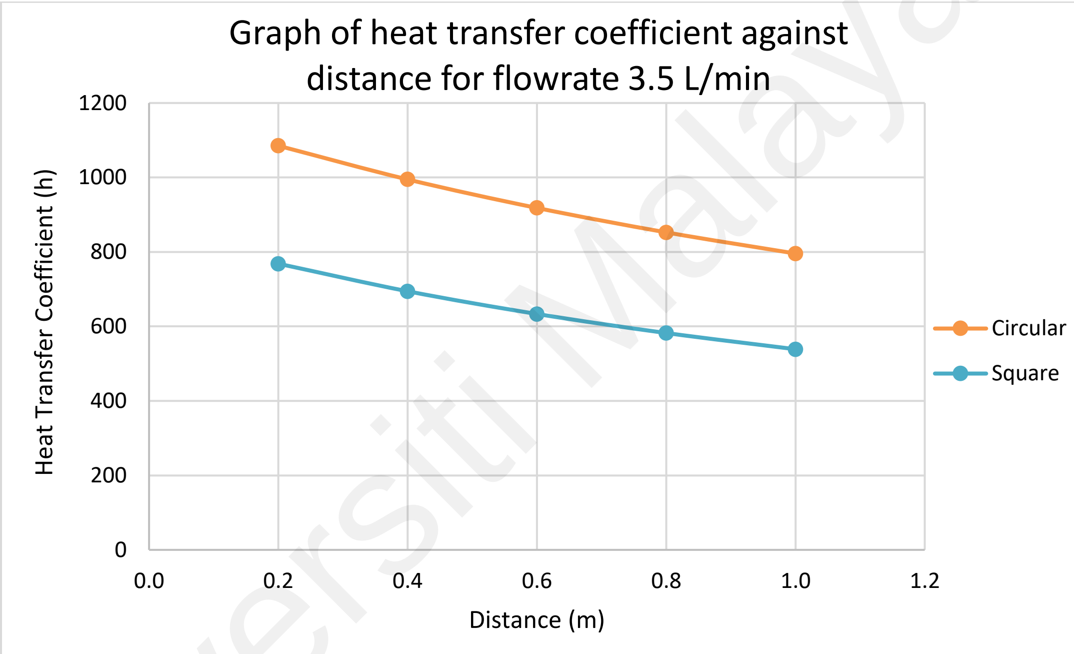

Figure 4.18: Graph of heat transfer coefficient against distance at flowrate 3.5L/min of water

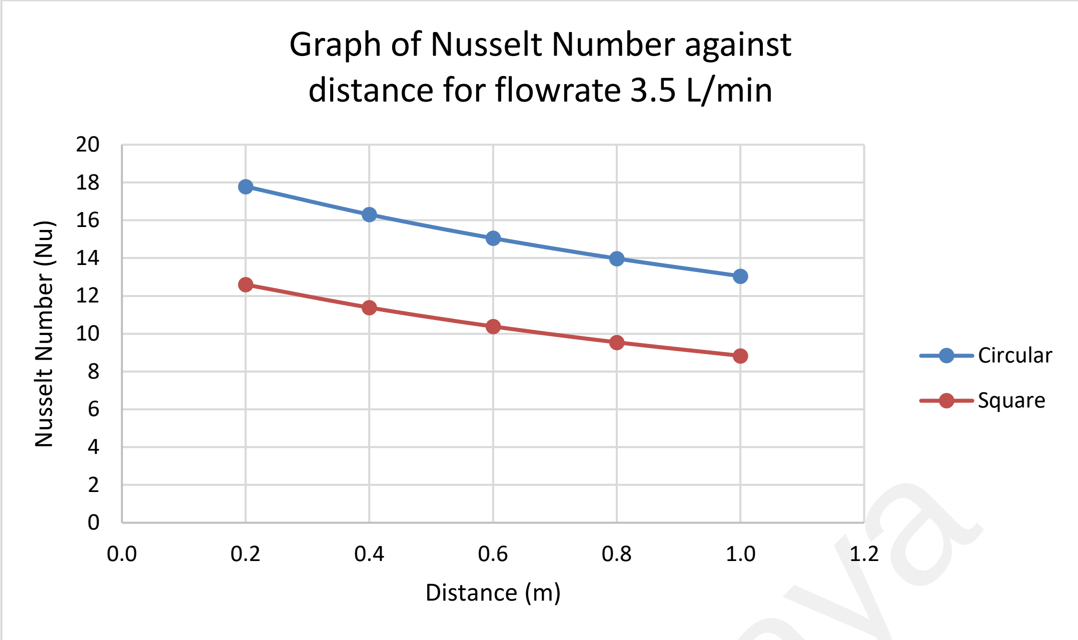

Figure 4.19: Graph of Nusselt number against distance at flowrate 3.5L/min of water

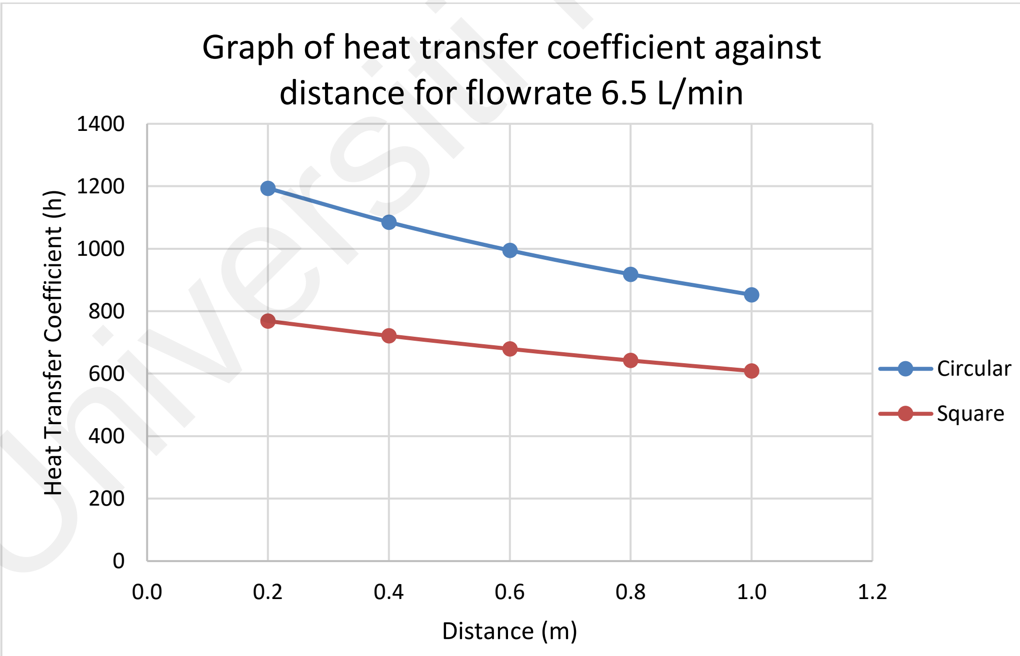

Figure 4.20: Graph of heat transfer coefficient against distance at flowrate 6.5L/min of water

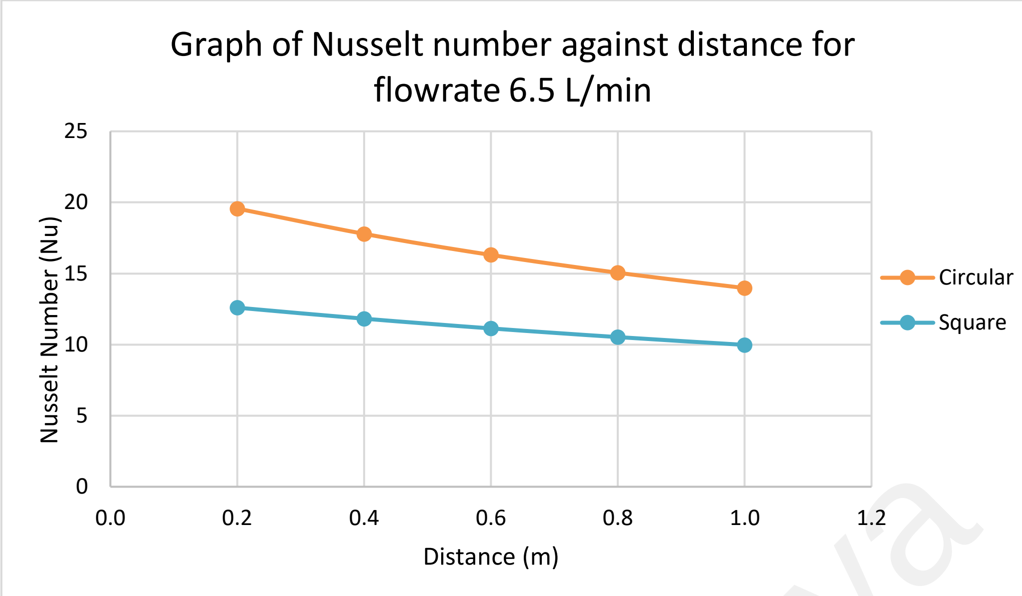

Figure 4.21: Graph of Nusselt number against distance at flowrate 6.5L/min of water

Form the graph it can be concluded that the heat transfer coefficient and Nusselt number is higher for the circular tube compared to square tube. As of Figure 4.18 and 4.19, at flowrate 3.5 l/min, there is an increase of about 30% in the heat transfer coefficient and Nusselt number of circular tube at the 0.2m mark. As of the Figure 4.20 and 4.21, there is also an increase of about 35% at 0.2 m in the circular tube and and a comparative increase at 1m of about 29%. This hence also proves that circular tube is a better option for heat transfer

4.2.1.2 0.1% GNP

Table 4-17: Heat transfer coefficient and Nusselt number of 0.1% GNP at flowrate 3.5 L/min

	Flowrate 3.5 - Circular		Flowrate 3.5 - Square	
Distance	Heat Transfer Coefficient	Nusselt number	Heat Transfer Coefficient	Nusselt number
0.2	1387.979155	20.71610679	1065.340909	15.90061058
0.4	1341.193341	20.01781105	892.8571429	13.32622601
0.6	1243.397993	18.558179	732.421875	10.93166978
0.8	1181.843637	17.63945727	625	9.328358209
1.0	1126.096295	16.80740739	600.9615385	8.969575201

Table 4-18: Heat transfer coefficient and Nusselt number of water at flowrate 6.5 L/min

	Flowrate 6.5 - Circular		Flowrate 6.5 - Square	
Distance	Heat Transfer Coefficient	Nusselt number	Heat Transfer Coefficient	Nusselt number
0.2	1510.96465	22.55171119	986.8421053	14.72898665
0.4	1372.025371	20.47799062	937.5	13.99253731
0.6	1256.486393	18.75352825	892.8571429	13.32622601
0.8	1158.895217	17.29694353	860.0917431	12.8371902
1.0	1075.371237	16.05031697	815.2173913	12.16742375

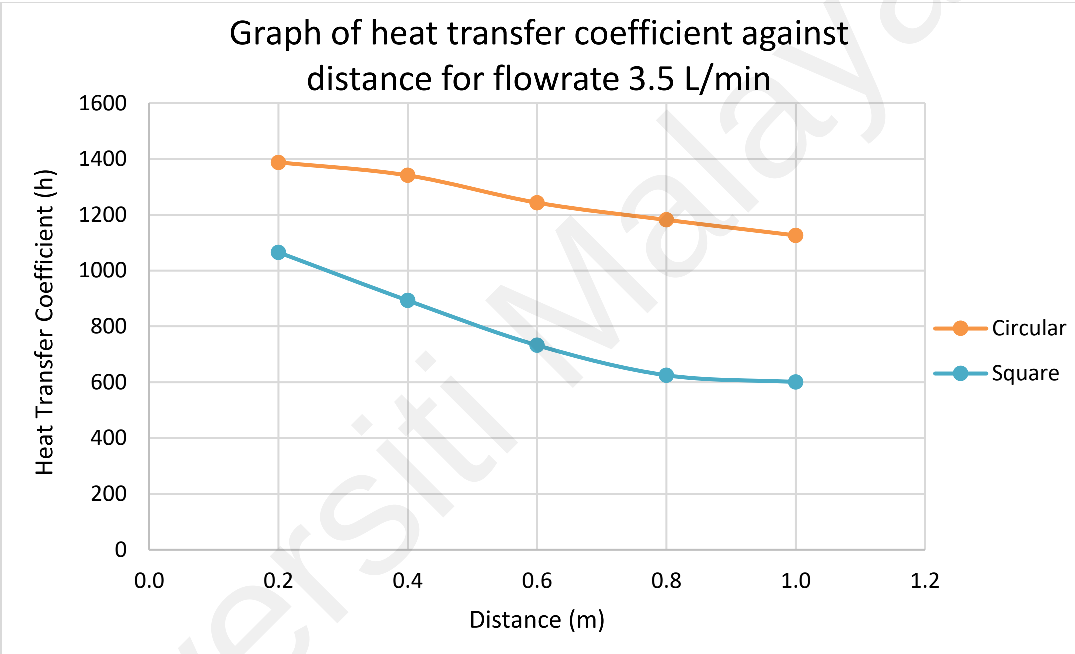

Figure 4.22: Graph of heat transfer coefficient against distance at flowrate 3.5L/min of 0.1% GNP

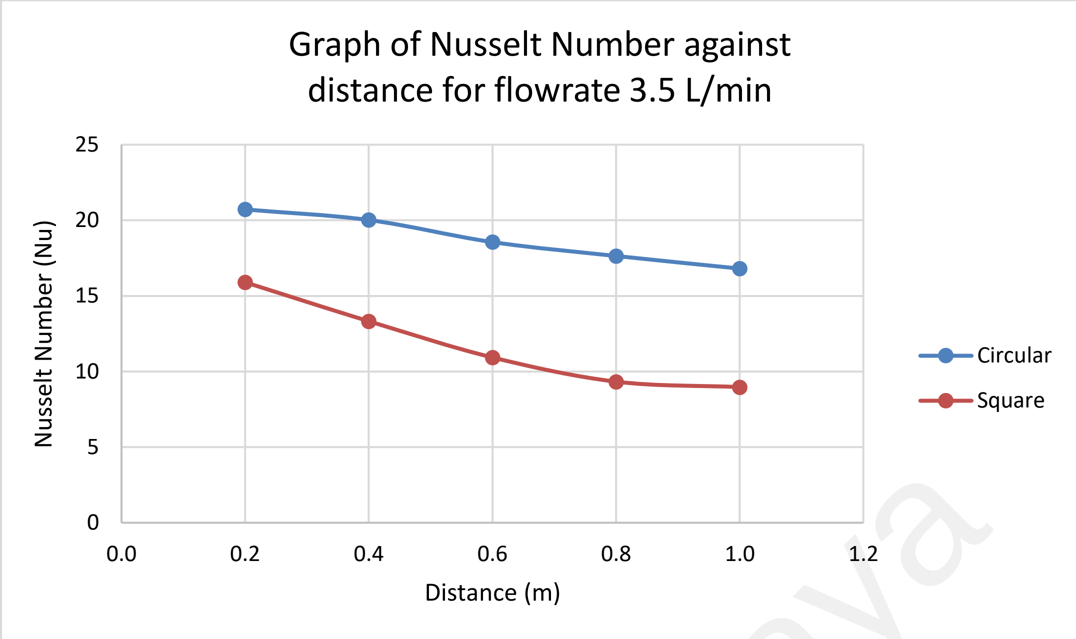

Figure 4.23: Graph of Nusselt number against distance at flowrate 3.5L/min of 0.1% GNP

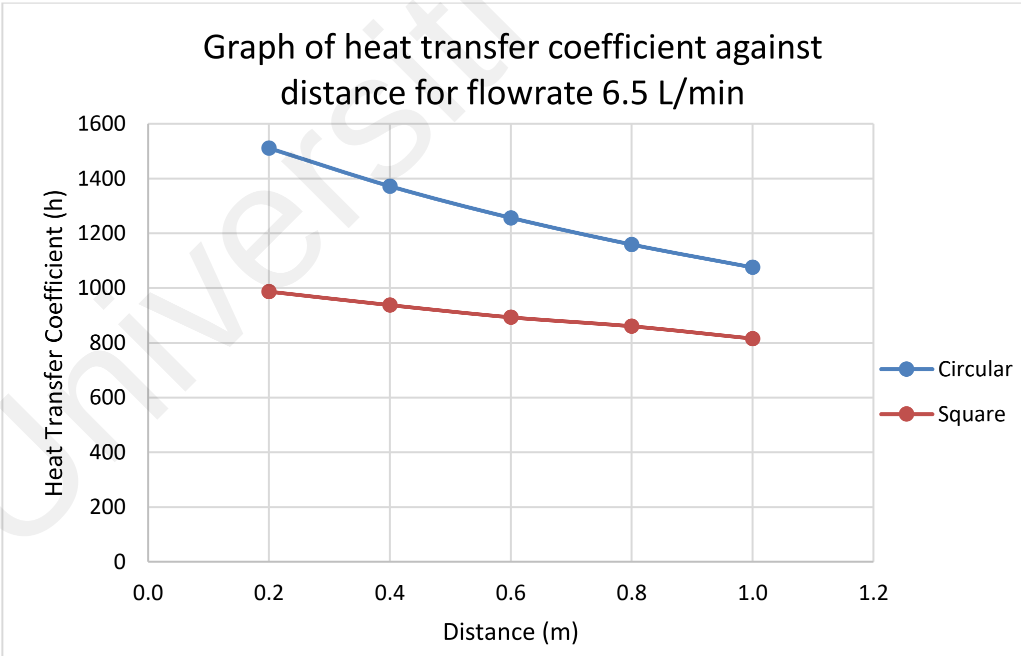

Figure 4.24: Graph of heat transfer coefficient against distance at flowrate 6.5L/min of 0.1% GNP

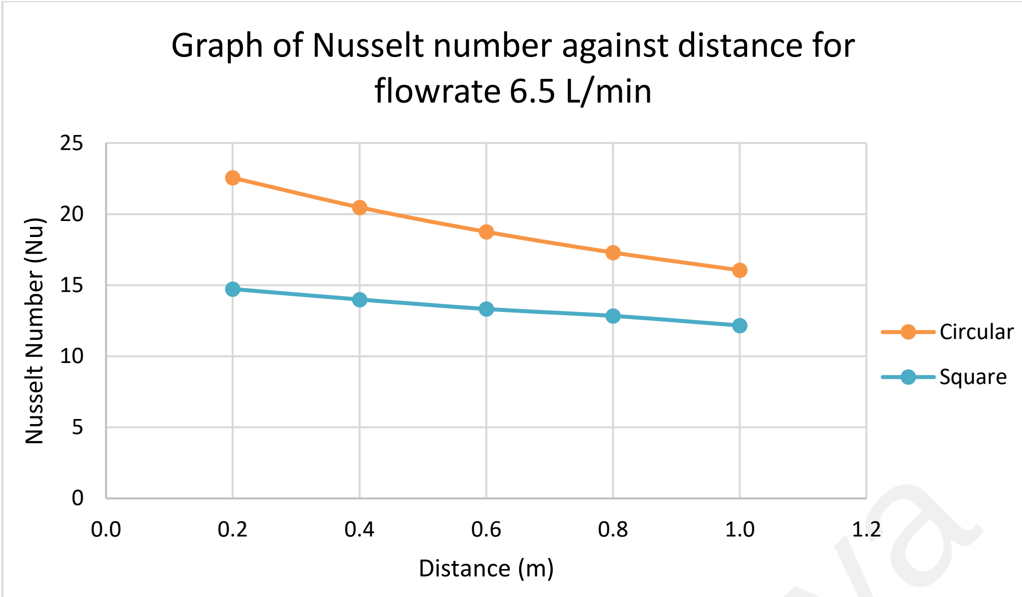

Figure 4.25: Graph of Nusselt number against distance at flowrate 6.5L/min of 0.1% GNP

Form the graph it can be concluded that the heat transfer coefficient and Nusselt number is higher for the circular tube compared to square tube. As of Figure 4.22 and 4.23, at flowrate 3.5 l/min, there is an increase of about 24% in the heat transfer coefficient and at the 0.2m mark there was a significant increase of 47% at 1m. As of the Figure 4.24 and 4.25, there is also an increase of about 35% at 0.2 m in the circular tube and and a comparative increase at 1m of about 25%. This hence once again shows that circular tube promotes heat transfer much better than other geometries. Nusselt number had a similar percentage trend to that of heat transfer coefficient for both the 3.5 l/min and 6.5 l/min.

4.2.1.3 0.05% GNP

Table 4-19: Heat transfer coefficient and Nusselt number of 0.05% GNP at flowrate 3.5 L/min

Flowrate 3.5 - Circular			Flowrate 3.5 - Square	
Distance	Heat Transfer Coefficient	Nusselt number	Heat Transfer Coefficient	Nusselt number
0.2	1218.022524	18.73880806	884.4339623	13.2005069
0.4	1158.895217	17.82915718	815.2173913	12.16742375
0.6	1147.751993	17.65772298	715.648855	10.68132619
0.8	1108.664464	17.05637637	597.133758	8.912444149
1.0	1078.610307	16.59400472	480.7692308	7.175660161

Table 4-20 Heat transfer coefficient and Nusselt number of 0.05% GNP at flowrate 6.5 L/min

Flowrate 6.5 - Circular			Flowrate 6.5 - Square	
Distance	Heat Transfer Coefficient	Nusselt number	Heat Transfer Coefficient	Nusselt number
0.2	1311.716564	20.18025483	1255.580357	18.74000533
0.4	1256.486393	19.33055989	916.1237785	13.67348923
0.6	1230.579457	18.93199164	721.1538462	10.76349024
0.8	1181.843637	18.1822098	625	9.328358209
1.0	1142.260357	17.57323626	551.4705882	8.230904302

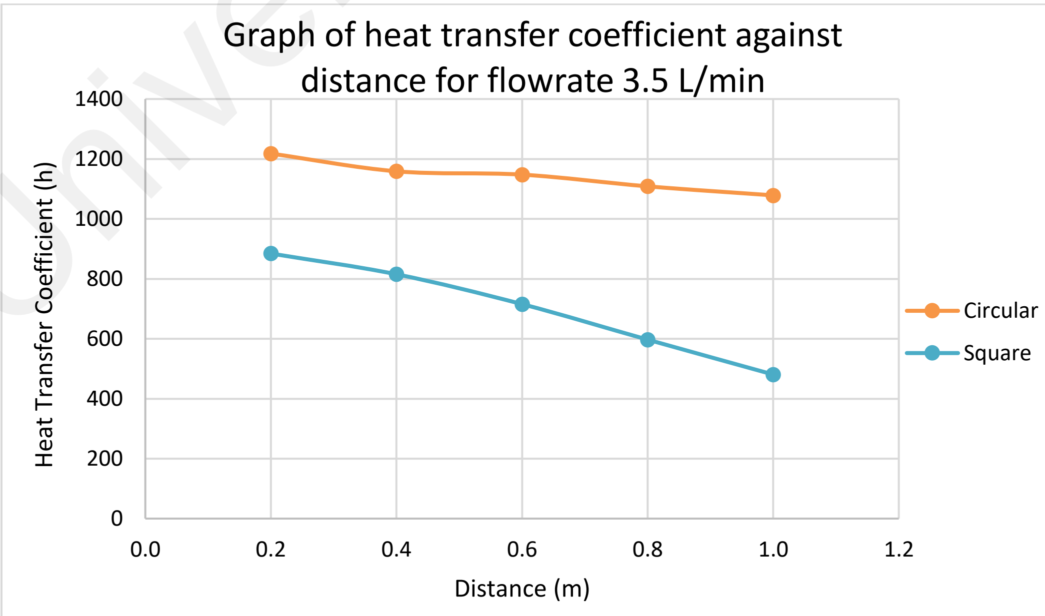

Figure 4.26: Graph of heat transfer coefficient against distance at flowrate 3.5L/min of 0.05% GNP

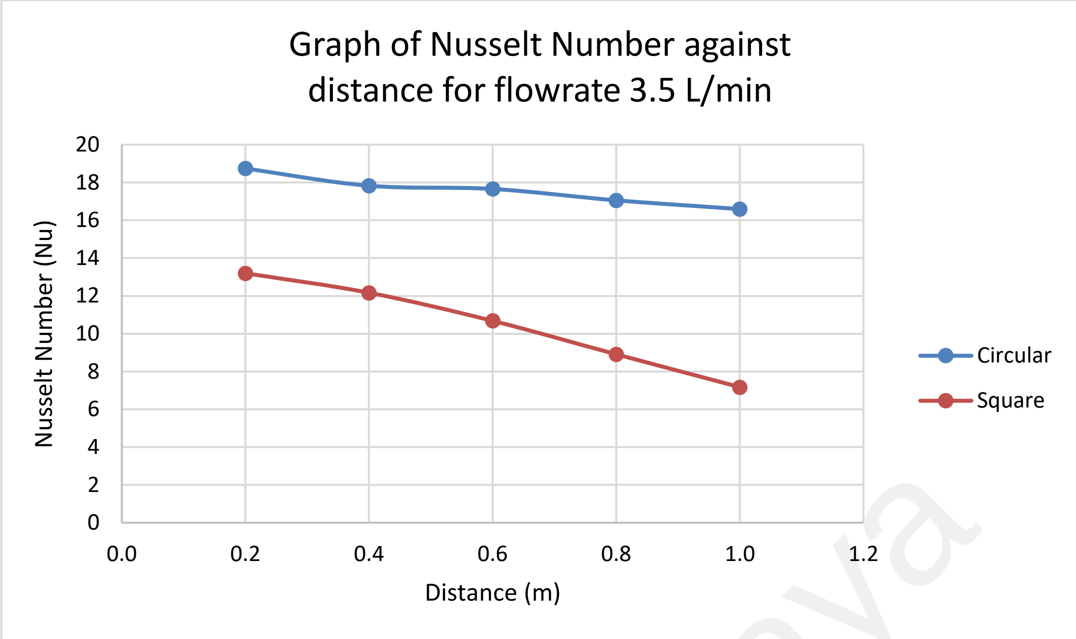

Figure 4.27: Graph of Nusselt number against distance at flowrate 3.5L/min of 0.05% GNP

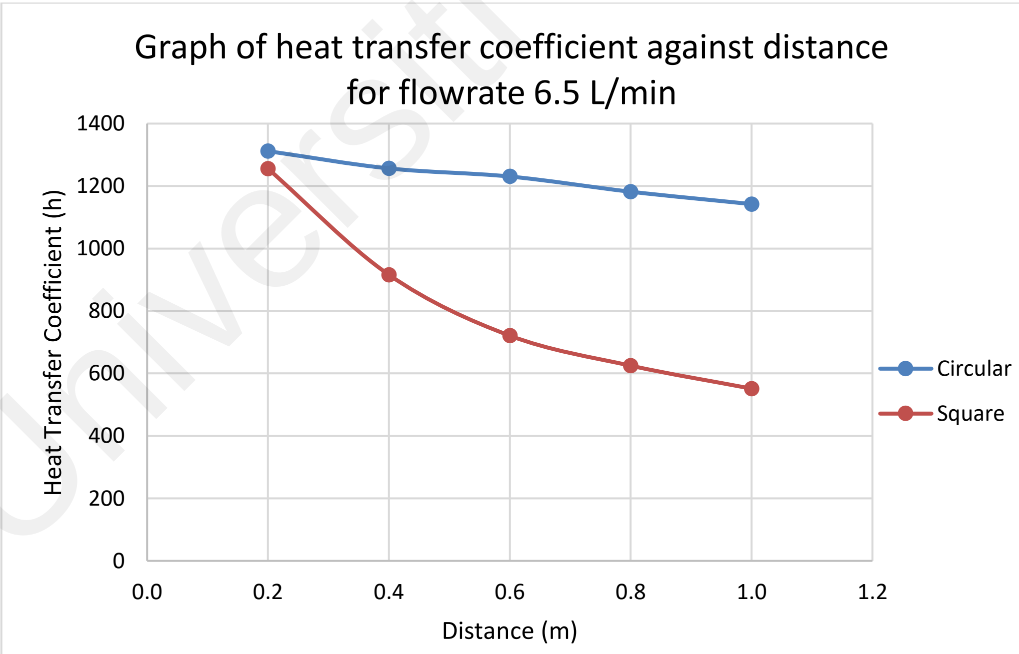

Figure 4.28: Graph of heat transfer coefficient against distance at flowrate 6.5L/min of 0.05% GNP

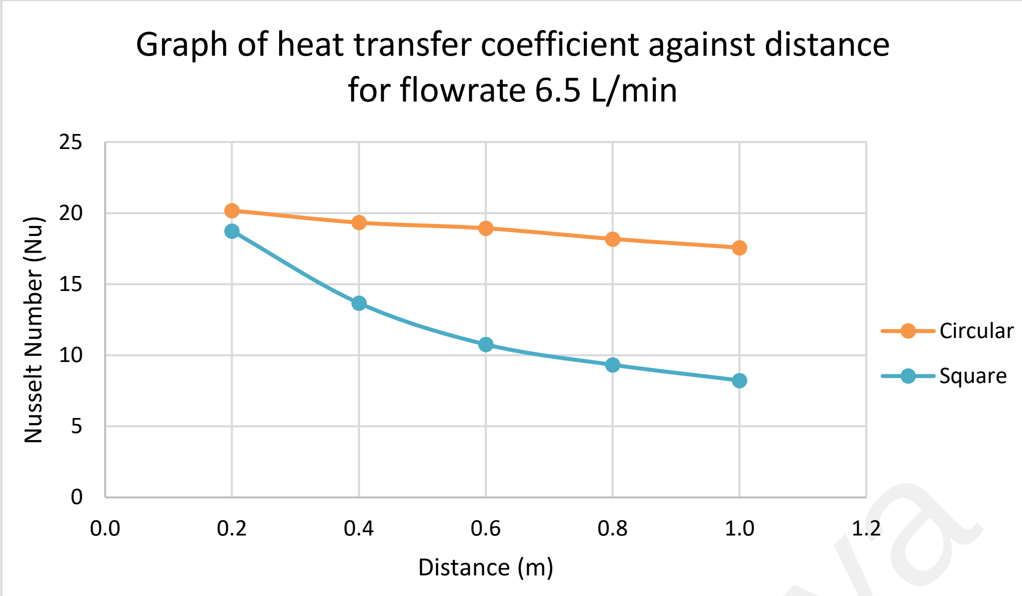

Figure 4.29: Graph of Nusselt number against distance at flowrate 6.5L/min of 0.05% GNP

Form the graph it can be concluded that the heat transfer coefficient and Nusselt number is higher for the circular tube compared to square tube. As of Figure 4.26 and 4.27, at flowrate 3.5 l/min, there is an increase of about 27% in the heat transfer coefficient and at the 0.2m mark there was a significant increase of 56% at 1m. As of the Figure 4.28 and 4.29, there is also an increase of about 5% at 0.2 m in the circular tube and and a significant increase at 1m of about 52%.

This hence once again shows that circular tube promotes heat transfer much better than other geometries. In addition, it was also quite evident that the heat transfer rate and the capability of absorbing larger amount of heat by the nanofluid is high at lower flowrate. Nusselt number had a similar percentage trend to that of heat transfer coefficient for both the 3.5 l/min and 6.5 l/min.

4.2.1.4 0.025% GNP

Table 4-21: Heat transfer coefficient and Nusselt number of 0.025% GNP at flowrate 3.5 L/min

Flowrate 3.5 - Circular			Flowrate 3.5 - Square	
Distance	Heat Transfer Coefficient	Nusselt number	Heat Transfer Coefficient	Nusselt number
0.2	1256.486393	19.94422846	860.0917431	12.8371902
0.4	1136.821022	18.04477813	726.744186	10.84692815
0.6	1037.96702	16.47566699	629.1946309	9.39096464
0.8	954.9296586	15.15761363	554.7337278	8.279607878
1.0	884.1941283	14.03482743	496.031746	7.403458896

Table 4-22: Heat transfer coefficient and Nusselt number of 0.025% GNP at flowrate 6.5 L/min

Flowrate 6.5 - Circular			Flowrate 6.5 - Square	
Distance	Heat Transfer Coefficient	Nusselt number	Heat Transfer Coefficient	Nusselt number
0.2	1326.291192	21.05224115	910.1941748	13.58498768
0.4	1193.662073	18.94701703	794.4915254	11.85808247
0.6	1085.147339	17.22456094	704.887218	10.52070475
0.8	994.7183943	15.78918086	633.4459459	9.454417104
1.0	918.2015948	14.57462849	575.1533742	8.58437872

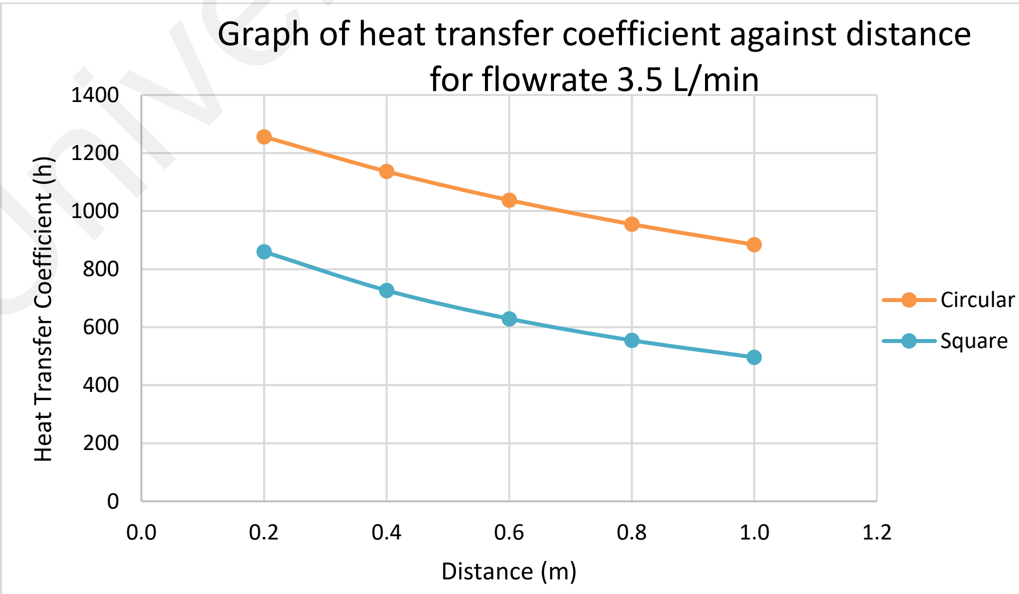

Figure 4.30: Graph of heat transfer coefficient against distance at flowrate 3.5L/min of 0.025% GNP

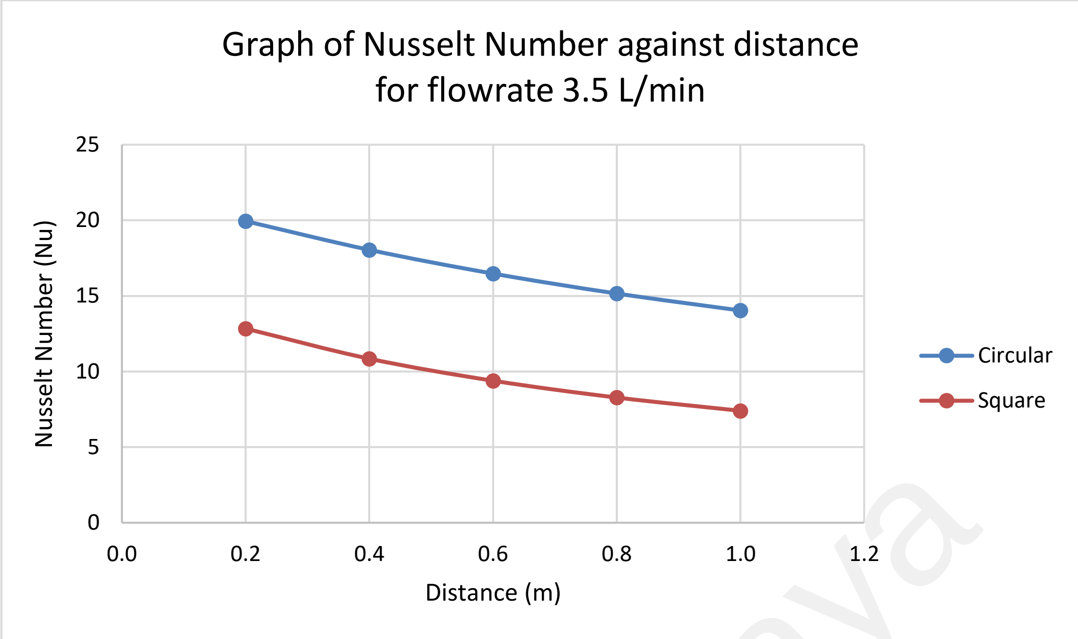

Figure 4.31: Graph of Nusselt number against distance at flowrate 3.5L/min of 0.05% GNP

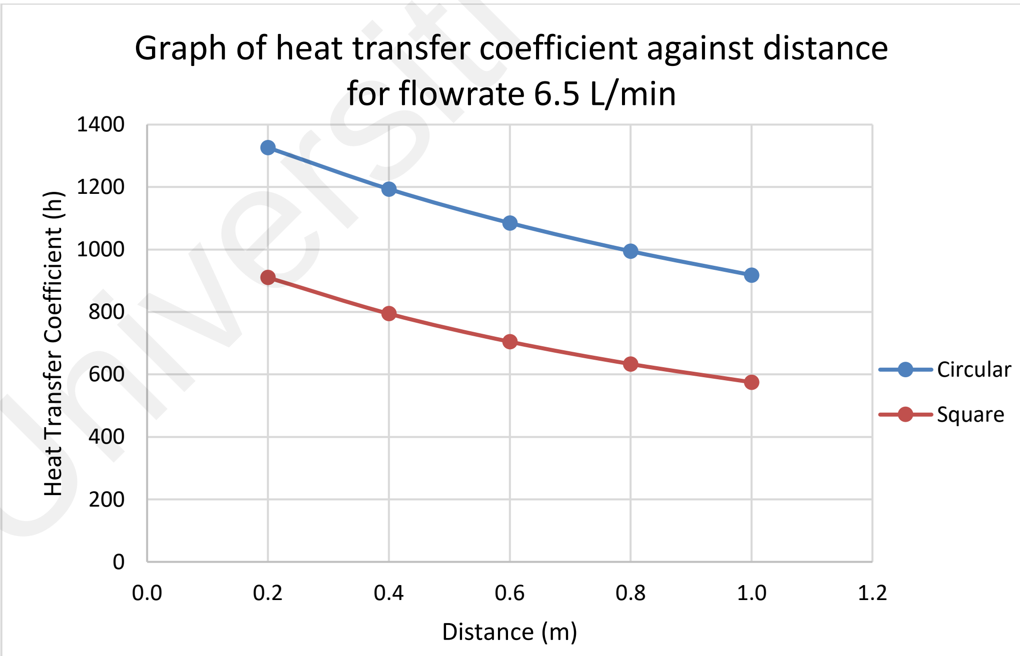

Figure 4.32: Graph of heat transfer coefficient against distance at flowrate 6.5L/min of 0.025% GNP

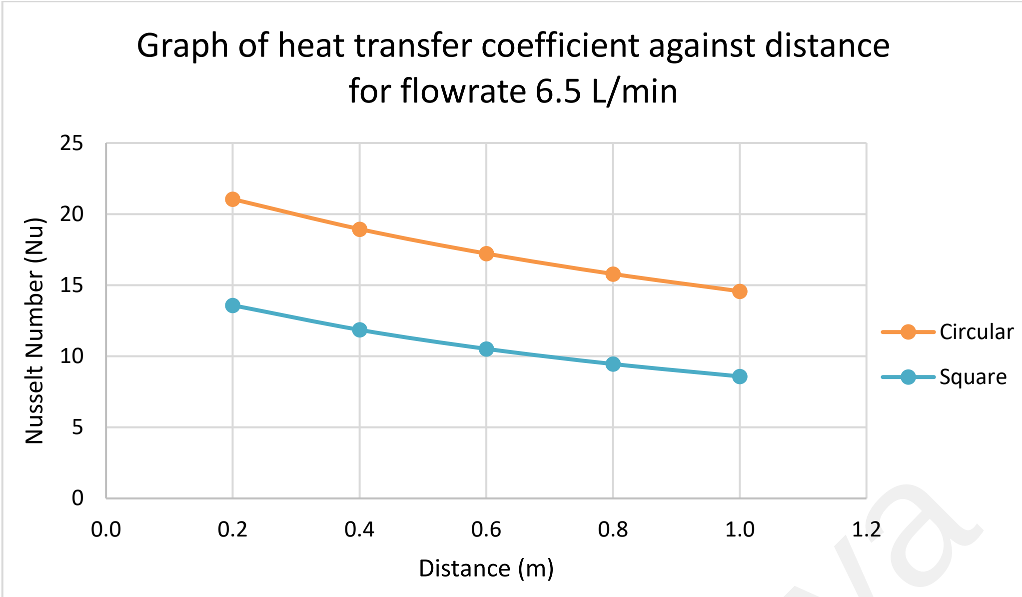

Figure 4.33: Graph of Nusselt number against distance at flowrate 6.5L/min of 0.05% GNP

Form the graph it can be concluded that the heat transfer coefficient and Nusselt number is higher for the circular tube compared to square tube. As of Figure 4.30 and 4.31, at flowrate 3.5 l/min, there is an increase of about 31% in the heat transfer coefficient and at the 0.2m mark there was a significant increase of 44% at 1m. Meanwhile at flowrate of 6.5 l/min, as of the Figure 4.32 and 4.33, there is also an increase of about 31% at 0.2 m in the circular tube and and a significant increase at 1m of about 37%.

This hence once again shows that circular tube promotes heat transfer much better than other geometries. In addition, it was also quite evident that the heat transfer rate and the capability of absorbing larger amount of heat by the nanofluid is high at lower flowrate. Nusselt number had a similar percentage trend to that of heat transfer coefficient for both the 3.5 l/min and 6.5 l/min.

4.2.1.5 Summary

Based on the findings, conduit geometry does have a significant impact on the heat transfer rate from the test section. From the graphical and data analysis, it can be solidly said that, circular tube is the structure that should be selected as heat exchanger wall profile. This is because, the rate of increase in heat transfer in terms percentage is relatively high at an average range of 30 – 50%. This is a significant improvement in comparison to that of conventional working fluid, water, for instance.

4.2.2 Concentration of GNP and Thermal Properties

The aim is to study the effect of different concentrations on the capacity of heat transfer. The concentration studied in this experiment are 0.1%, 0.05% and 0.025%. On top of that, water was also used as one of the working fluid as a control parameter as it is one of the conventionally used working fluids in real world applications. A total of 6 different flowrates were studied. All the data is tabulated and presented in graphical manner. All the conditions, varying flowrate and concentration, was subjected to both circular tube and square tube.

4.2.2.1 Circular tube - water

Table 4-23: Temperature relative to flowrate and position on test section

Temperature (°C)					
Length (m)	**0.2**	**0.4**	**0.6**	**0.8**	**1**
Flow3.5	38.5	38.2	37.7	39.8	44.5
Flow4.5	38.0	39.3	38.5	40.9	46.5
Flow5.5	37.5	38.2	38.7	40.9	47.0
Flow6.5	37.0	38.5	39.1	41.2	47.3
Flow7.5	36.5	38.5	39.0	41.1	47.4
Flow8.5	36.0	38.5	38.8	40.9	47.5

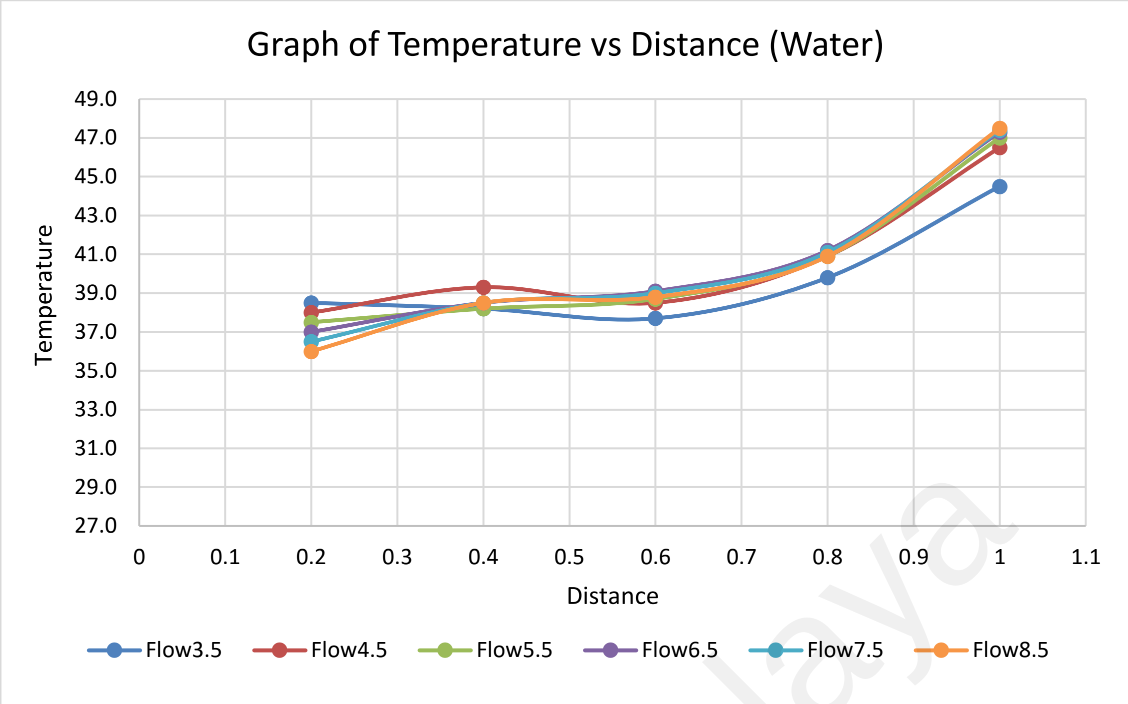

Figure 4.34: Graph of temperature against distance for water run

From Figure 4.34, it can be seen that, as the flowrate increases, the temperature decreases. Due to some anomaly, the decrement in the temperature not quite evident. Considering flowrate 5.5 l/min, the temperature at 0.2m is 37.5 ºC which then eventually increases to 47 ºC. Similar trend of increasing surface temperature can be observed for the consecutive flowrates too whereby for instance temperature at 0.2 m for 7.5 L/min is 36.5 ºC which is followed by increasing temperature of 38.5 ºC, 39.0 ºC, 41.1 ºC and 47.4 ºC.

Table 4-24: Heat transfer coefficient relative to position on test section

Heat transfer Coeff (W/m²K)					
Length (m)	**0.2**	**0.4**	**0.6**	**0.8**	**1**
Flow3.5	1085.15	1263.13	1333.70	1080.24	757.88
Flow4.5	1147.75	1056.34	1136.82	925.32	645.22
Flow5.5	1158.90	1158.90	1105.24	918.20	624.95
Flow6.5	1193.66	1131.43	1070.55	900.88	616.88
Flow7.5	1193.66	1126.10	1075.37	904.29	612.13
Flow8.5	1326.29	1110.38	1080.24	907.73	604.39

Table 4-25: Nusselt number relative to position on test section

Nusselt Number					
Length (m)	**0.2**	**0.4**	**`**	**0.8**	**1**
Flow3.5	17.79	20.71	21.86	17.71	12.42
Flow4.5	18.82	17.32	18.64	15.17	10.58
Flow5.5	19.00	19.00	18.12	15.05	10.25
Flow6.5	19.57	18.55	17.55	14.77	10.11
Flow7.5	19.57	18.46	17.63	14.82	10.03
Flow8.5	21.74	18.20	17.71	14.88	9.91

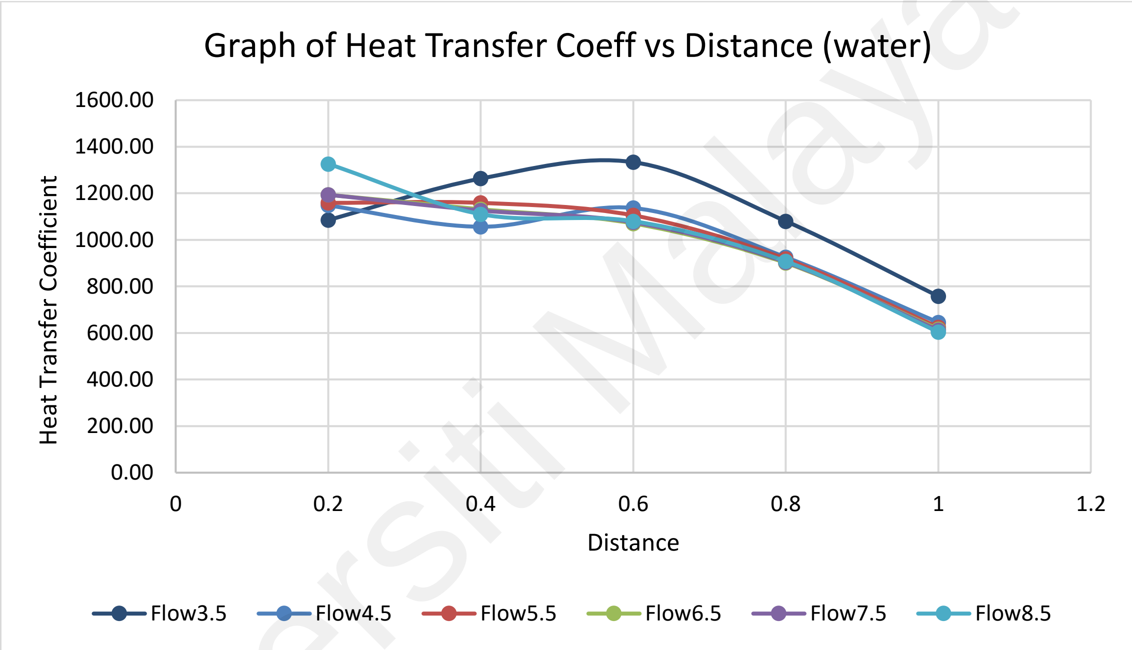

Figure 4.35: Graph of heat transfer against distance for water run

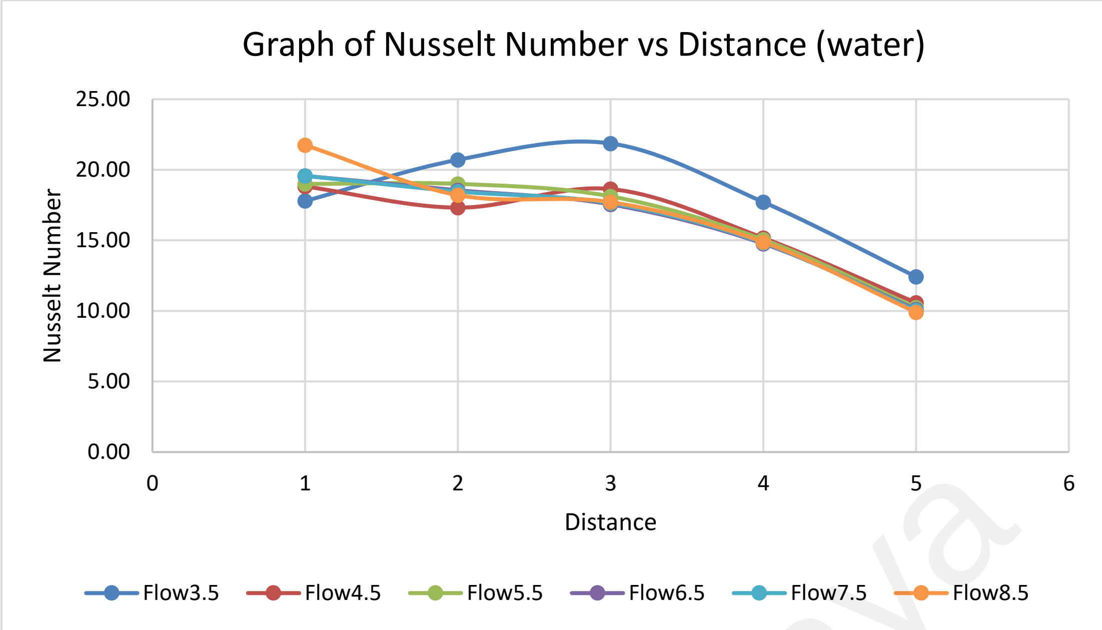

Figure 4.36: Graph of Nusselt number against distance for water run

From Figure 4.35 and 4.36, it can be seen that flowrate 8.5 is with one the highest heat transfer coefficient and Nusselt number. At 0.2 m, a value of 1326.29 W/m^{2}K was recorded. This corresponds to the highest of Nusselt number at the exact same local point on the test section. It can also be concluded that, the Nusselt number trendline follows that of heat transfer coefficient, whereby when flowrate is increased, the heat transfer coefficient and Nusselt number increases.

Flowrate 3.5 l/min does not sync with the other lines. This may be due to irregular placement of the thermocouple whereby the thermocouple is not properly in contact with the surface of the test section.

4.2.2.2 Square tube – water

Table 4-26: Temperature relative to flowrate and position on test section

Temperature (°C)					
Length (m)	**0.2**	**0.4**	**0.6**	**0.8**	**1**
Flow3.5	37.2	38.5	39.8	41.1	42.4
Flow4.5	37.0	38.2	39.4	40.6	41.8
Flow5.5	36.8	37.9	39.0	40.1	41.2
Flow6.5	37.2	38.0	38.8	39.6	40.4
Flow7.5	36.9	37.5	38.1	38.8	39.0
Flow8.5	37.0	37.3	37.6	38.6	38.2

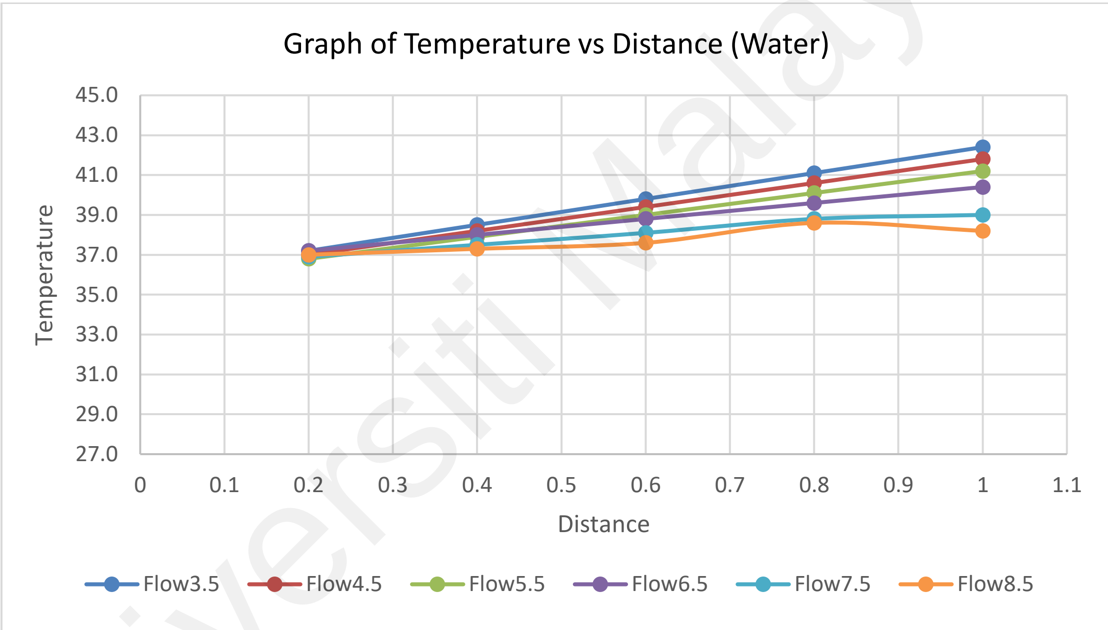

Figure 4.37: Graph of temperature against distance for water run

From Figure 4.37, it can be seen that, as the flowrate increases, the temperature decreases. This can be seen at 0.6m distance, whereby the temperature at the local point decreases throughout the flowrate. Considering flowrate 3.5 l/min, the temperature at 0.2m is 37.2 ºC which then eventually increases to 42.4 ºC. Similar trend of increasing surface temperature can be observed for the consecutive flowrates too whereby for instance temperature at 0.2 m for 7.5 L/min is 36.9 ºC which is followed by increasing temperature of 37.5 ºC, 38.1 ºC, 38.8 ºC and 39.0 ºC.

Table 4-27: Heat transfer coefficient relative to position on test section

Heat transfer Coeff (W/m²K)					
Length (m)	**0.2**	**0.4**	**0.6**	**0.8**	**1**
Flow3.5	768.4426	694.4444	633.4459	582.2981	538.7931
Flow4.5	781.2500	710.2273	651.0417	600.9615	558.0357
Flow5.5	794.4915	726.7442	669.6429	620.8609	578.7037
Flow6.5	768.4426	721.1538	679.3478	642.1233	608.7662
Flow7.5	787.8151	750.0000	715.6489	679.3478	669.6429
Flow8.5	781.2500	762.1951	744.0476	689.3382	710.2273

Table 4-28: Nusselt number relative to position on test section

Nusselt Number					
Length (m)	**0.2**	**0.4**	**0.6**	**0.8**	**1**
Flow3.5	12.59742	11.38434	10.38436	9.54587	8.83267
Flow4.5	12.80738	11.64307	10.67281	9.85183	9.14813
Flow5.5	13.02445	11.91384	10.97775	10.17805	9.48695
Flow6.5	12.59742	11.82219	11.13685	10.52661	9.97977
Flow7.5	12.91500	12.29508	11.73195	11.13685	10.97775
Flow8.5	12.80738	12.49500	12.19750	11.30063	11.64307

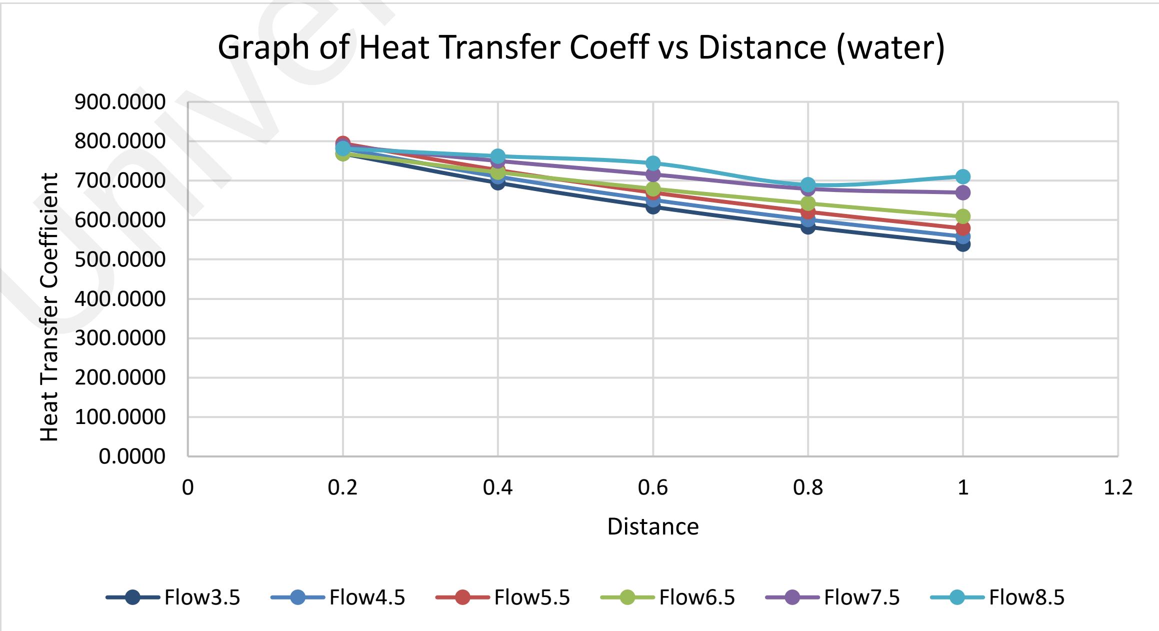

Figure 4.38: Graph of heat transfer coefficient against distance for water run

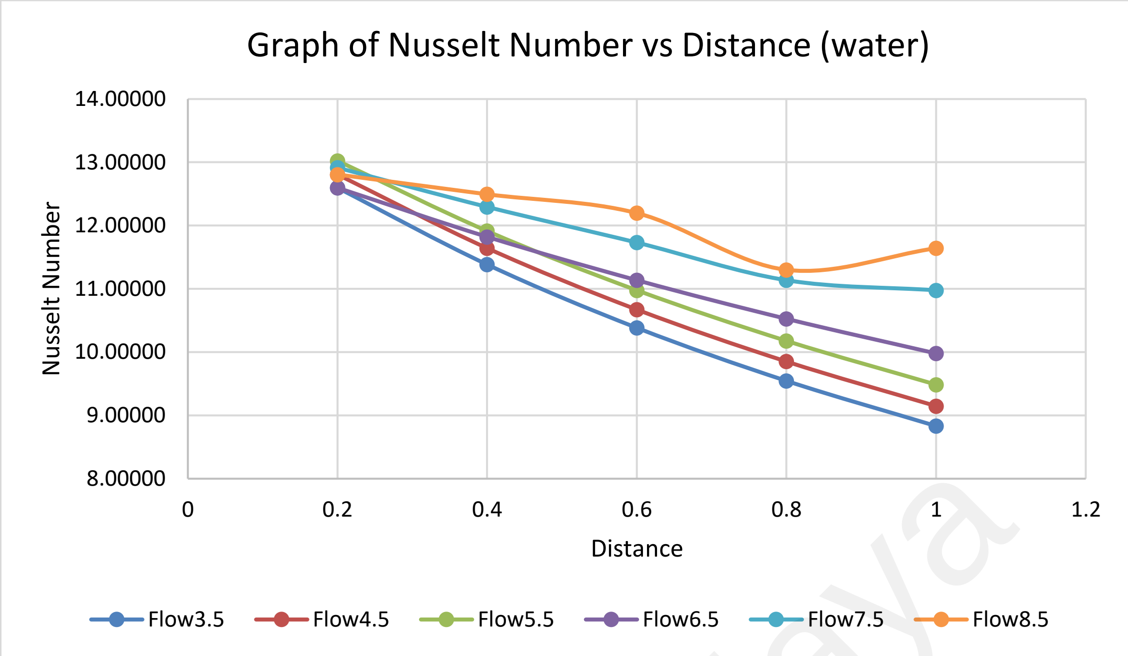

Figure 4.39: Graph of Nusselt number against distance for water run

From the graph, it can be observed that the heat transfer coefficient for the flow rate of 8.5 L/m is the highest in comparison to the other flowrates. The highest heat transfer coefficient is recorded at the 0.2 distance for the 8.5 L/m flowrate which is 781.21 W/(m^2K). The lowest heat transfer coefficient is recorded by the 3.5 L/m flowrate at the distance of 1m which is 538 W/(m^2K).

From the graph, it can be observed that the Nusselt number for the flow rate of 8.5 l/min is the highest in comparison to the other flowrates. The highest Nusselt number is recorded at the 0.6 distance for the 8.5 L/m flowrate which is 12.20. The lowest Nusselt number is recorded by the 3.5 L/m flowrate at the distance of 1m which is 8.83.

It can also be concluded that, the Nusselt number trendline follows that of heat transfer coefficient, whereby when flowrate is increased, the heat transfer coefficient and Nusselt number increases.

4.2.2.3 0.1% GNP – Circular tube

Table 4-29: Temperature relative to flowrate and position on test section

Temperature (°C)					
Length (m)	**0.2**	**0.4**	**0.6**	**0.8**	**1**
Flow3.5	39.5	39.8	40.5	41.0	41.5
Flow4.5	39.0	39.5	40.0	40.5	41.0
Flow5.5	38.5	39.0	39.5	40.0	40.5
Flow6.5	37.7	38.5	39.3	40.1	40.9
Flow7.5	37.3	38.0	38.7	39.4	40.1
Flow8.5	37.0	38.0	39.0	40.0	40.6

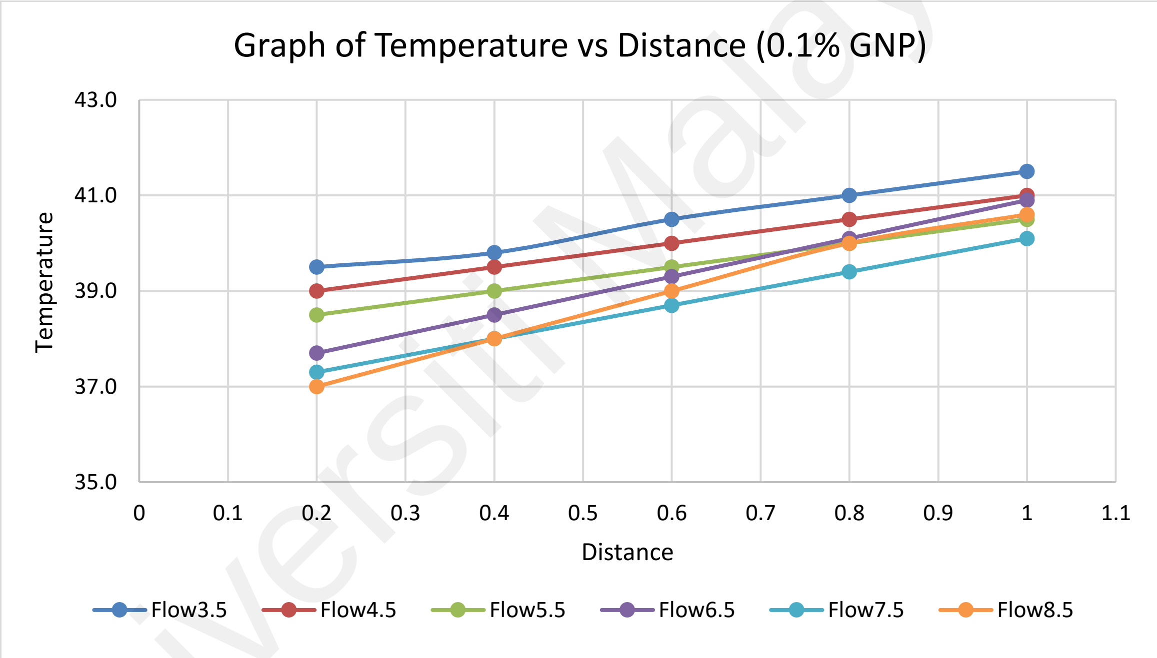

Figure 4.40: Graph of temperature against distance for 0.1% GNP run

From Figure 4.40, it can be seen that, as the flowrate increases, the temperature decreases. This can be seen at 0.2m distance, whereby the temperature at the local point decreases throughout the flowrate. Considering flowrate 3.5 l/min, the temperature at 0.2m is 39.5 ºC which then eventually increases to 41.5 ºC, similar trend of increasing surface temperature can be observed for the consecutive flowrates too whereby for instance temperature at 0.2 m for 8.5 L/min is 37.0 ºC which is followed by increment of temperature to 40.6 ºC

Table 4-30: Heat transfer coefficient relative to position on test section

Heat transfer Coeff (W/m^{2}K)					
Length (m)	**0.2**	**0.4**	**0.6**	**0.8**	**1**
Flow3.5	1387.98	1341.19	1243.40	1181.84	1126.10
Flow4.5	1404.31	1326.29	1256.49	1193.66	1136.82
Flow5.5	1421.03	1341.19	1269.85	1205.72	1147.75
Flow6.5	1510.96	1372.03	1256.49	1158.90	1075.37
Flow7.5	1570.61	1438.15	1326.29	1230.58	1147.75
Flow8.5	1681.21	1473.66	1311.72	1181.84	1115.57

Table 4-31: Nusselt number relative to position on test section

Nusselt Number					
Length (m)	**0.2**	**0.4**	**0.6**	**0.8**	**1**
Flow3.5	20.72	20.02	18.56	17.64	16.81
Flow4.5	20.96	19.80	18.75	17.82	16.97
Flow5.5	21.21	20.02	18.95	18.00	17.13
Flow6.5	22.55	20.48	18.75	17.30	16.05
Flow7.5	23.44	21.46	19.80	18.37	17.13
Flow8.5	25.09	21.99	19.58	17.64	16.65

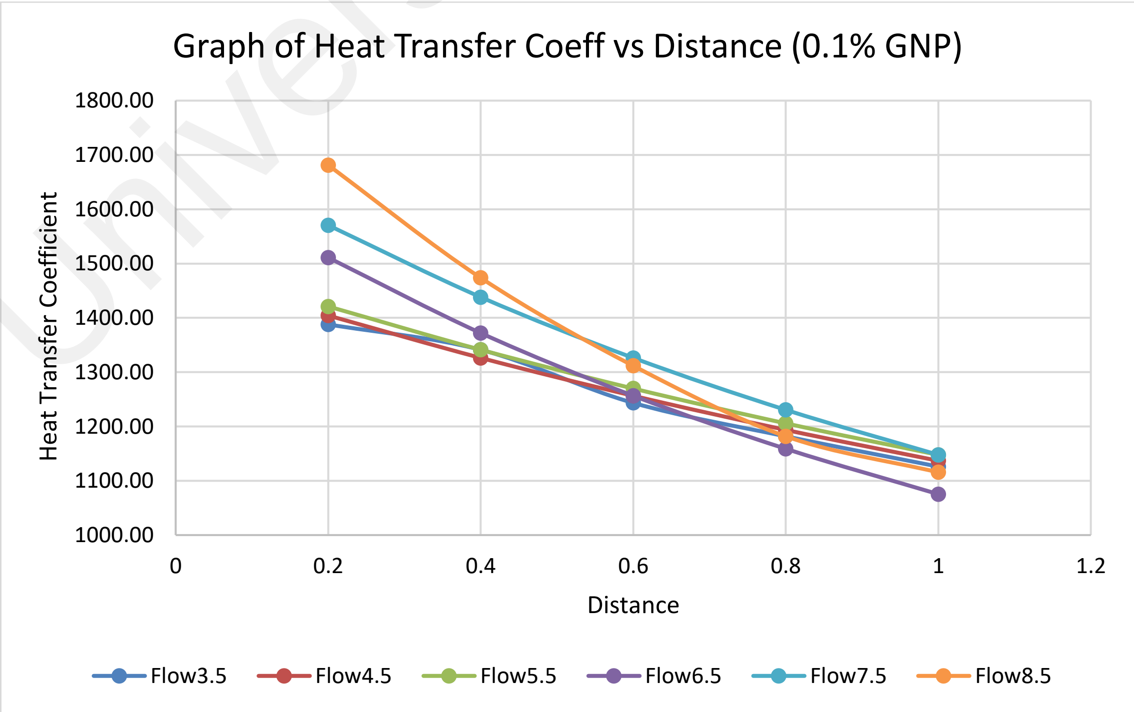

Figure 4.41: Graph of heat transfer coefficient against distance for 0.1% GNP

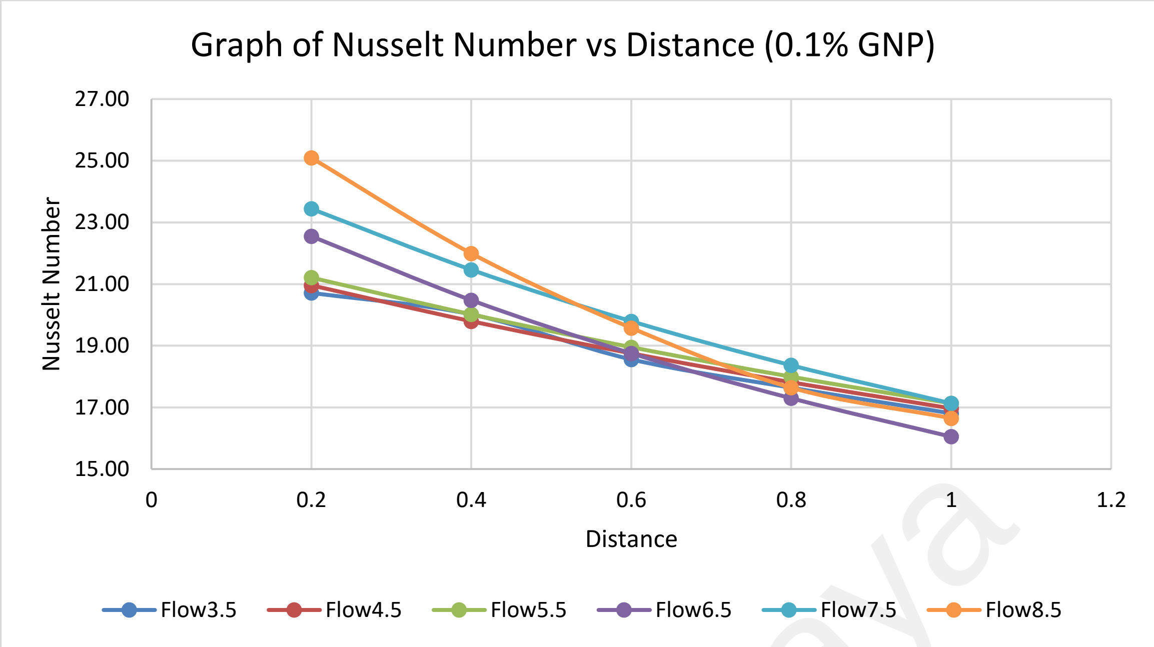

Figure 4.42: Graph of Nusselt number against distance for 0.1% GNP

From the graph, it can be observed that the heat transfer coefficient for the flow rate of 8.5 L/m is the highest in comparison to the other flowrates. The highest heat transfer coefficient is recorded at the 0.2 distance for the 8.5 L/m flowrate which is 1681.21 W/(m^2K). One of the lowest heat transfer coefficient is recorded by the 3.5 L/m flowrate at the distance of 1m which is 1126.10 W/(m^2K).

From the graph, it can be observed that the Nusselt number for the flow rate of 8.5 l/min is the highest in comparison to the other flowrates. The highest Nusselt number is recorded at the 0.6 distance for the 8.5 L/m flowrate which is 25.09. One of the lowest Nusselt number is recorded by the 3.5 L/m flowrate at the distance of 1m which is 16.81.

It can also be concluded that, the Nusselt number trendline follows that of heat transfer coefficient, whereby when flowrate is increased, the heat transfer coefficient and Nusselt number increases.

4.2.2.4 0.1% GNP – Square tube

Table 4-32: Temperature relative to flowrate and position on test section

Temperature (°C)					
Length (m)	**0.2**	**0.4**	**0.6**	**0.8**	**1**
Flow3.5	37.8	39.5	41.8	44.0	44.6
Flow4.5	37.5	38.2	38.9	39.6	40.3
Flow5.5	37.2	38.0	38.8	39.6	40.4
Flow6.5	38.0	38.5	39.0	39.4	40.0
Flow7.5	37.5	38.0	38.2	38.4	38.6
Flow8.5	37.0	37.5	38.0	38.5	39.0

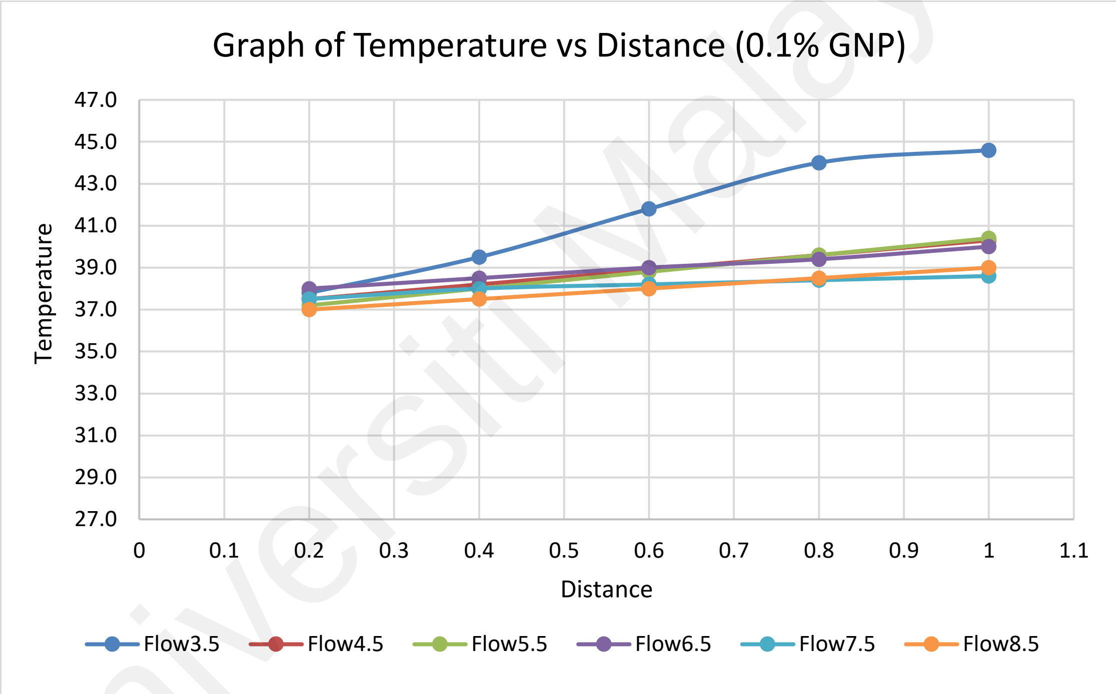

Figure 4.43: Graph of temperature against distance for 0.1% GNP run

From Figure 4.43, it can be seen that, as the flowrate increases, the temperature decreases. This can be seen at 0.2m distance, whereby the temperature at the local point decreases throughout the increasing flowrate. The similar can be seen at 1m too. Considering flowrate 3.5 l/min, the temperature at 0.2m is 37.8 °C which then eventually increases to 44.6 °C, similar trend of increasing surface temperature can be observed for the consecutive flowrates too whereby for instance temperature at 0.2 m for 8.5 L/min is 37.0 ºC which is followed by increment of temperature to 39.0 ºC.

Table 4-33: Heat transfer coefficient relative to position on test section

Heat transfer Coeff (W/m2K)					
Length (m)	**0.2**	**0.4**	**0.6**	**0.8**	**1**
Flow3.5	1065.3409	892.8571	732.4219	625.0000	600.9615
Flow4.5	986.8421	919.1176	860.0917	808.1897	762.1951
Flow5.5	1077.5862	986.8421	910.1942	844.5946	787.8151
Flow6.5	986.8421	937.5000	892.8571	860.0917	815.2174
Flow7.5	1008.0645	956.6327	937.5000	919.1176	901.4423
Flow8.5	1171.8750	1102.9412	1041.6667	986.8421	937.5000

Table 4-34: Nusselt number relative to position on test section

Nusselt Number					
Length (m)	**0.2**	**0.4**	**0.6**	**0.8**	**1**
Flow3.5	15.9006	13.3262	10.9317	9.3284	8.9696
Flow4.5	14.7290	13.7182	12.8372	12.0625	11.3760
Flow5.5	16.0834	14.7290	13.5850	12.6059	11.7584
Flow6.5	14.7290	13.9925	13.3262	12.8372	12.1674
Flow7.5	15.0457	14.2781	13.9925	13.7182	13.4544
Flow8.5	17.4907	16.4618	15.5473	14.7290	13.9925

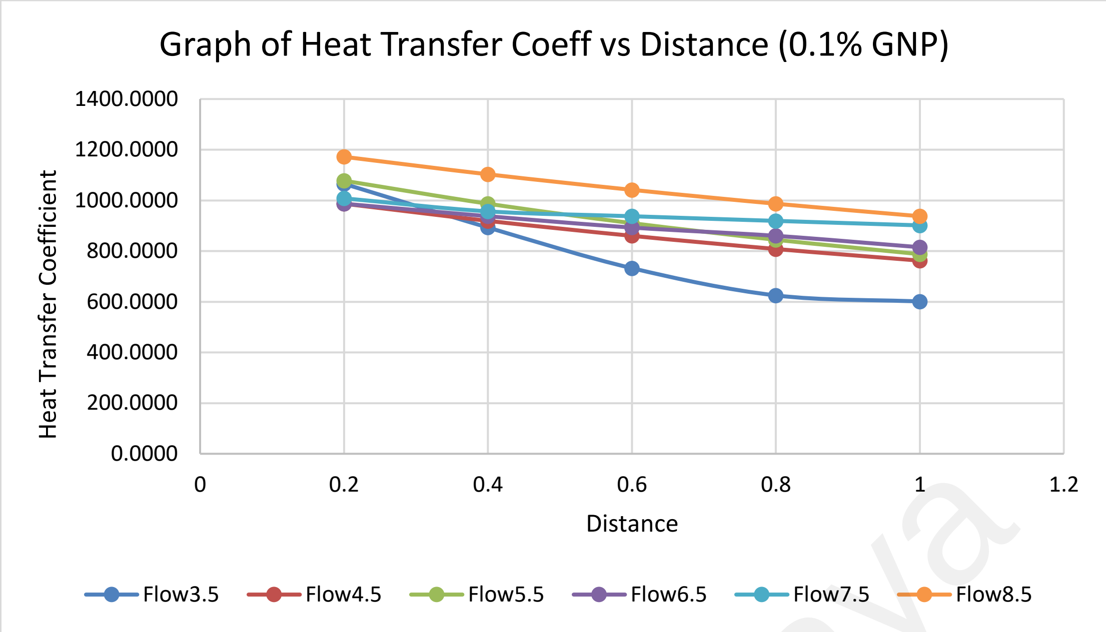

Figure 4.44: Graph of heat transfer coefficient against distance for 0.1% GNP

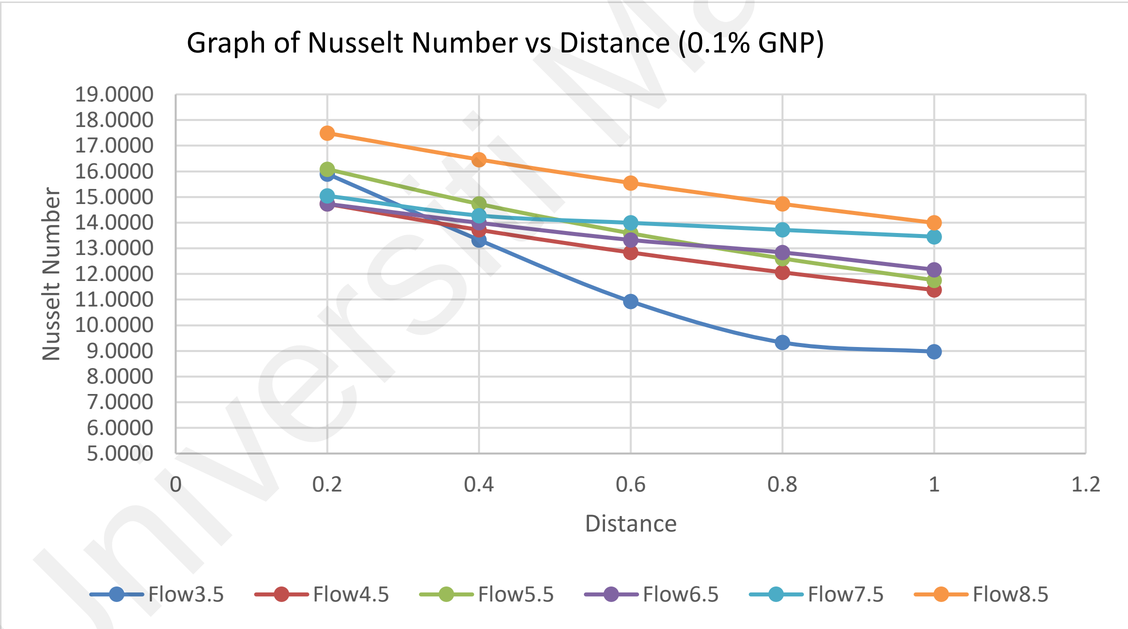

Figure 4.45: Graph of Nusselt number against distance for 0.1% GNP

From the graph, it can be observed that the heat transfer coefficient for the flow rate of 8.5 L/m is the highest in comparison to the other flowrates. The highest heat transfer coefficient is recorded at the 0.2 distance for the 8.5 L/m flowrate which is 1172.88 W/(m^2K). One of the lowest heat transfer coefficient is recorded by the 3.5 L/m flowrate at the distance of 1m which is 600.96 W/(m^2K).

From the graph, it can be observed that the Nusselt number for the flow rate of 8.5 l/min is the highest in comparison to the other flowrates. The highest Nusselt number is recorded at the 0.2 distance for the 8.5 L/m flowrate which is 17.49. One of the lowest Nusselt number is recorded by the 3.5 L/m flowrate at the distance of 1m which is 8.97.

It can also be concluded that, the Nusselt number trendline follows that of heat transfer coefficient, whereby when flowrate is increased, the heat transfer coefficient and Nusselt number increases.

4.2.2.5 0.05% GNP – Circular tube

Table 4-35: Temperature relative to flowrate and position on test section

Temperature (°C)					
Length (m)	**0.2**	**0.4**	**0.6**	**0.8**	**1**
Flow3.5	38.0	38.5	38.6	39.0	39.3
Flow4.5	37.8	38.3	38.5	38.9	39.3
Flow5.5	37.6	38.0	38.2	38.6	39.0
Flow6.5	37.4	37.8	38.0	38.4	38.8
Flow7.5	37.2	37.7	37.9	38.2	38.5
Flow8.5	37.0	37.3	37.5	38.0	38.4

Table 4-36: Heat transfer coefficient relative to position on test section

Heat transfer Coeff (W/m^2K)					
Length (m)	**0.2**	**0.4**	**0.6**	**0.8**	**1**
Flow3.5	1218.02	1158.90	1147.75	1108.66	1078.61
Flow4.5	1243.40	1181.84	1158.90	1115.57	1080.24
Flow5.5	1318.96	1263.13	1236.96	1187.72	1147.75
Flow6.5	1311.72	1256.49	1230.58	1181.84	1142.26
Flow7.5	1387.98	1311.72	1283.51	1243.40	1205.72
Flow8.5	1326.29	1283.51	1256.49	1197.65	1151.44

Table 4-37: Nusselt number relative to position on test section

Nusselt Number					
Length (m)	**0.2**	**0.4**	**0.6**	**0.8**	**1**
Flow3.5	18.74	17.83	17.66	17.06	16.59
Flow4.5	19.13	18.18	17.83	17.16	16.62
Flow5.5	20.29	19.43	19.03	18.27	17.66
Flow6.5	20.18	19.33	18.93	18.18	17.57
Flow7.5	21.35	20.18	19.75	19.13	18.55
Flow8.5	20.40	19.75	19.33	18.43	17.71

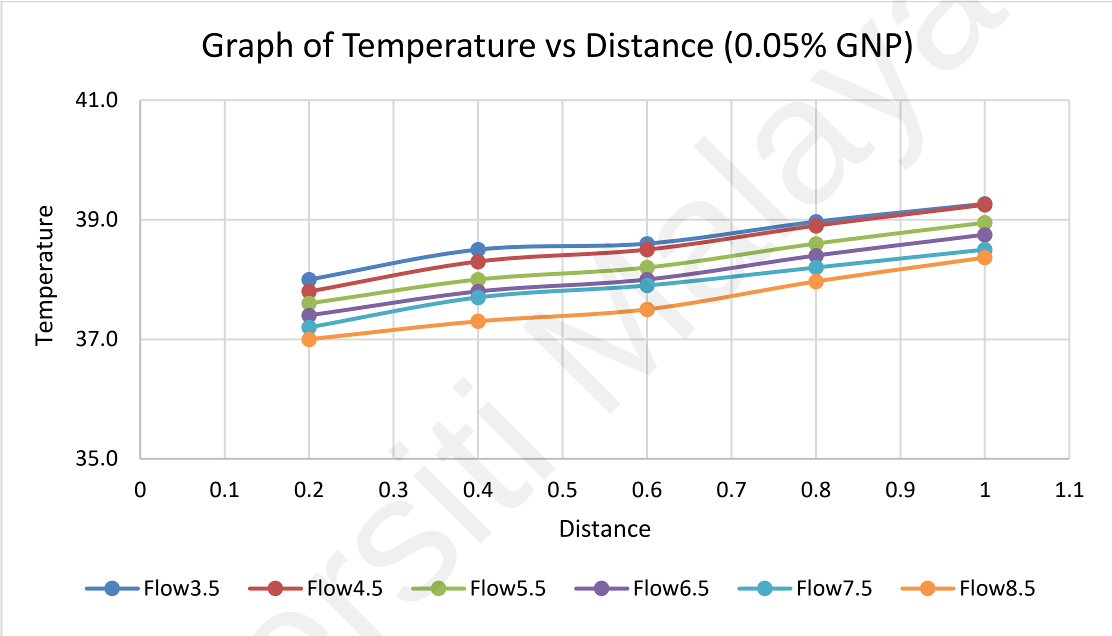

Figure 4.46: Graph of temperature against distance for 0.05% GNP run

From Figure 4.46, it can be seen that, as the flowrate increases, the temperature decreases. This can be seen at 0.2m distance, whereby the temperature at the local point decreases throughout the increasing flowrate. The similar can be seen at 1m too. Considering flowrate 3.5 l/min, the temperature at 0.2m is 38.0 °C which then eventually increases to 39.3 °C, similar trend of increasing surface temperature can be observed for the consecutive flowrates too.

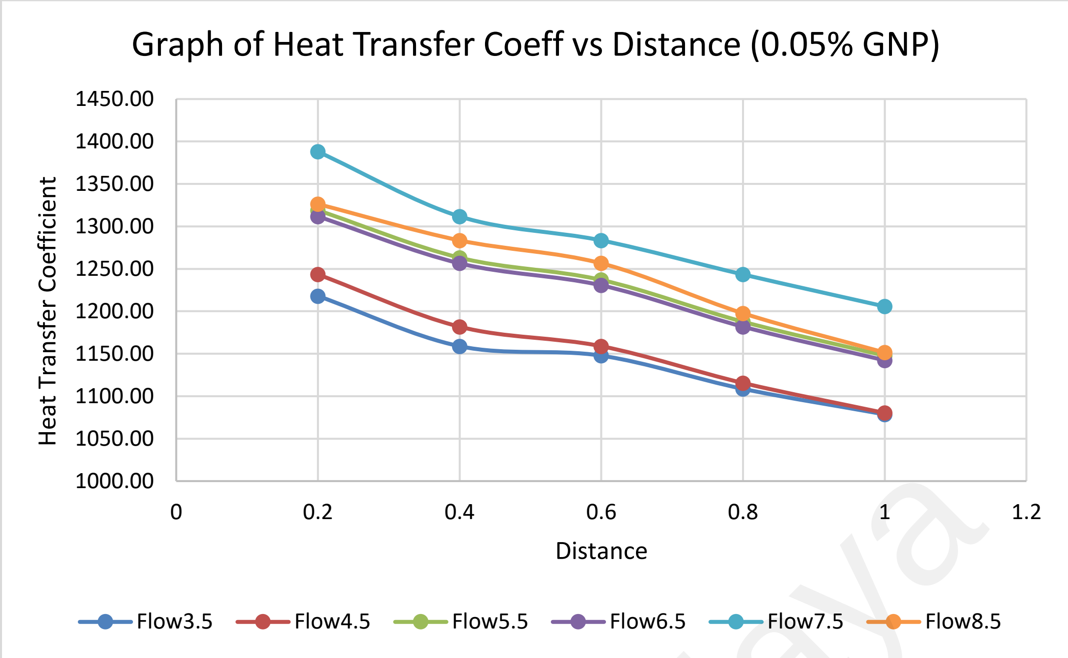

Figure 4.47: Graph of heat transfer coefficient against distance for 0.05% GNP

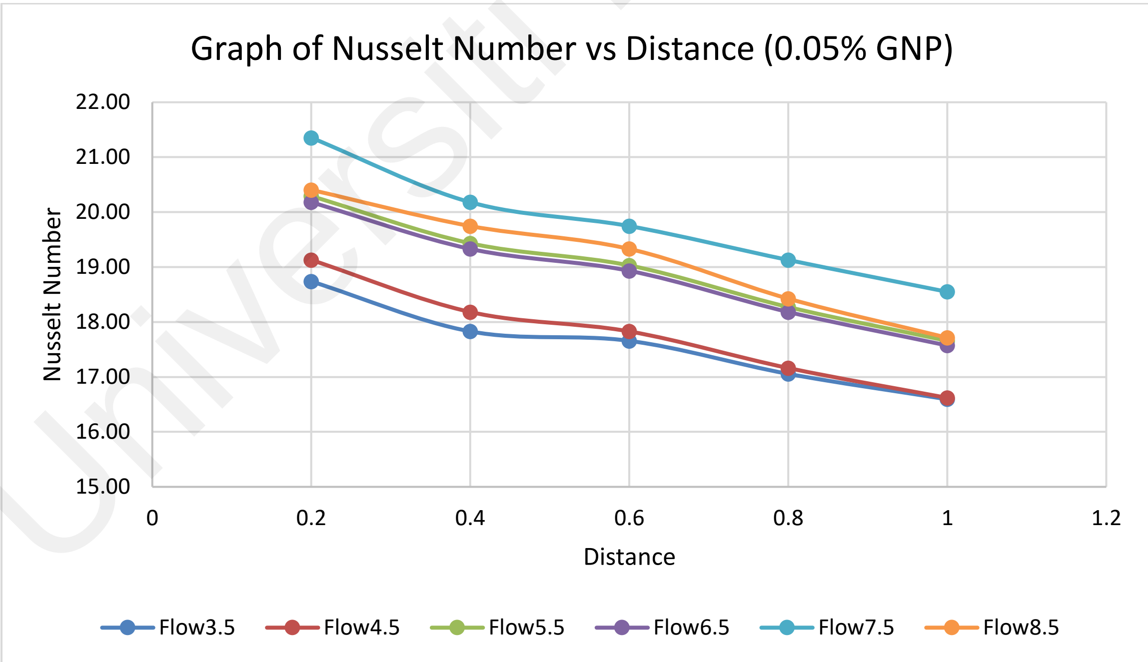

Figure 4.48: Graph of Nusselt number against distance for 0.05% GNP

From the graph, it can be observed that the heat transfer coefficient for the flow rate of 8.5 L/m is the highest in comparison to the other flowrates. The highest heat transfer coefficient is recorded at the 0.2 distance for the 8.5 L/m flowrate which is 1326.29

W/(m²K). The data for 7.5 l/min is avoided as there seems to be anomaly in the reading recorded by the thermocouple. One of the lowest heat transfer coefficient is recorded by the 3.5 L/m flowrate at the distance of 1m which is 1078.61 W/(m²K).

From the graph, it can be observed that the Nusselt number for the flow rate of 8.5 l/min is the highest in comparison to the other flowrates. The highest Nusselt number is recorded at the 0.2 distance for the 8.5 L/m flowrate which is 20.40. One of the lowest Nusselt number is recorded by the 3.5 L/m flowrate at the distance of 1m which is 16.59.

It can also be concluded that, the Nusselt number trendline follows that of heat transfer coefficient, whereby when flowrate is increased, the heat transfer coefficient and Nusselt number increases.

4.2.2.6 0.05% GNP – Square tube

Table 4-38: Temperature relative to flowrate and position on test section

Temperature (°C)					
Length (m)	**0.2**	**0.4**	**0.6**	**0.8**	**1**
Flow3.5	40.0	40.9	42.5	45.1	48.9
Flow4.5	37.9	40.0	42.0	44.7	48.0
Flow5.5	37.5	39.5	41.7	44.3	47.0
Flow6.5	36.0	38.7	41.5	43.5	45.5
Flow7.5	34.7	38.0	41.3	44.2	46.3
Flow8.5	33.5	37.3	40.0	41.7	43.6

Table 4-39: Heat transfer coefficient relative to position on test section

Heat transfer Coeff (W/m^2K)					
Length (m)	**0.2**	**0.4**	**0.6**	**0.8**	**1**
Flow3.5	884.4340	815.2174	715.6489	597.1338	480.7692
Flow4.5	1053.3708	852.2727	721.1538	597.1338	493.4211
Flow5.5	1065.3409	868.0556	721.1538	600.9615	512.2951
Flow6.5	1255.5804	916.1238	721.1538	625.0000	551.4706
Flow7.5	1508.0429	983.3916	729.5720	597.1338	526.6854
Flow8.5	1714.9390	1004.4643	781.2500	684.3066	600.9615

Table 4-40: Nusselt number relative to position on test section

Nusselt Number					
Length (m)	**0.2**	**0.4**	**0.6**	**0.8**	**1**
Flow3.5	13.2005	12.1674	10.6813	8.9124	7.1757
Flow4.5	15.7220	12.7205	10.7635	8.9124	7.3645
Flow5.5	15.9006	12.9561	10.7635	8.9696	7.6462
Flow6.5	18.7400	13.6735	10.7635	9.3284	8.2309
Flow7.5	22.5081	14.6775	10.8891	8.9124	7.8610
Flow8.5	25.5961	14.9920	11.6604	10.2135	8.9696

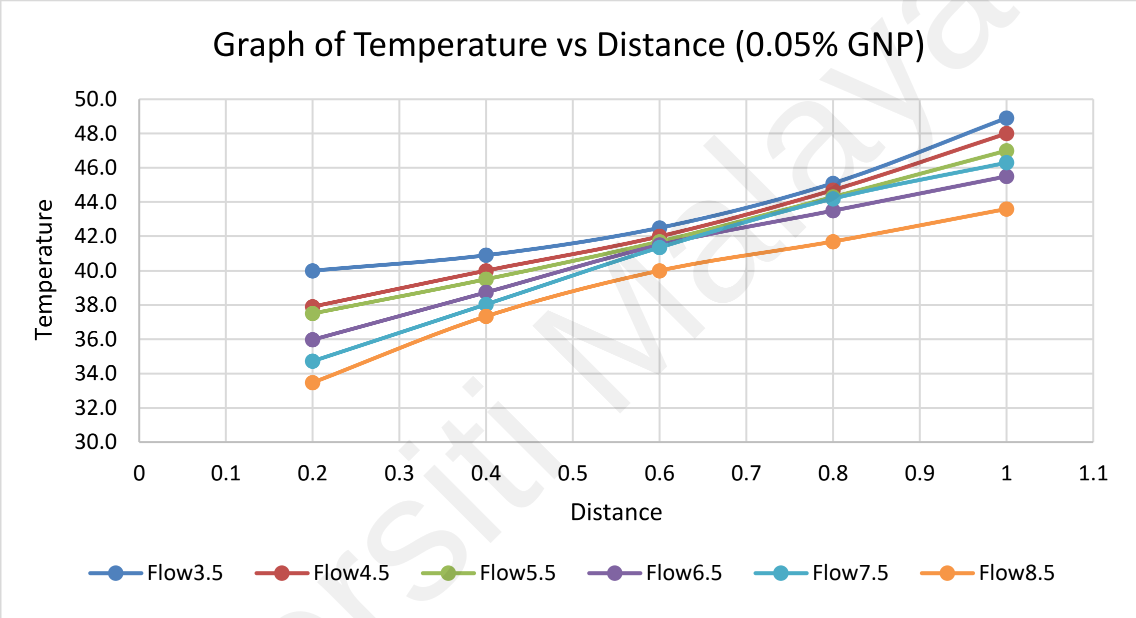

Figure 4.49: Graph of temperature against distance for 0.05% GNP run

From Figure 4.49, it can be seen that, as the flowrate increases, the temperature decreases. This can be seen at 0.2m distance, whereby the temperature at the local point decreases throughout the increasing flowrate. The similar can be seen at 1m too. Considering flowrate 3.5 l/min, the temperature at 0.2m is 40.0 ºC which then eventually increases to 48.9 ºC, similar trend of increasing surface temperature can be observed for the consecutive flowrates too.

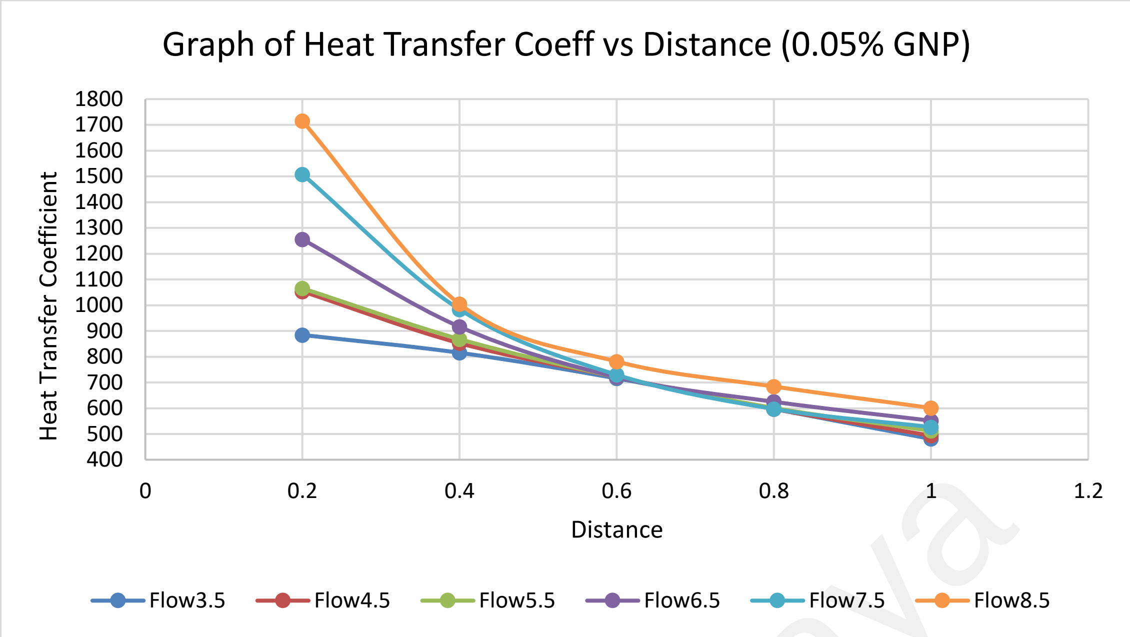

Figure 4.50: Graph of heat transfer coefficient against distance for 0.05% GNP

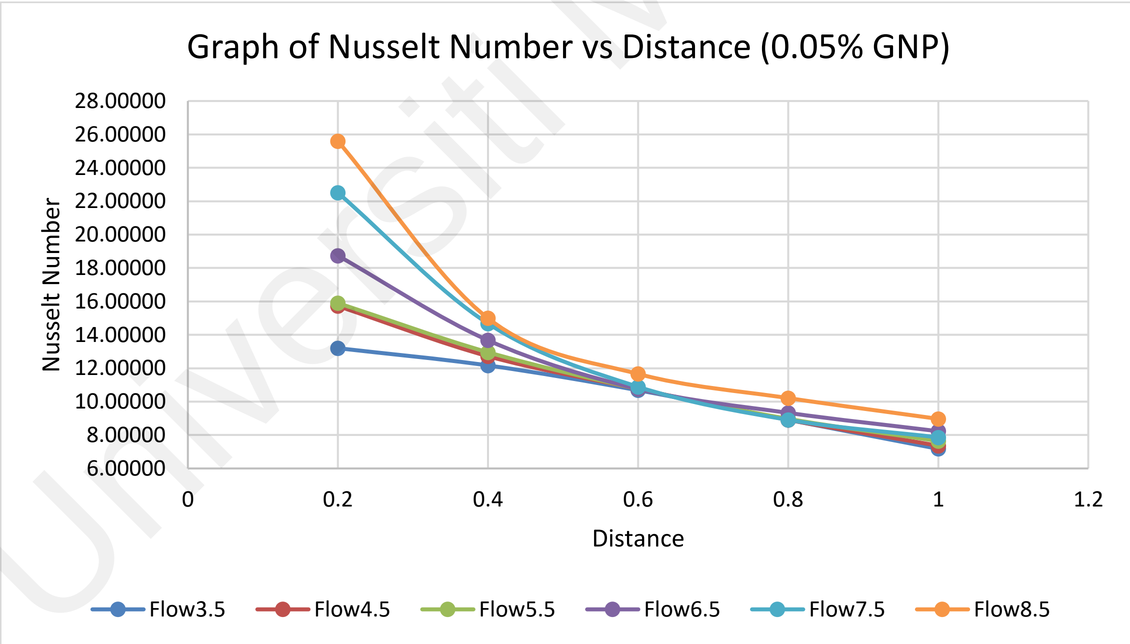

Figure 4.51: Graph of Nusselt number against distance for 0.05% GNP

From the graph, it can be observed that the heat transfer coefficient for the flow rate of 8.5 L/m is the highest in comparison to the other flowrates. The highest heat transfer coefficient is recorded at the 0.2 distance for the 8.5 L/m flowrate which is 1714.94

W/(m^2K). One of the lowest heat transfer coefficient is recorded by the 3.5 L/m flowrate at the distance of 1m which is 480.77 W/(m^2K).

From the graph, it can be observed that the Nusselt number for the flow rate of 8.5 l/min is the highest in comparison to the other flowrates. The highest Nusselt number is recorded at the 0.2 distance for the 8.5 L/m flowrate which is 25.60. One of the lowest Nusselt number is recorded by the 3.5 L/m flowrate at the distance of 1m which is 7.18.

It can also be concluded that, the Nusselt number trendline follows that of heat transfer coefficient, whereby when flowrate is increased, the heat transfer coefficient and Nusselt number increases.

4.2.3 Pressure Loss in Flow Passages

As any fluid flows in a passage it will be subjected to pressure drop. This pressure drop results from the resistance the flow undergoes throughout the flow passage. Commonly friction between the fluid and the wall is one of the major resistance the flow undergoes

When fluid flows through a pipe there will be a pressure drop that occurs as a result of resistance to flow. There may also be a pressure gain/loss due a change in elevation between the start and end of the pipe. ... Friction between the fluid and the wall of the pipe. Outcome of the pressure drop is plotted against flowrate for water and 0.1% concentration.

Table 4-41: Pressure Drop in Circular Tubes

	Pressure Drop, ▲p			
Velocity	**Water**	**0.10%**	**0.05%**	**0.03%**
0.7427231	1615.0	2620.0	1505.0	1525.0
0.96554	2070.0	2970.0	2620.0	2230.0
1.1671362	2565.0	3130.0	2810.0	2900.0
1.3793428	3240.0	3540.0	3330.0	3480.0
1.5915494	4250.0	4100.0	4020.0	3850.0
1.803756	5130.0	4800.0	5040.0	4725.0

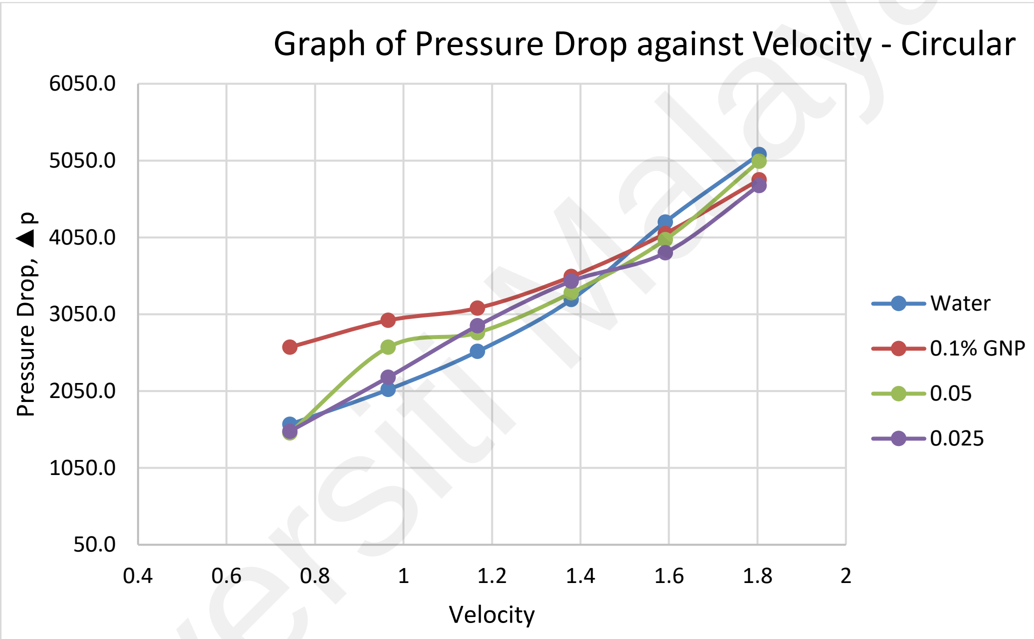

Figure 4.52: Graph of Pressure Drop against Flowrate – Circular tube

Table 4-42: Pressure Drop in Square Tubes

	Pressure Drop, ▲p			
Velocity	**Water**	**0.10%**	**0.05%**	**0.03%**
0.742723	1510.0	3430.0	3420.0	3380.0
0.96554	1920.0	3940.0	4200.0	3600.0
1.167136	2480.0	4300.0	4100.0	4000.0
1.379343	3350.0	4450.0	4470.0	4500.0
1.591549	4300.0	5080.0	4980.0	4720.0
1.803756	5050.0	6080.0	5720.0	5710.0

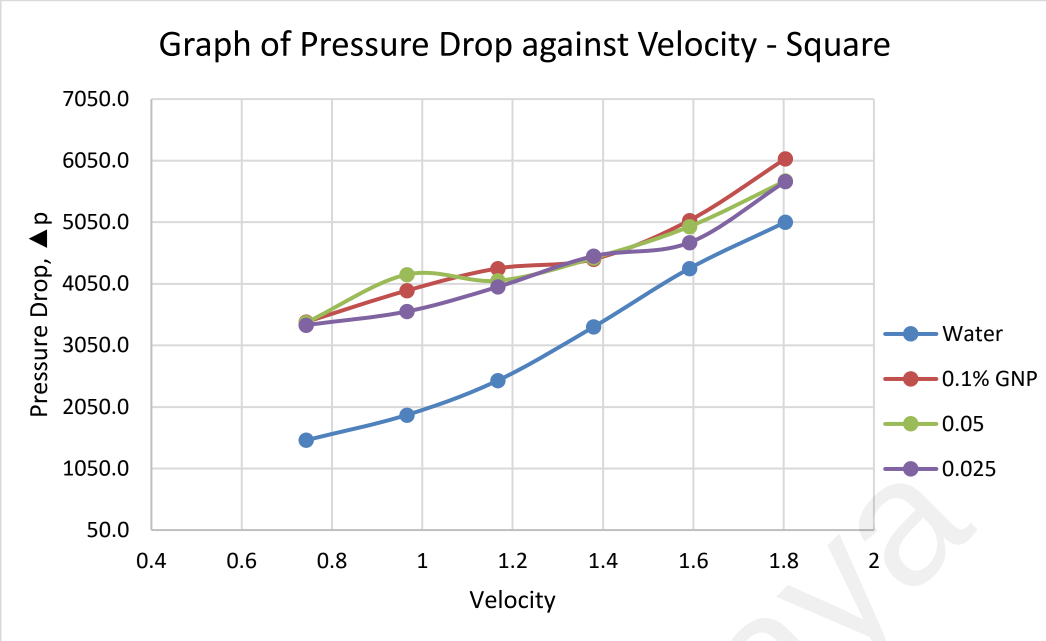

Figure 4.53: Graph of Pressure Drop against Flowrate – Square tube

From Figure 4.52 and 4.53, it can be observed that as the velocity increases, the pressure drop increases. Pressure drop is directly proportional to velocity. Similar scenario is observed on the circular and square tube flows.

4.3 Summary

As a conclusion, it can be said that as the flowrate increases, the temperature decreases. But for a given flowrate, the temperature increases across the test section. This can be seen from the temperatures at the local points on the test section. Comparison of heat transfer coefficient and Nusselt number for all concentrations

Table 4-43: Average heat transfer coefficient number against the velocity and concentration for circular tube

Velocity (m/s)	H avg (water)	H avg (0.1%)	H avg (0.05%)	H avg (0.025%)
0.7427	929.2916	1256.1021	1142.3889	1054.0796
0.9549	975.4359	1263.5138	1155.9892	1054.0796
1.1884	983.5819	1277.1088	1230.9058	1103.6041
1.3793	1008.8690	1274.7486	1224.5773	1103.6041
1.5915	1008.8690	1342.6755	1286.4641	1124.7652
1.8038	1103.6041	1352.8007	1243.0764	1158.1025

Table 4-44: Average Nusselt number against the velocity and concentration for circular tube

Velocity (m/s)	Nu avg (Water)	Nu avg (0.1%)	Nu avg (0.05%)	Nu avg (0.025%)
0.7427	15.2343	18.7478	17.5752	16.7314
0.9549	15.9908	18.8584	17.7844	16.7314
1.1884	16.1243	19.0613	18.9370	17.5175
1.3793	16.5388	19.0261	18.8397	17.5175
1.5915	16.5388	20.0399	19.7918	17.8534
1.8038	18.0919	20.1911	19.1243	18.3826

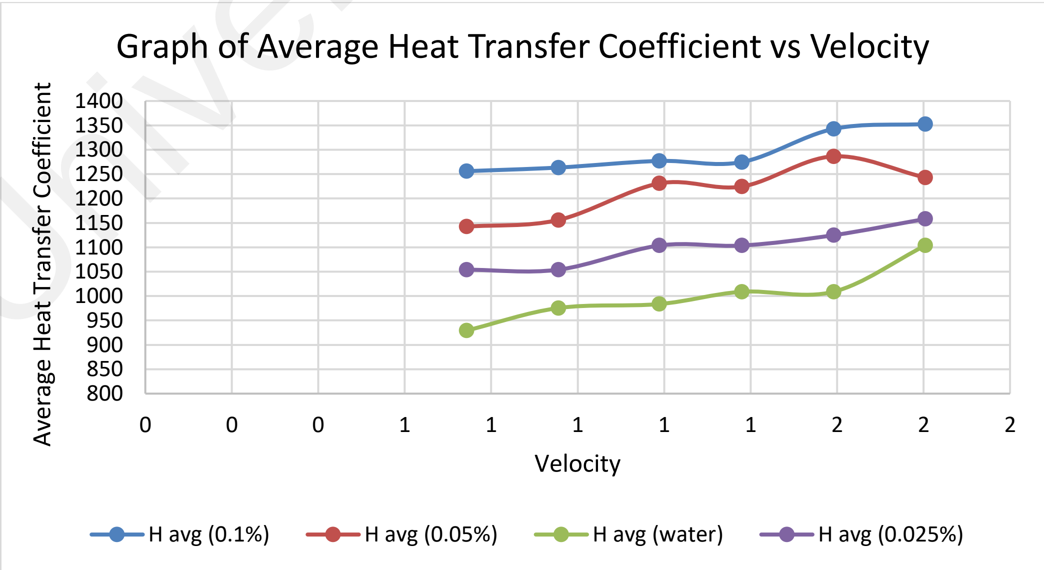

Figure 4.54: Graph of average heat transfer coefficient against velocity

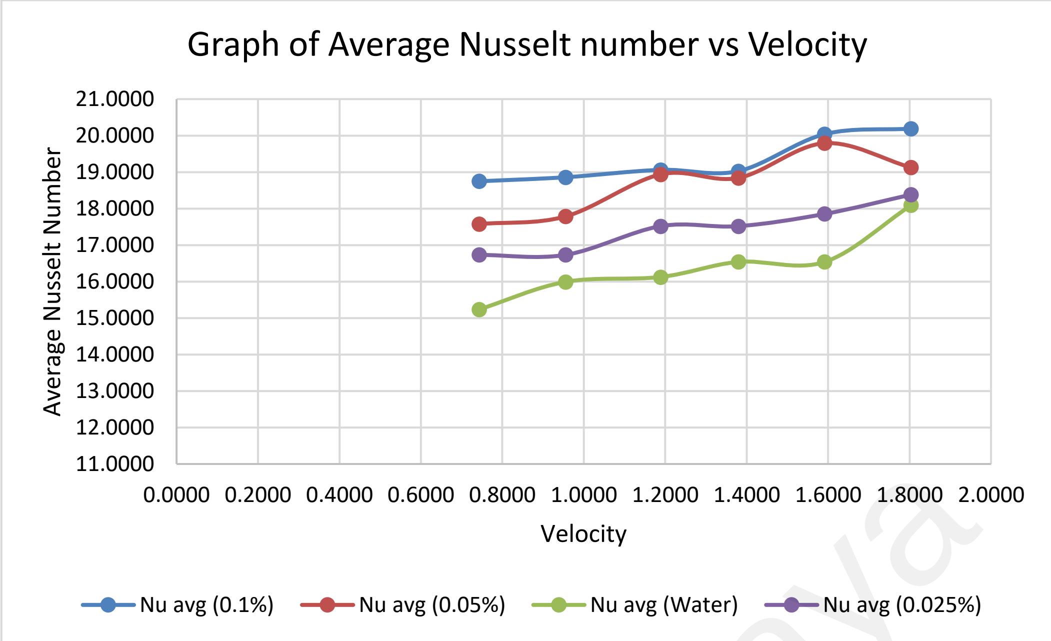

Figure 4.55: Graph of average Nusselt number against velocity

Table 4-45: Average heat transfer coefficient number against the velocity and concentration for square tube

Velocity (m/s)	H avg (water)	H avg (0.1%)	H avg (0.05%)	H avg (0.025%)
0.7427	643.4849	783.3163	698.6406	653.3592
0.9549	660.3032	867.2873	743.4704	672.8695
1.1884	678.0886	921.4064	753.5614	701.0961
1.3793	683.9668	898.5017	813.8657	723.6344
1.5915	720.4909	944.5514	868.9651	751.9140
1.8038	737.4116	1048.1650	957.1843	778.2152

Table 4-46: Average Nusselt number against the velocity and concentration for square tube

Velocity (m/s)	Nu avg (Water)	Nu avg (0.1%)	Nu avg (0.05%)	Nu avg (0.025%)
0.7427	10.5489	11.6913	12.1674	9.7516
0.9549	10.8246	12.9446	12.7205	10.0428
1.1884	11.1162	13.7523	12.9561	10.4641
1.3793	11.2126	13.4105	13.6735	10.8005
1.5915	11.8113	14.0978	14.6775	11.2226
1.8038	12.0887	15.6443	14.9920	11.6152

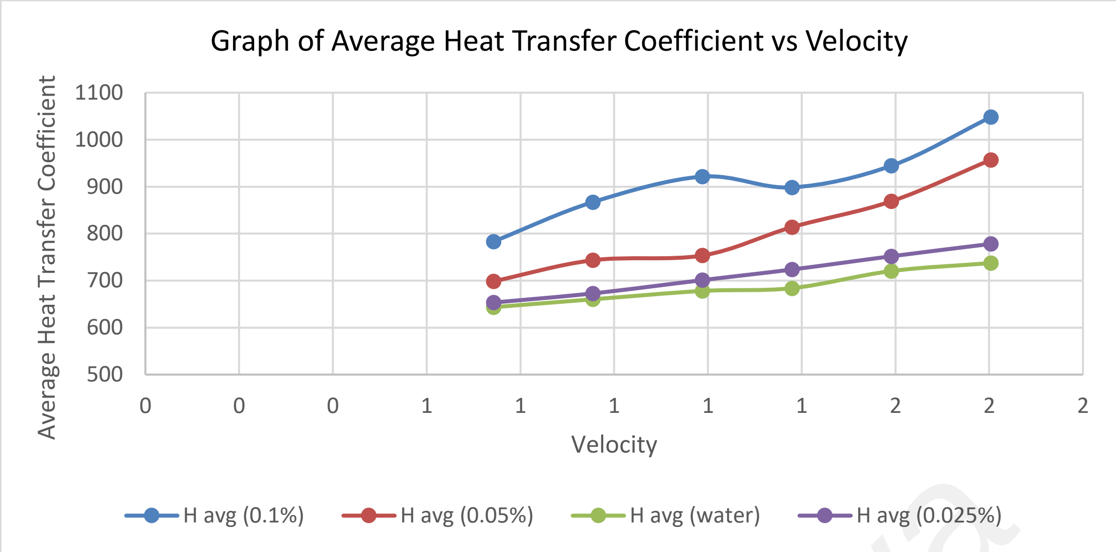

Figure 4.56: Graph of average heat transfer coefficient against velocity

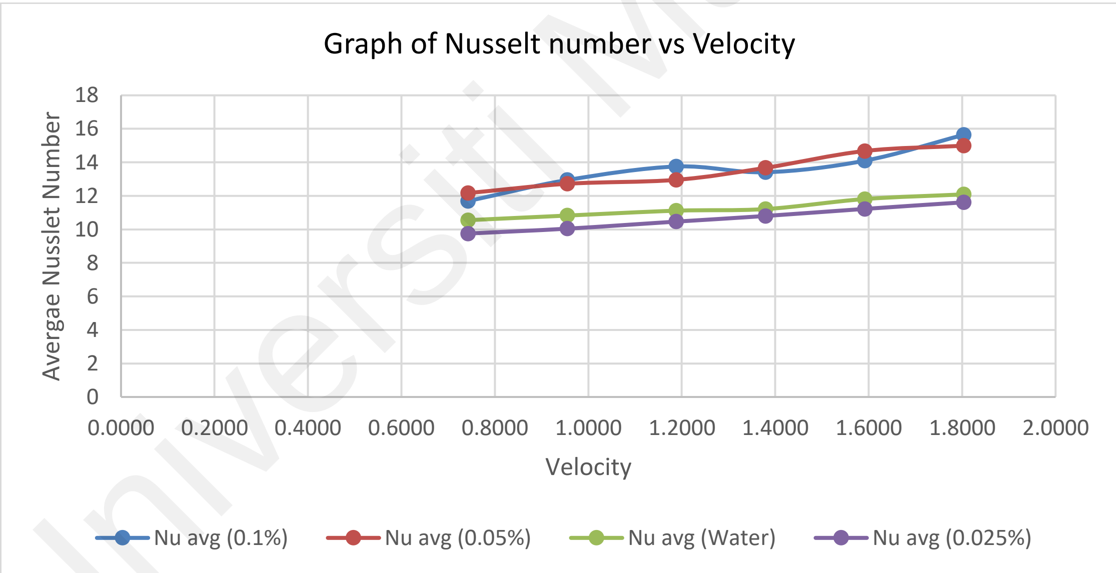

Figure 4.57: Graph of average Nusselt number against velocity

From the graphs, it can be seen that the average heat transfer coefficient and average Nusselt number increases as the velocity increases for all concentration. This suggests that, concentration does affect the overall heat transfer of a working fluid

CHAPTER 5: CONCLUSION

The objectives of the study is thoroughly discussed and reviewed in results and discussion section.

As a conclusion, it can be said that, concentration of nanofluid does have a significant effect on the heat transfer capacity of the particular fluid. This is because, as the concentration increases, the number of nanoparticles in the fluid increases too. This enables the nanoparticle to absorb more heat than nanofluid with lower concentration.

In addition, the geometry of the test section is also a deciding factor on the heat transfer rate. Based on the study, it was evident that, circular tube have a more promising heat transfer capability when compare to square. This can be proven based on the high heat transfer coefficient and Nusselt number obtained from the test runs. The reason behind this geometry effect is that, circular tube has more surface area than the square tube.

To support this arguments, simulation done on ANSYS Fluent also indicate that nanofluid with high concentration have better thermal properties which assist for much improved heat transfer. Simulation also indicated that circular tube is a better heat transfer geometry than square.

5.1 Recommendations

Current work only focused on improving the working fluid and the geometry of the test section. More researches shall be done to study the most suitable base fluid such as distilled water or any oil based fluid which may improve the overall heat transfer much better than phenolic acid treated GNP. Besides that, the material used to fabrication heat exchanger shall be looked into too. Material with better heat conductivity shall be used for much improved cooling.

CHAPTER 6: REFERENCE

Al-aswadi, A. A., Mohammed, H. A., Shuaib, N. H., & Campo, A. (2010). Laminar forced convection flow over a backward facing step using nanofluids. *International Communications in Heat and Mass Transfer, 37*(8), 950-957. doi:https://doi.org/10.1016/j.icheatmasstransfer.2010.06.007

Assael, M., Metaxa, I., Arvanitidis, J., Christofilos, D., & Lioutas, C. (2005). Thermal Conductivity Enhancement in Aqueous Suspensions of Carbon Multi-Walled and Double-Walled Nanotubes in the Presence of Two Different Dispersants. *International Journal of Thermophysics, 26*, 647-664. doi:10.1007/s10765-005-5569-3

Chen, H., Ding, Y., He, Y., & Tan, C. (2007). Rheological behaviour of ethylene glycol based titania nanofluids. *Chemical Physics Letters, 444*(4), 333-337. doi:https://doi.org/10.1016/j.cplett.2007.07.046

Chen, L., Xie, H., Li, Y., & Yu, W. (2008). Nanofluids containing carbon nanotubes treated by mechanochemical reaction. *Thermochimica Acta, 477*(1), 21-24. doi:https://doi.org/10.1016/j.tca.2008.08.001

Cheremisinoff, N. P. (1986). *Encyclopedia of fluid mechanics Volume 2 Dynamics of single-fluid flows and mixing*. United States: Gulf Publishing Co.

Chevalier, J., Tillement, O., & Ayela, F. (2007). Rheological properties of nanofluids flowing through microchannels. *Applied Physics Letters, 91*(23), 233103. doi:10.1063/1.2821117

Duangthongsuk, W., & Wongwises, S. (2009). Heat transfer enhancement and pressure drop characteristics of TiO2–water nanofluid in a double-tube counter flow heat exchanger. *International Journal of Heat and Mass Transfer, 52*(7), 2059-2067. doi:https://doi.org/10.1016/j.ijheatmasstransfer.2008.10.023

Dul, S., Fambri, L., Merlini, C., Barra, G., Bersani, M., Vanzetti, L., & Pegoretti, A. (2017). *Effect of Graphene Nanoplatelets Structure on the Properties of Acrylonitrile-Butadiene-Styrene Composites*.

Eastman, J., S. Choi, U., Li, S., J. Thompson, L., & Lee, S. (1996). Enhanced Thermal Conductivity Through the Development of Nanofluids. *MRS Proceedings, 457*. doi:10.1557/PROC-457-3

Eastman, J., U. S. Choi, S., Li, S., Yu, W., & J. Thompson, L. (2001). Anomalously Increased Effective Thermal Conductivity of Ethylene Glycol-Based Nanofluids Containing Copper Nanoparticles. *Applied Physics Letters, 78*, 718-720. doi:10.1063/1.1341218

Gangadevi, R., Vinayagam, B. K., & Senthilraja, S. (2018). Effects of sonication time and temperature on thermal conductivity of CuO/water and Al2O3/water nanofluids with and without surfactant. *Materials Today: Proceedings, 5*(2, Part 3), 9004-9011. doi:https://doi.org/10.1016/j.matpr.2017.12.347

Georgakilas, V., Otyepka, M., Bourlinos, A. B., Chandra, V., Kim, N., Kemp, K. C., . . . Kim, K. S. (2012). Functionalization of Graphene: Covalent and Non-Covalent Approaches, Derivatives and Applications. *Chemical Reviews, 112*(11), 6156-6214. doi:10.1021/cr3000412

Ghadimi, A., Saidur, R., & Metselaar, H. S. C. (2011). A review of nanofluid stability properties and characterization in stationary conditions. *International Journal of Heat and Mass Transfer, 54*(17), 4051-4068. doi:https://doi.org/10.1016/j.ijheatmasstransfer.2011.04.014

Godson, L., Raja, B., Lal, D. M., & Wongwises, S. (2010). Experimental Investigation on the Thermal Conductivity and Viscosity of Silver-Deionized Water Nanofluid. *Experimental Heat Transfer, 23*(4), 317-332. doi:10.1080/08916150903564796

Hosseini, M., Abdelrazek, A. H., Sadri, R., Mallah, A. R., Kazi, S. N., Chew, B. T., . . . Yusoff, N. (2018). Numerical study of turbulent heat transfer of nanofluids containing eco-friendly treated carbon nanotubes through a concentric annular heat exchanger. *International Journal of Heat and Mass Transfer, 127*, 403-412. doi:https://doi.org/10.1016/j.ijheatmasstransfer.2018.08.040

Hwang, Y., Lee, J.-K., Lee, J.-K., Jeong, Y.-M., Cheong, S.-i., Ahn, Y.-C., & Kim, S. H. (2008). Production and dispersion stability of nanoparticles in nanofluids. *Powder Technology, 186*(2), 145-153. doi:https://doi.org/10.1016/j.powtec.2007.11.020

Jiang, L., Gao, L., & Sun, J. (2003). Production of aqueous colloidal dispersions of carbon nanotubes. *Journal of Colloid and Interface Science, 260*(1), 89-94. doi:https://doi.org/10.1016/S0021-9797(02)00176-5

Khoshvaght-Aliabadi, M. (2014). Influence of different design parameters and Al2O3-water nanofluid flow on heat transfer and flow characteristics of sinusoidal-corrugated channels. *Energy Conversion and Management, 88*, 96-105. doi:https://doi.org/10.1016/j.enconman.2014.08.042

Kulkarni, S., Chapman, C., & Shah, H. (2016). *Computational Fluid Dynamics (CFD) Mesh Independency Study of A Straight Blade Horizontal Axis Tidal Turbine*.

Kumar, N., Singh, P., Redhewal, A. K., & Bhandari, P. (2015). A Review on Nanofluids Applications for Heat Transfer in Micro-channels. *Procedia Engineering, 127*, 1197-1202. doi:https://doi.org/10.1016/j.proeng.2015.11.461

Le, J.-L., Du, H., & Pang, S. D. (2014). Use of 2D Graphene Nanoplatelets (GNP) in cement composites for structural health evaluation. *Composites Part B: Engineering, 67*, 555-563. doi:https://doi.org/10.1016/j.compositesb.2014.08.005

Li, X., Zhu, D., & Wang, X. (2007). Evaluation on dispersion behavior of the aqueous copper nano-suspensions. *Journal of Colloid and Interface Science, 310*(2), 456-463. doi:https://doi.org/10.1016/j.jcis.2007.02.067

Li, Y., Zhou, J. e., Tung, S., Schneider, E., & Xi, S. (2009). A review on development of nanofluid preparation and characterization. *Powder Technology, 196*(2), 89-101. doi:https://doi.org/10.1016/j.powtec.2009.07.025

Liu, L., Ding, N., Shi, J., Xu, N., Guo, W., & Wu, C.-M. L. (2016). Failure analysis of tube-to-tubesheet welded joints in a shell-tube heat exchanger. *Case Studies in Engineering Failure Analysis, 7*, 32-40. doi:https://doi.org/10.1016/j.csefa.2016.06.002

M Hussein, A., Sharma, K., Abu Bakar, R., & Kadirgama, K. (2013). *The Effect of Nanofluid Volume Concentration on Heat Transfer and Friction Factor inside a Horizontal Tube* (Vol. 2013).

Mirzaei, M., Hajabdollahi, H., & Fadakar, H. (2017). Multi-objective optimization of shell-and-tube heat exchanger by constructal theory. *Applied Thermal Engineering, 125*, 9-19. doi:https://doi.org/10.1016/j.applthermaleng.2017.06.137

Mukherjee, S., & Paria, S. (2013). Preparation and Stability of Nanofluids-A Review. *IOSR Journal of Mechanical and Civil Engineering (IOSR-JMCE), 9*, 63-69. doi:10.9790/1684-0926369

Narendar, G., Gupta, A. V. S. S. K. S., Krishnaiah, A., & Satyanarayana, M. G. V. (2017). Experimental investigation on the preparation and applications of Nano fluids. *Materials Today: Proceedings, 4*(2, Part A), 3926-3931. doi:https://doi.org/10.1016/j.matpr.2017.02.292

Nguyen, C. T., Desgranges, F., Roy, G., Galanis, N., Maré, T., Boucher, S., & Angue Mintsa, H. (2007). Temperature and particle-size dependent viscosity data for water-based nanofluids – Hysteresis phenomenon. *International Journal of Heat and Fluid Flow, 28*(6), 1492-1506. doi:https://doi.org/10.1016/j.ijheatfluidflow.2007.02.004

Novoselov, K. S., Geim, A. K., Morozov, S. V., Jiang, D., Zhang, Y., Dubonos, S. V., . . . Firsov, A. A. (2004). Electric Field Effect in Atomically Thin Carbon Films. *Science, 306*(5696), 666. doi:10.1126/science.1102896

Oon, C. S., Amiri, A., Chew, B. T., Kazi, S. N., Shaw, A., & Al-Shamma'a, A. (2018). INCREASE IN CONVECTIVE HEAT TRANSFER OVER A BACKWARD-FACING STEP IMMERSED IN A WATER-BASED TiO₂ NANOFLUID. *49*(15), 1419-1429. doi:10.1615/HeatTransRes.2018017043

Oon, C. S., Togun, H., Kazi, S. N., Badarudin, A., & Sadeghinezhad, E. (2013). Computational simulation of heat transfer to separation fluid flow in an annular passage. *International Communications in Heat and Mass Transfer, 46*, 92-96. doi:https://doi.org/10.1016/j.icheatmasstransfer.2013.05.005

Pak, B. C., & Cho, Y. I. (1998). HYDRODYNAMIC AND HEAT TRANSFER STUDY OF DISPERSED FLUIDS WITH SUBMICRON METALLIC OXIDE PARTICLES. *Experimental Heat Transfer, 11*(2), 151-170. doi:10.1080/08916159808946559

Pantzali, M. N., Kanaris, A. G., Antoniadis, K. D., Mouza, A. A., & Paras, S. V. (2009). Effect of nanofluids on the performance of a miniature plate heat exchanger with modulated surface. *International Journal of Heat and Fluid Flow, 30*(4), 691-699. doi:https://doi.org/10.1016/j.ijheatfluidflow.2009.02.005

Patel, H. E., Das, S. K., Sundararajan, T., Sreekumaran Nair, A., George, B., & Pradeep, T. (2003). Thermal conductivities of naked and monolayer protected metal nanoparticle based nanofluids: Manifestation of anomalous enhancement and chemical effects. *Applied Physics Letters, 83*(14), 2931-2933. doi:10.1063/1.1602578

Peng, H., Ding, G., & Hu, H. (2011). Effect of surfactant additives on nucleate pool boiling heat transfer of refrigerant-based nanofluid. *Experimental Thermal and Fluid Science, 35*(6), 960-970. doi:https://doi.org/10.1016/j.expthermflusci.2011.01.016

Sabiha, M. A., Saidur, R., Hassani, S., Said, Z., & Mekhilef, S. (2015). Energy performance of an evacuated tube solar collector using single walled carbon nanotubes nanofluids. *Energy Conversion and Management, 105*, 1377-1388. doi:https://doi.org/10.1016/j.enconman.2015.09.009

Sadri, R., Hosseini, M., Kazi, S. N., Bagheri, S., Zubir, N., Ahmadi, G., . . . Zaharinie, T. (2017). *A novel, eco-friendly technique for covalent functionalization of graphene nanoplatelets and the potential of their nanofluids for heat transfer applications* (Vol. 675).

Sridhar, V., Jeon, J.-H., & Oh, I.-K. (2010). Synthesis of graphene nano-sheets using eco-friendly chemicals and microwave radiation. *Carbon, 48*(10), 2953-2957. doi:https://doi.org/10.1016/j.carbon.2010.04.034

Syam Sundar, L., Venkata Ramana, E., Singh, M. K., & De Sousa, A. C. M. (2012). Viscosity of low volume concentrations of magnetic Fe3O4 nanoparticles dispersed in ethylene glycol and water mixture. *Chemical Physics Letters, 554*, 236-242. doi:https://doi.org/10.1016/j.cplett.2012.10.042

Timofeeva, E. V., Gavrilov, A. N., McCloskey, J. M., Tolmachev, Y. V., Sprunt, S., Lopatina, L. M., & Selinger, J. V. (2007). Thermal conductivity and particle agglomeration in alumina nanofluids: Experiment and theory. *Physical Review E, 76*(6), 061203. doi:10.1103/PhysRevE.76.061203

Vajjha, R. S., Das, D. K., & Mahagaonkar, B. M. (2009). Density Measurement of Different Nanofluids and Their Comparison With Theory. *Petroleum Science and Technology, 27*(6), 612-624. doi:10.1080/10916460701857714

Wang, X.-Q., & Mujumdar, A. S. (2008). A review on nanofluids - part II: experiments and applications. *Brazilian Journal of Chemical Engineering, 25*, 631-648.

Wong, K. V., & De Leon, O. (2010). Applications of Nanofluids: Current and Future. *Advances in Mechanical Engineering, 2*, 519659. doi:10.1155/2010/519659

Xie, H., Lee, H., Youn, W., & Choi, M. (2003). Nanofluids containing multiwalled carbon nanotubes and their enhanced thermal conductivities. *Journal of Applied Physics, 94*(8), 4967-4971. doi:10.1063/1.1613374

Xuan, Y., & Roetzel, W. (2000). Conceptions for heat transfer correlation of nanofluids. *International Journal of Heat and Mass Transfer, 43*(19), 3701-3707. doi:https://doi.org/10.1016/S0017-9310(99)00369-5

Yarmand, H., Gharehkhani, S., Kazi, S. N., Sadeghinezhad, E., & Safaei, M. R. (2014). Numerical Investigation of Heat Transfer Enhancement in a Rectangular Heated Pipe for Turbulent Nanofluid. *The Scientific World Journal, 2014*, 9. doi:10.1155/2014/369593

Yu, W., Xie, H., & Bao, D. (2009). Enhanced thermal conductivities of nanofluids containing graphene oxide nanosheets. *Nanotechnology, 21*(5), 055705. doi:10.1088/0957-4484/21/5/055705

Yuan, X., Tao, Z., Li, H., & Tian, Y. (2016). Experimental investigation of surface roughness effects on flow behavior and heat transfer characteristics for circular microchannels. *Chinese Journal of Aeronautics, 29*(6), 1575-1581. doi:https://doi.org/10.1016/j.cja.2016.10.006

Zhu, H., Zhang, C., Tang, Y., Wang, J., Ren, B., & Yin, Y. (2007). Preparation and thermal conductivity of suspensions of graphite nanoparticles. *Carbon, 45*, 226-228. doi:10.1016/j.carbon.2006.07.005